Zootaxa 3848 (1): 001–066
www.mapress.com/zootaxa/

Monograph

ISSN 1175-5326 (print edition)
ZOOTAXA
ISSN 1175-5334 (online edition)

http://dx.doi.org/10.11646/zootaxa.3848.1.1
http://zoobank.org/urn:lsid:zoobank.org:pub:B72CF242-610B-45E8-A0C4-813EB115FD5B

ZOOTAXA

3848

A new titanosauriform sauropod (Dinosauria: Saurischia) from the Lower Cretaceous of Hyogo, Japan

HARUO SAEGUSA[1,2,3] & TADAHIRO IKEDA[1,2]

[1]*Institute of Natural and Environmental Sciences, University of Hyogo, Hyogo 669-1546, Japan*
[2]*Museum of Nature and Human Activities, Hyogo, Hyogo 669-1546, Japan*
[3]*Corresponding author. E-mail: saegusa@hitohaku.jp*

Magnolia Press
Auckland, New Zealand

Accepted by S. Brusatte: 5 Jun. 2014; published: 12 Aug. 2014

HARUO SAEGUSA & TADAHIRO IKEDA
A new titanosauriform sauropod (Dinosauria: Saurischia) from the Lower Cretaceous of Hyogo, Japan
(*Zootaxa* 3848)

66 pp.; 30 cm.

12 Aug. 2014

ISBN 978-1-77557-465-1 (paperback)

ISBN 978-1-77557-466-8 (Online edition)

FIRST PUBLISHED IN 2014 BY

Magnolia Press

P.O. Box 41-383

Auckland 1346

New Zealand

e-mail: zootaxa@mapress.com

http://www.mapress.com/zootaxa/

ISSN 1175-5326 (Print edition)

ISSN 1175-5334 (Online edition)

Table of contents

Abstract

A new genus and species of titanosauriform sauropod is erected based on a partial skeleton found in the Lower Cretaceous Sasayama Group of Hyogo Prefecture, SW Japan. The new taxon is here named as *Tambatitanis amicitiae* **gen. et sp. nov.**, which is diagnosed by the following features of the caudal vertebrae, chevrons and braincase: the postzygapophysis and the summit of the neural spine of the anterior caudal vertebrae are located beyond the posterior border of the centrum, the spine of the anterior caudal vertebrae is curved strongly anteriorly and bow-shaped in lateral view, the summit of the neural spine is expanded and hemispherical with its anterior face excavated by the posterodorsal extension of a deep and narrow SPRF, the transverse process of the anterior caudal vertebrae are short and L shaped, the anterior chevron is the longest among sauropods in proportion to body size, the distal ends of the anterior chevrons are rod-shaped, the distal ends of the mid chevrons are transversely thin and anteroposteriorly long without cranial processes, and the dorsal border of the shaft of the paroccipital process that forms the ventral margin of the posttemporal fenestra is short mediolaterally and V-shaped in posterior view. A phylogenetic analysis suggests that *T. amicitiae* is a basal titanosauriform, possibly belonging to the East Asian endemic clade Euhelopodidae. The caudals and chevrons are described in detail in order to document highly autapomorphic features of the new taxon as well as potentially phylogenetically informative characters. The discovery of *T. amicitiae* suggests that East Asian basal titanosauriforms were diverse not only in the number of the taxa but also in the morphological variation of the caudal elements.

Key words: Sauropoda, Titanosauriform, Early Cretaceous, Sasayama Group, Japan, East Asia

Introduction

Titanosauriform sauropods diversified during the Cretaceous, and represent the only sauropod clade that persisted until the very end of the Cretaceous. Their high diversity during the Cretaceous has been mostly documented from the southern continents, especially from South America (Mannion and Otero 2012), but during the last decade, it has been increasingly recognized that titanosauriforms were more diversified in northern continents during the Cretaceous than previously thought. This re-evaluation of the global sauropod diversity pattern is prompted by the revisions of existing remains and the new finding of Cretaceous sauropod remains from North America (*e.g.,* D'Emic 2013 and the references therein), Europe (*e.g.,* Díez Díaz *et al*. 2013 and the references therein), and Asia (*e.g.*, D'Emic *et al*. 2013 and the references therein), although the number of titanosauriforms, especially that of titanosaurs known from the southern continents, is still overwhelmingly larger than that of the northern continents. Recently, phylogenetic analyses of basal titanosauriforms were conducted by two sets of authors (D'Emic 2012; Mannion *et al*. 2013), based on comprehensive revision of the fossils of the group, including the recently found East Asian titanosauriforms. They largely agreed in recovering a monophyletic group, Euhelopodidae, which was composed of most of the Early Cretaceous East Asian titanosauriforms, but one of the phylogenetic analyses of Mannion *et al.* (2013), in which quantitative characters were treated as continuous data, suggests that Euhelopodidae breaks up to form a paraphyletic grade. In order to resolve this issue, arguments on the adequacy of

the phylogenetic method applied to the morphological data seem to be critical. At the same time, however, the amount of reliable data available for the analysis is also crucial. As noted by D'Emic *et al*. (2013), most of the remains of East Asian titanosauriforms have yet to be adequately described, and this situation made the further investigation of the evolutionary history of the East Asian titanosauriforms difficult.

Here we report a new basal titanosauriform sauropod dinosaur from the Early Cretaceous of Japan. The materials described here have been excavated from the Early Cretaceous Sasayama Group of Hyogo Prefecture, SW Japan. This partial skeleton was found in 2006 by amateur paleontologists Messrs. K. Adachi and S. Murakami on the riverbed of the Sasayama River in Kamitaki, Sannan-cho, Tamba City, Hyogo Prefecture, Japan (Fig.1) (the locality is referred to as Kamitaki Quarry hereafter). It took five seasons to retrieve the fossils from a hard, reddish mudstone bed of the Sasayama Group exposed at the Kamitaki Quarry, because the bed on the riverbed can be excavated only during the limited time in winter when the water level of the river becomes lowest due to a decrease in local precipitation (Saegusa *et al*. 2008, 2010). Teeth, a braincase, a dentary, an atlas, a fragmental cervical vertebra, dorsal ribs, two fragmental dorsal vertebrae, a pubis, an ilium, sacral spines, presumable first sacral ribs, 22 caudal vertebrae and 17 chevrons of a single individual of a sauropod have been collected from the quarry, but much of the materials are still being prepared, because the hard matrix and the highly fractured condition of the bones are hindering the preparation.

A full description of all of the sauropod material excavated so far will be not given here, because much of the material is still being prepared. Our aim in this paper is to establish a new taxon of titanosauriform sauropod based on the detailed description of a braincase, caudal vertebrae and chevrons, which are completely prepared, and to give a preliminary account of the phylogenetic position of the new taxon. As for the other sauropod skeletal elements excavated from Kamitaki Quarry, only a brief description of the features necessary for the scoring of the character matrix used for the phylogenetic analysis and/or the generic and specific distinction between the present taxon and some Asian titanosauriforms are given. The detailed description of the elements other than the cranial and caudal elements will be published elsewhere, together with the augmented phylogenetic analyses, when the preparation of the sauropod material from Kamitaki Quarry is completed.

The quarry map shown in this paper depicts only the position of the braincase, caudals, chevrons, ilium, sacral spines and presumable first sacral ribs (Fig. 2). The quarry map of the other excavated elements is yet to be completed, because their precise shapes are mostly still not clear due to matrix coverage, although the location of the all the specimens in the quarry was precisely recorded three dimensionally. The complete site map will be published elsewhere, together with a detailed account of the taphonomy of the site.

Institutional abbreviations: **AMNH**, American Museum of Natural History, New York, USA; **CM**: Carnegie Museum of Natural History, Pittsburgh, Pennsylvania, USA; **CPT**, Museo Fundacíon Conjunto Paleontológico de Teruel, Teruel, Spain; **DFMMh**, Dinosaurier-Freilichtmuseum, Münchehagen, Germany; **GMNH**, Gunma Museum of Natural History, Gunma, Japan; **HMN**, Humboldt Museum für Naturkunde, Berlin, Germany; **MACN**, Museo Argentino de Ciencias Naturales, "Bernadino Rivadavia", Buenos Aires, Argentina; **Mal**, Malawi Department of Antiquities Collection, Lilongwe and Nguludi, Malawi; **MCF-PVPH**, Museuo Carmen Fuens, Plaza Huincul, Neuquén, Argentina; **MGPIFDGR**, Museo de Geología y Paleontología del Instituto de Formación Docente Continua de General Roca, Río Negro, Argentina; **MIWG**, Museum of Isle of Wight Geology (now Dinosaur Isle Visitor Centre), Sandown, Isle of Wight, United Kingdom; **MML**, Museo Municipal de General Roca, Río Negro, Argentina; **MNHAH**, Museum of Nature and Human Activities, Hyogo, Japan; **MUCP**, Museo de Geología y Paleontología de la Universidad Nacional del Comahue Neuquén, Argentina; **PMU**, Palaeontological Museum, University of Uppsala, Sweden; **SM**, Sirindhorn Museum, Changwat Kalasin, Thailand; **YPM**, Yale Peabody Museum of Natural History, New Haven, Connecticut, USA; **Z. PAL**, Palaeobiological Institute of the Polish Academy of Sciences, Warsaw.

Terminology and anatomical abbreviations

For the anatomical structures listed below and discussed in text, we use ''Romerian'' terms for the structures (*e.g.,* ''centrum,'' not ''corpus'') and for their orientation (*e.g.,* ''anterior,'' not ''cranial''). The terminology for vertebral lamination and fossa follows the nomenclatures of Wilson (1999, 2012) and Wilson *et al*. (2011) respectively.

Anatomical Abbreviations: **afc**, anterior articular facet for chevron; **ba**, foramen for basilar artery; **bc**, braincase; **bp**, basipterygoid process; **bt**, basal tubera; **c**, centrum; **ca**, crista antotica; **ch**, chamber; **cp**, crista prootica; **Cd**, caudal vertebra; **CPOL**, centropostzygapophyseal lamina; **CPRL**, centroprezygapophyseal lamina; **ct**, crista tuberalis; **d**, diapophysis; **ds**, dorsum sellae; **dp**, depression; **eof**, external occipital foramen; **fm**, foramen

magnum; **fmt**, fenestra metotica; **fo**, fenestra ovalis; **fr,** foramen; **fs**, fossa; **gr,** groove; **Ha**, haemal arch or chevron; **ic**, foramen for internal carotid artery; **il**, ilium; **mdCPRL**: medial division of the centroprezygapophyseal lamina; **msf**, median subcondylar foramen; **nc**, neural canal; **nuc**, nuchal crest; **ns**, neural spine; **oc,** occipital condyle; **ocf**, orbitocerebral foramen; **pa**, pierced area; **pf,** pituitary fossa; **pfc**, posterior articular facet for chevron; **pl**, pleurocoel; **poz**, postzygapophysis; **POCDF**, postzygapophyseal centrodiapophyseal fossa; **PODL**, postzygodiapophyseal lamina; **POSDF**, postzygapophyseal spinodiapophyseal fossa; **POSL**, postspinal lamina; **prz**, prezygapophysis; **pop**, paroccipital process; **re**, recess; **PRDL**, prezygodiapophyseal lamina; **PRSL**, prespinal lamina; **ptf**, posttemporal foramen; **rd**, ridge; **rg,** rugosity; **SDF**, spinodiapophyseal fossa; **SPDL**, spinodiapophyseal lamina; **SPOF**, spinopostzygapophyseal fossa; **speo**, suture between prootic and exoccipital-opisthotic complex; **spl**, suture between prootic and laterosphenoid; **SPOL**, spinopostzygapophyseal lamina; **SPRF**, spinoprezygapophyseal fossa; **SPRL**, spinoprezygapophyseal lamina; **SPRLp,** SPRL process; **sr**, sacral rib; **ssp**, sacral spine; **tb**, tuberosity; **tp**, transverse process; **tu**, tubercle; **vlf**, ventral longitudinal fossa; **III–XII**, cranial nerve openings.

Taphonomical Abbreviations: bf, bone fragment; **tf**, trace fossil.

CT and laser scanning.

CT scanning of the caudal vertebrae Cd1 to Cd6 of MNHAH D-1029280 took place at Fukui Prefectural Dinosaur Museum, in Katsuyama, Japan, using the model TESCO Corporation, TXS320-ACTIS. These specimens were scanned with the following settings: an interslice spacing of 0.1mm, a slice thickness of 0.2mm, 290 kV, and 270μA. Data were output from the scanner in DICOM format, and then imported into Amira ver. 5.3 for viewing, analysis and preparation of the transverse sections.

We reconstructed the ilium of MNHAH D-1029280 from 3D images of the 19 broken pieces of the ilium virtually, because these fragments, especially those of sacral ribs, are too fragile to be fitted together. We used a ZScanner 700 (Z Corporation, Burlington, MA, USA) to capture the 3D surface geometry of these fragments, and then we assembled their 3D images in Rapidform XOS2 (INUS Technology, Seoul, South Korea).

Geologic setting.

The sauropod specimens reported here were collected from the "Lower Formation" of the Cretaceous Sasayama Group, which crops out in the eastern part of Hyogo Prefecture, Japan (Saegusa *et al*. 2008). The Sasayama Group unconformably overlies a Permo–Triassic accretionary complex, and is unconformably overlain by the Upper Cretaceous Arima Group. The Sasayama Group, which consists of the "Lower" and "Upper" Formations, is mainly composed of terrestrial clastic rocks (Yoshikawa 1993); the "Lower Formation" consists mainly of conglomerates, sandstones, and mudstones, and intercalated acidic tuff beds in the lower part, whereas the "Upper Formation" consists mainly of andesites, andesitic pyroclastic rocks, and tuffaceous sandstones and mudstones. Zircon fission-track (FT) ages and biostratigraphical correlations have been used to date the Group, with the age of the "Lower" and the "Upper" formations assigned to the Tithonian to Cenomanian and Aptian to Cenomanian, respectively (Matsuura *et al*.1992; Hayashi *et al*. 2010). Recently, SHRIMP U-Pb dating of a tuff bed in the lower part of the "Lower Formation" and an andesite in the lower part of the "Upper Formation" have given ages of 112.1±0.4 Ma (early Albian) and 106.4 ± 0.4 Ma (late Albian), respectively (Kusuhashi *et al.* 2013).

The fossils described here have all been recovered from a reddish mudstone bed of flood plain origin in the "Lower Formation", at Kamitaki Quarry, Sannan-cho, Tamba City (Fig 1). Besides a partial sauropod skeleton reported here, this bed contains various micro-vertebrate remains, including numerous frog bones (including several complete skeletons), tooth and jaw remains of scincomorph lizards, and shed teeth of various dinosaurs including basal hadrosauroids, ankylosaurs, therizinosauroids, undefined theropods, as well as premaxillary teeth of a basal tyrannosauroid. Strong development of slickensides and the high calcareous concretions in the reddish paleosol mudstones suggest that the deposition of the bone bed took place under a climate with intense seasonal temperature and precipitation fluctuations (Saegusa *et al.* 2010).

Anterior caudal vertebrae, pelvic elements and ribs of a sauropod were found lying roughly in anatomical order in an area of approximately 6m x 4m. Thousands of bone fragments, most of which are irregular shaped, and thin fragments, presumably derived from the shattered sacral and presacral centra, were found piled up on these semi-articulated axial elements of the sauropod. Other skeletal elements, including the braincase and dentary, were found scattered and jumbled with bone fragments within and around the above area. Significantly, all of the skeletal elements mentioned above are found in a single horizon situated at the middle of the 2m thick reddish mudstone

bed and no duplication of elements was found among them, at least among those prepared so far. This association of skeletal elements strongly suggests the presence of a single sauropod individual.

Although a sedimentary gap is not directly observed on the outcrop of the mudstone bed containing the sauropod remains, the presence of a hiatus between sedimentary episodes is inferred because the sides of the bones facing upward in the bed are selectively damaged, as described below in the section of the postmortem distortion of the caudals. This selective damage of the bones must be related to the thickness of the sediment left by a single depositional event. The skeletal parts not covered by the initial sedimentary event may have been destroyed by various ground surface process prior to the completion of burial by succeeding sedimentary events (for the taphonomy of caudal elements, see Appendix).

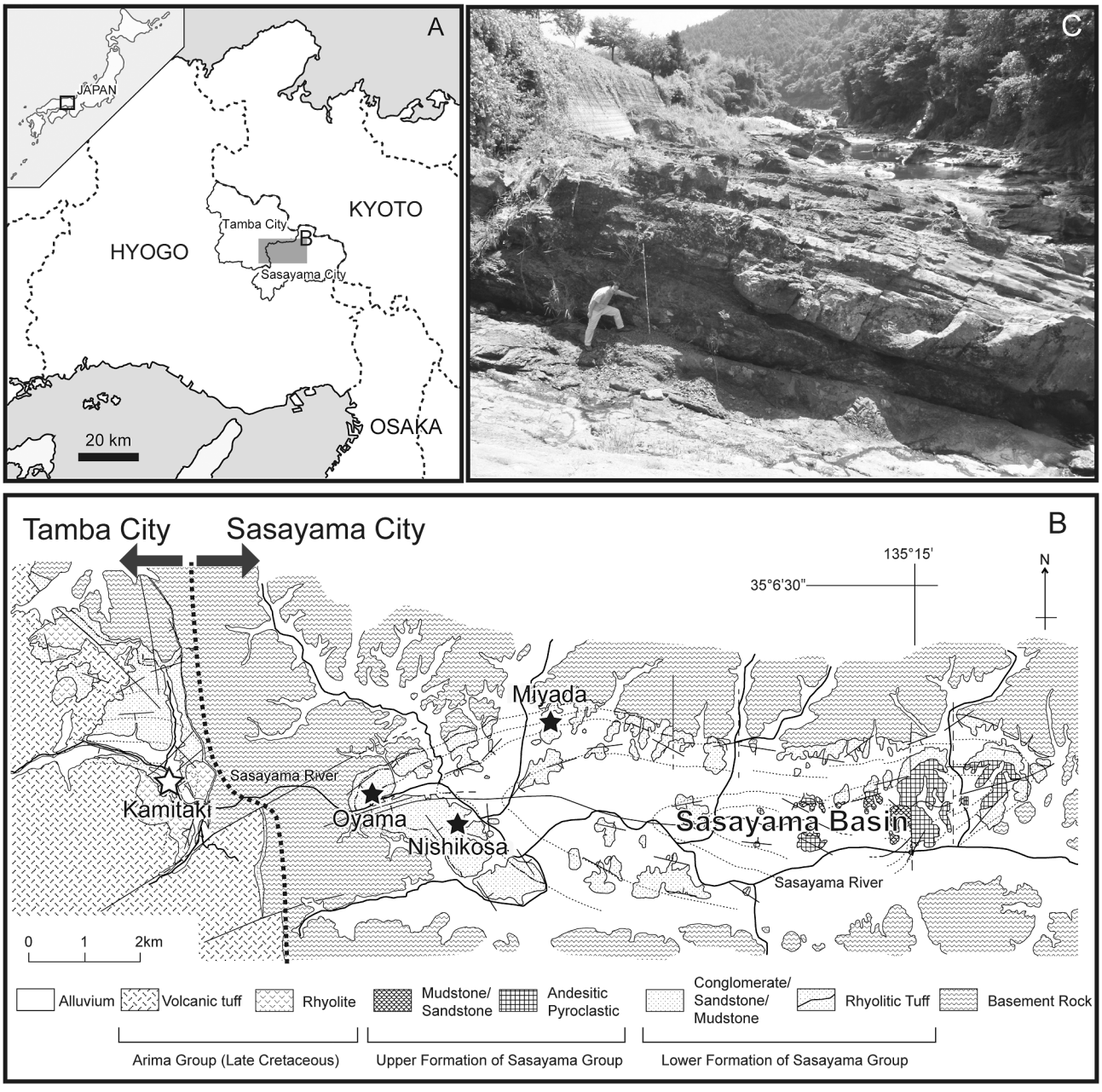

FIGURE 1. A, Map showing the geographical location of Tamba and Sasayama City, Hyogo, Japan. The gray area denotes the distributional area of the Sasayama Group. **B,** Geological map of Tamba-Sasayama Area; modified after Yoshikawa (1993). The white star represents the type locality (Kamitaki Quarry) of *Tambatitanis amicitiae* **gen. et sp. nov.** The black stars indicate other localities of fossil vertebrate assemblages. **C,** a view of Kamitaki Quarry.

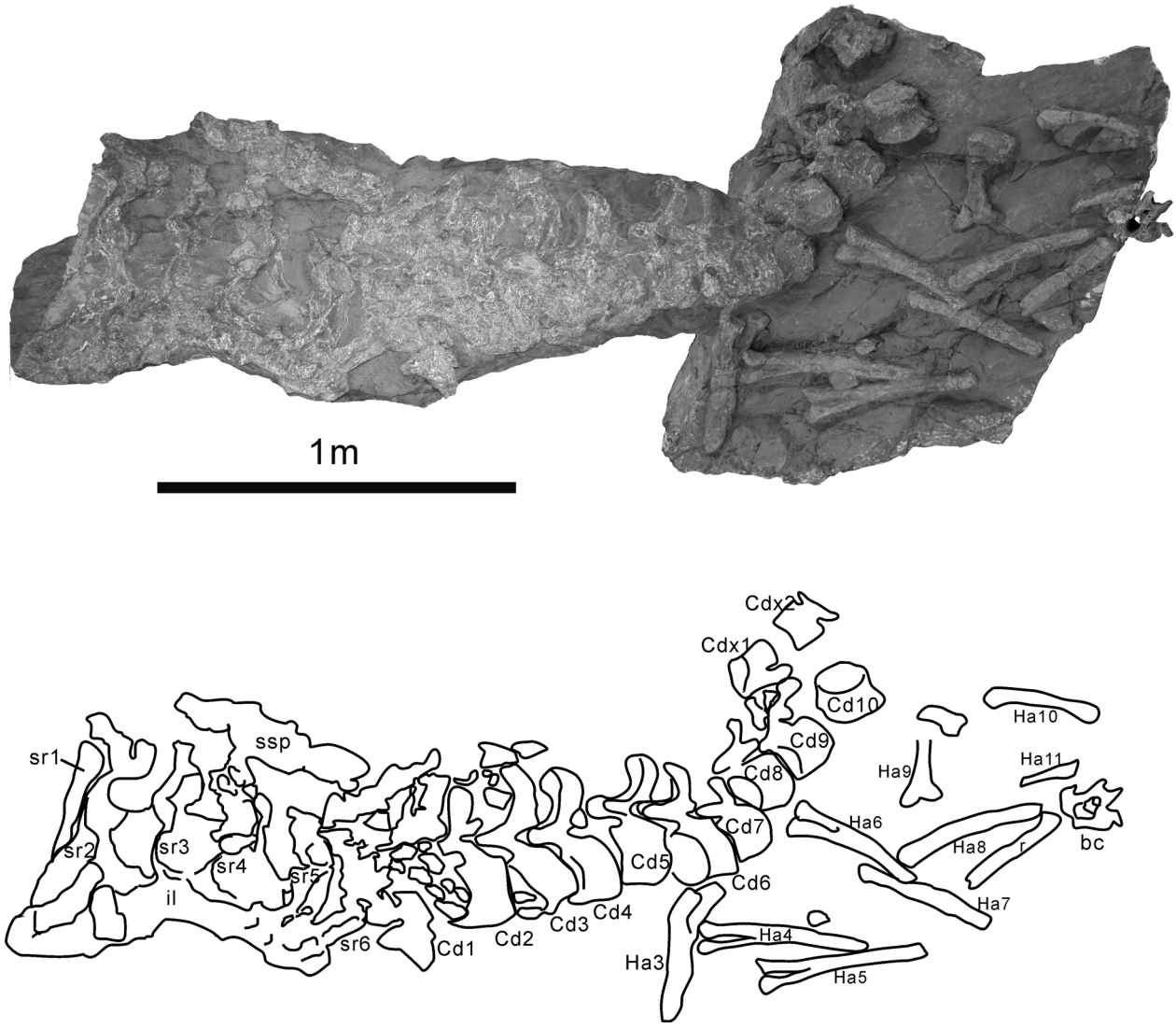

FIGURE 2. *Tambatitanis amicitiae* **gen. et sp. nov.**, holotype (MNHAH D-1029280). Disposition of pelvic and caudal elements in the bed. Adapted from Saegusa *et al.* (2008). See text for abbreviations.

Systematic paleontology

Dinosauria Owen, 1842

Saurischia Seeley, 1887

Sauropoda Marsh, 1878

Macronaria Wilson and Sereno, 1998

Titanosauriformes Salgado, Coria, and Calvo, 1997

Somphospondyli Wilson and Sereno, 1998

***Tambatitanis* gen. nov.**

Type species: *Tambatitanis amicitiae* **sp. nov.**; see below.

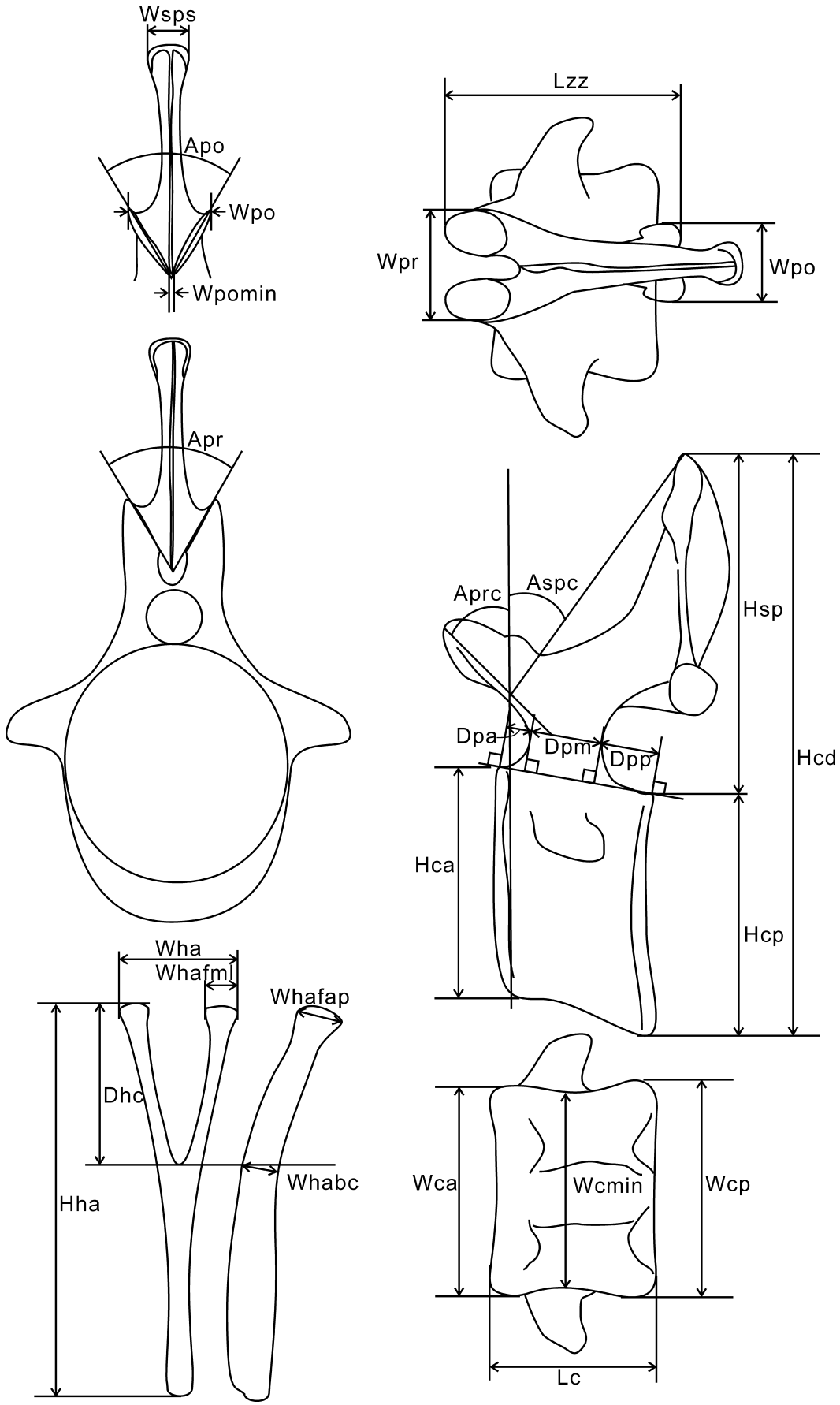
Wsps
Apo
Wpo
Wpomin
Lzz
Wpr
Wpo
Apr
Aprc
Aspc
Hsp
Hcd
Dpa
Dpm
Dpp
Hca
Hcp
Wha
Whafml
Whafap
Dhc
Whabc
Hha
Wca
Wcmin
Wcp
Lc

Etymology. In reference to the Tamba, the northwestern region of Kansai Area, SW Japan, where the type specimen was collected; and *titanis*, from Greek, refers to giants, symbolic of the great size of the specimen.

Diagnosis. As for the type and only known species.

Tambatitanis amicitiae sp. nov.

Holotype. Museum of Nature and Human Activities, MNHAH D-1029280: a partial skeleton represented by teeth, a braincase, a dentary, an atlas, a fragmentary cervical vertebra, fragmentary dorsal vertebrae, dorsal ribs, first sacral ribs, spine of sacral vertebrae, a pubis, an ilium, caudal vertebrae and chevrons

Type locality. Kamitaki, Sannan-cho, Tamba City, Hyogo Prefecture, Japan

Type horizon and age: 'Lower' Formation of the Sasayama Group, Early Cretaceous (probably early Albian).

Etymology. *amicitia* (Latin), meaning friendship, refers to the friendship between Messrs. Murakami Shigeru and Adachi Kiyoshi who found the holotype skeleton of this new species, in August, 2006.

Diagnosis. *Tambatitanis amicitiae* **gen. et sp. nov.** is characterized by 8 unique characters: (1) the postzygapophysis and the summit of the neural spine of the anterior caudal vertebrae are located beyond the posterior border of the centrum; (2) the spine of the anterior caudal vertebrae is curved strongly anteriorly and bow-shaped in lateral view; (3) the summit of the neural spine is expanded and hemispherical with its anterior face excavated by the posterodorsal extension of a deep and narrow SPRF; (4) the transverse processes of the anterior caudal vertebrae are short and L shaped; (5) the anterior chevron is longest among sauropods in proportion to body size; (6) the distal ends of the anterior chevrons are rod-shaped; (7) the distal ends of the mid chevrons are transversely thin and long anteroposteriorly, without cranial process; (8) the dorsal border of the shaft of the paroccipital process that forms the ventral margin of the posttemporal fenestra is short mediolaterally and V-shaped in posterior view.

Description and comparisons.

Braincase. The preserved braincase consists of a supraoccipital, basioccipital, exoccipital, opisthotic, prootic, basisphenoid, laterosphenoid and orbitosphenoid. Most of the orbitosphenoid in front of the foramina for cranial nerves III and IV was lost by postmortem damage. Skull roof elements, including the frontal and parietal, are not present in the materials prepared so far.

The braincase is, as a whole, very short anteroposteriorly. This feature is not due to the postmortem distortion because no cleavage is seen on thin structures, such as crista prootica and crista interfenestralis, which might be vulnerable to compression forces exerted by sedimentary loads.

Because of the strong coossification of the elements constituting the braincase, the sutures between them cannot be discerned except for those between the prootic and exoccipital-opisthotic complex and between the prootic and laterosphenoid (see below). The occipital surface is nearly flat, barely concave transversely and slightly convex dorsoventrally (Fig. 4A).

FIGURE 3. Measurements taken on caudal vertebrae and chevrons: Apo = angle between articular facets of postzygapophyses; Apr = angle between articular facets of prezygapophyses; Aprc = inclination of the prezygapophysis; Aspc = the angle between the plane parallel to the articular surface of the centrum and the line connecting the lowest point of SPRL just behind the process and the summit of the spine; Dhc = dorsoventral height of haemal canal; Dpa = distance from anterior end of centrum to anterior end of the pedicle of neural arch measured parallel to the dorsal border of the centrum; Dpm = anteroposterior width of the pedicle of neural arch measured parallel to the dorsal border of the centrum; Dpp = distance from posterior end of centrum to posterior end of the pedicle of neural arch measured parallel to the dorsal border of the centrum; Hca = anterior centrum height (excluding chevron facets); Hcd = total height of caudal (measured from the ventral margin of the posterior articular surface of the centrum up to the neural spine summit); Hcp = posterior centrum height (excluding chevron facets); Hha = dorsoventral height of chevron; Hsp = neural spine height (measured from the dorsal surface of the centrum up to the neural spine summit); Lc = centrum length; Lzz = distance from anterior end of prezygapophysis to posterior end of the postzygapophysis; Wca = anterior centrum width; Wcp = posterior centrum width; Wha = mediolateral width across proximal end chevron; Whabc = anteroposterior width of shaft immediately below haemal canal; Whafap = anteroposterior width of proximal articular facet of chevron; Whafml = mediolateral width across one proximal articular facet of chevron; Wcmin = minimal centrum width; Wpo = maximum distance between the articular surfaces of postzygapophyses; Wpomin = minimum distance between the articular surfaces of postzygapophyses; Wpr = maximum distance between the articular surfaces of prezygapophyses; Wsps = width of neural spine summit.

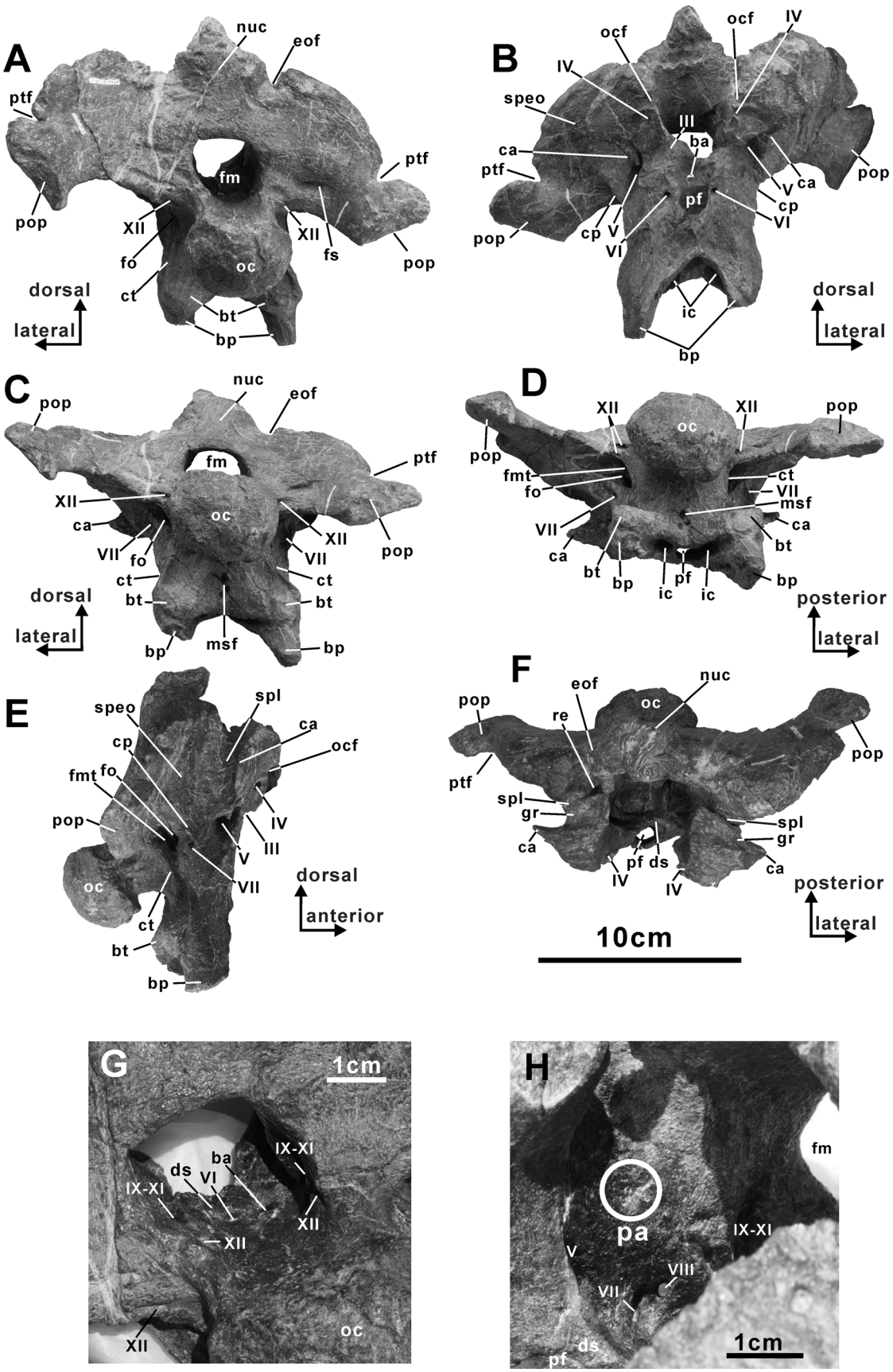

FIGURE 4. *Tambatitanis amicitiae* **gen. et sp. nov.**, holotype (MNHAH D-1029280). Braincase. **A,** posterior view. **B,** anterior view. **C,** posteroventral view. **D,** ventral view. **E,** right lateral view. **F,** dorsal view. **G,** posterodorsal view of the endocranial cavity. **H,** dorsomedial view of the endocranial cavity. See text for abbreviations.

The dorsal apex of the supraoccipital is triangular in posterior view. A blunt sagittal crest extends ventrally from it, gradually diminishes ventrally, and then becomes non-existent halfway down the occiput. Shallow depressions are present just lateral to the sagittal crest on the dorsal half of the occiput. Ventral to these depressions, there are faint elevations which may represent the articular surfaces for the proatlas.

There is a small triangular notch just lateral to the dorsal apex of the supraoccipital (eof in Fig. 4A, C and F). This notch may represent the ventral margin of a foramen described by Balanoff *et al.* (2010) and Marpmann *et al.* (2014) as the external occipital foramen, which is considered to have accommodated the caudal middle cerebral vein (Witmer and Ridgely 2009). As preserved, this notch communicates with a recess that is located at the dorsoposterior corner of the preserved endocranial cavity (re in Fig. 4F). A small foramen located about 6mm lateroventral from this notch may represent a subdivision of the external occipital foramen but its communication with the endocranial cavity is obliterated by the distortion.

From the notch that presumably represents the ventral margin of the external occipital foramen, the dorsal border of the exoccipital-opisthotic complex extends ventrolaterally to a V-shaped notch (ptf in Fig. 4A, B, C, F). This notch represents the ventral margin of the posttemporal foramen, but compared to those of other sauropods, it is extremely narrow mediolaterally. In some titanosauriformes (*e.g., Phuwiangosaurus* [Suteethorn *et al.* 2009: fig. 9]; *Malawisaurus* [Gomani 2005: fig. 6]; *Nemegtosaurus* and *Quaesitosaurus* [Wilson 2005: figs. 9, 18]; *Rapetosaurus* [Curry Rogers and Forster 2004: fig.19]; *Jainosaurus* [Wilson *et al.* 2009: fig.6]), the shaft of the paroccipital process that forms the ventral margin of the posttemporal foramen is shorter mediolaterally compared to the condition in some basal sauropods (*e.g., Spinophorosaurus* [Knoll *et al.* 2012: fig. 3]) and diplodocoids (*e.g., Suuwassea* [Harris and Dodson 2004: fig.1]; *Diplodocus* and *Apatosaurus* [Berman and McIntosh 1978: figs. 3, 11]). However, that of *Tambatitanis* is notable for its extremely mediolaterally shortened paroccipital processes, a condition that is clearly autapomorphic.

The left paroccipital process is displaced dorsally from its original position by a series of small cracks running dorsoventrally on the middle of the exoccipital-opisthotic complex. The left and right paroccipital processes are well preserved except for their ventrolateral extremities, so that the presence or absence of the non articular ventral process of the paroccipital process cannot be established. On the right exoccipital-opisthotic complex, a small elliptical depression is located about 15mm lateral from the lateral rim of the foramen magnum.

The dorsal and ventral borders of the foramen magnum are located 6 cm and 9.5 cm, respectively, ventral to the dorsal end of the preserved supraoccipital. Due to the complete fusion between occipital elements, their relative contribution to the foramen magnum is not known. In posterior view, the foramen magnum is skewed leftward due to postmortem distortion. It is dorsoventrally higher than transversely wide (Table 1). The dorsoventral height of the exoccipital is about 1.7 times greater than that of the foramen magnum (Table 1).

TABLE 1. Size measurements of (in mm) braincase of *Tambatitanis amicitiae* **gen. et sp. nov.**, holotype (MNHAH D-1029280).

Disance from dorsal apex of supraoccipital to ventral border of basal tubera	136
Disance from dorsal apex of supraoccipital to dorsal margin of foramen magnum	54
Disance from ventral border of the neck of the occipital condyle to ventral border of basal tubera	26
Transverse width of occipital condyle	48
Dorsoventral height of occipital condyle	39
Anteroposteiror length of occipital condyle	23
Transverse width of foramen magnum	29
Dorsoventral height of foramen magnum	32
Transverse width of basal tubera	63
Anteroposterior width of the base of the right basipterygoid process	20
Transverse width of the base of the right basipterygoid process	14
Transverse width of braincase across paroccipital proccess (as preserved)	188
Transverse width of braincase across fenestrae metotica	42
Basal tubera:occipital condyle width	1.31
Occipital condyle width:height	1.23

The occipital condyle is posteroventrally oriented: the plane of occiput meets the dorsal surface of the occipital neck and the axis of condyle at about 115 and 145 degrees, respectively. In posterior view, the dorsal rim of the articular surface of the occipital condyle is slightly concave dorsally, and on the dorsal surface of its neck, a very shallow longitudinal trough extends anteriorly from the dorsal rim of the articular surface of the condyle to the floor of the endocranial cavity. The occipital condyle of *Tambatitanis* is most similar to *Bonatitan* (MACN-PV RN821) in width/height ratio (Table 1; Mannion 2011: table 1) as well as in its outline in posterior view (Martinelli and Forasiepi 2004: fig.7). However, these traits of the occipital condyle are probably not diagnostic, because a wide range of the individual variation in the size and shape of the condyle is seen in *Camarasaurus* (Berman and McIntosh 1978: figs. 3, 11; Ikejiri 2008).

The basal tubera are sheet-like and broad laterally, extending well beyond the lateral margin of the occipital condyle. In the ratio between the transverse widths of the basal tubera and occipital condyle (Table 1), *Tambatitanis* is similar to some neosauropods (*Apatosaurus ajax* (YPM 1860), *Camarasaurus lentus* (CM 11338), *Europasaurus* (DFMMh 291) and *Nemegtosaurus* (Z. PAL MgD-I/9) [Mannion 2011: table 1]) and a eusauropod, *Turiasaurus* (CPT-1211 [Royo-Torres and Upchurch 2012: appendix 1]). Other sauropods have wider (most titanosaurs and basal macronarians) or narrower (most diplodocoids and *Giraffatitan*) basal tubera in relation to the transverse width of the occipital condyle compared to *Tambatitanis* (Mannion 2011: table 1). The basal tubera are short dorsoventrally and located very close to the occipital condyle (Table 1, Fig. 4E). In these features, *Tambatitanis* is similar to *Europasaurus* (Marpmann *et al.* 2014: fig. 13), *Giraffatitan* (Janensch 1935-6: fig. 58), an indeterminate North American titanosauriform (Tidwell and Carpenter 2003: fig.1), *Phuwiangosaurus* (Suteethorn *et al.* 2009: fig. 9), *Mongolosaurus* (Mannion 2011: fig. 2), *Nemegtosaurus* (Wilson 2005: fig. 9) and *Antarctosaurus* (Powell 2003: pl. 64).

In posterior view, the basal tubera diverge from the midline of the braincase by 70 degrees. The basal tubera are not separated from each other by deep a medial fossa as in some individuals of *Camarasaurus* (*e.g.,* Madsen *et al.* 1995: fig. 23), *Europasaurus* (Marpmann *et al.* 2014: fig. 13), *Giraffatitan* (Janensch 1935-6: fig. 58), and an indeterminate North American titanosauriform (Tidwell and Carpenter 2003: fig. 1), but rather are connected by a weak swelling extending along the midline from the ventral surface of the neck of the occipital condyle to the ventral border of the basal tubera. On the posterior surface of each basal tuber, there is a broad shallow fossa (Fig. 4C). This fossa is separated from its counterpart by the low swelling that connects the left and right basal tubera, bordered laterally by thin but distinct ridge (hereafter referred to as the crista tuberalis for simplicity, ct in Fig. 4) and bounded ventrally by the protuberance which marks the ventral end of the basal tubera (hereafter referred to as the ventral protuberance for simplicity). The crista tuberalis connects the paroccipital process above with the basal tuber below. It runs medially from the sharp ventral margin of the paroccipital process to the point just posterodorsally to the fenestra metotica (see below). From this point it passes down the lateral side of the base of the neck of the occipital condyle and then extends ventrolaterally along the lateral margin of the basal tuber to the ventrolateral corner of the ventral protuberance. *Ampelosaurus* also has a crista tuberalis that connects the paroccipital process above with the basal tuber below (Knoll *et al.* 2013: figs. S1–3).

The basal tubera have a broad, shallow depression on their posterior surface in *Jainosaurus* (Wilson *et al.* 2009), "Malagasy Taxon B" (Curry Rogers, unpublished data, in Wilson *et al.* 2009) , *Muyelensaurus* (Calvo *et al.* 2008), *Pitekunsaurus* (Filippi and Garrido 2008), and an indeterminate titanosaur braincase from Río Negro, Argentina (MML 194 [García *et al.* 2008]). The shallow depression on the basal tubera of these taxa differs from the similar depressions of *Tambatitanis* in being a single structure, undivided into left and right halves by low median bulge.

The ventral protuberance is weakly rugose, band-like (ca. 1.2cm wide) and runs medially and slightly dorsally from the ventrolateral end of the basal tuber to the midline of the basal tubera. The ventral margin of the ventral protuberance, which marks the ventral border of the basal tuber, is arched dorsally and widely V-shaped in posterior view (Fig. 4A , C).

The ventral protuberance is not as robust as those of *Rapetosaurus* (Curry Rogers and Foster 2004), *Phuwiangosaurus* (Suteethorn *et al.* 2009), *Lirainosaurus* (Díez Díaz *et al.* 2011) and an indeterminate titanosaur from Patagonia (García *et al.* 2008). *Nemegtosaurus* and *Quaesitosaurus,* and supposedly some titanosaurs such as *Jainosaurus* and *Rapetosaurus,* have a novel bony contact between the basal tubera and the quadrate (Wilson 2005; Wilson *et al.* 2009). *Tambatitanis* is not likely to have such bony connection between the basisphenoid and quadrate, because its ventral protuberance is weaker than those of titanosaurs that have or presumably had such a bony connection.

There are four small vertically aligned pits on the low swelling that connects the left and right basal tubera (msf in Fig. 4C, D). They are sharply bordered and range in diameter from 1.4 to 2.9 mm. Two of them that are located in the middle of the row are aligned slightly ventrolaterally and connected to each other by a sharply bordered shallow groove. Similar vertically aligned small fossae are present on the midline of the posterior surface of the basal tubera in *Phuwiangosaurus* (Suteethorn *et al.* 2009) and *Mongolosaurus* (Mannion 2011), whereas a single and larger fossa is present on the posterior surface of the basal tubera of *Saltasaurus*, *Amargasaurus*, *Limaysaurus* and *Nigersaurus* (Mannion 2011).

A concavity on an indeterminate titanosaur braincase (MUCPv 334) described by Calvo and Kellner (2006) as a 'basisphenoidal depression' appears to be comparable with the single fossa on the posterior surface of the basal tubera of *Saltasaurus*. This concavity on MUCPv 334 is considered to be located on the ventral margin of the basal tubera (*e.g.,* Mannion 2011). However, the sharp edge extending laterally from the concavity looks to be the result of breakage rather than the original ventral border of the basal tubera. If this interpretation is correct, the concavity in question is not located on the ventral margin of the basal tubera but on the middle of the tubera and should be compared with the single fossa on the basal tubera of *Saltasaurus* mentioned above. On the other hand, the single fossa of latter three diplodocoid taxa is fairly larger and located at a higher position on the basal tubera than those of the titanosauriforms, and appears to be not comparable with the latter.

The basipterygoid process is poorly preserved: only the basal 3 and 13 mm are preserved on the left and right sides, respectively. The preserved basal part of the right basipterygoid process is wider anteroposteriorly than transversely (Table 1), and is the shape of an isosceles triangle in horizontal cross-section. Because of the poor preservation, it is hard to measure the angle between the basipterygoid processes precisely, but judging from the remaining parts, the angle appears to be very small, presumably less than 20 degrees. The dorsal bases of the basipterygoid processes are widely separated from each other and rise just ventral to the ventrolateral end of the basal tubera. In these features of the basipterygoid processes, *Tambatitanis* is similar to some titanosaurs (*Bonatitan* [Martinelli and Forasiepi 2004: fig. 7], *Antarctosaurus* [Powell 2003: pl. 64], *Narambuenatitan* [Filippi *et al.* 2011: fig. 3], *Muyelensaurus* [Calvo *et al.* 2008: fig. 4], *Pitekunsaurus* [Filippi and Garrido 2008: fig. 3], indeterminate titanosaur [García *et al.* 2008: fig. 1]). On the other hand, the basipterygoid processes are more divergent ventrally and their bases are located more medially in *Phuwiangosaurus* (Suteethorn *et al.* 2009: fig. 9), *Mongolosaurus* (Mannion 2011: fig. 2) and some other titanosaurs (*Lirainosaurus* [Díez Díaz 2011: figs. 2, 5], *Jainosaurus* [Wilson *et al.* 2009: fig. 6], *Malawisaurus* [Gomani 2005: fig. 6], *Nemegtosaurus* [Wilson 2005: fig. 9], *Quaesitosaurus* [Wilson 2005: fig. 18]). *Rapetosaurus* exhibits an extremely derived state: its basipterygoid processes diverge only at their distal extremes and the angle between them is very small (Curry Rogers and Forster 2004; Mannion 2011). *Europasaurus* exhibits another condition: the basipterygoid processes are divergent and separated from each other beneath the ventral border of the basal tubera and their bases are located just ventral to the medioventral end of each basal tuber (Marpmann *et al.* 2014: fig. 13).

The angle between the skull roof and the basal region of the basipterygoid processes is not known in *Tambatitanis* because its skull roof elements have not been found thus far. However, the long axis of the remaining right basipterygoid process intersects the plane of the occiput at about 20 degrees in lateral view, suggesting that the basipterygoid processes are ventrolaterally oriented in relation to the skull roof in *Tambatitanis*, rather than anterolaterally as in diplodocoids (Calvo and Salgado 1995; Wilson 2002) and some titanosaurs such as *Rapetosaurus* and *Saltasaurus* (Curry Rogers and Forster 2004).

The basal tubera are not strongly offset posterior to the posterior surface of the basipterygoid processes: the most posterior point of the ventral protuberance is located only 0.8 cm from the plane passing through the posterior surface of the basipterygoid processes. However, the basal tubera are clearly separated from the basipterygoid processes by a thin sulcus that extends along the anterior side of the crista tuberalis from the ventral margin of the fenestra metotica (see below) to the ventrolateral corner of the basal tuber and then extends dorsomedially to merge with the opening for the internal carotid artery (see below).

The space between the ventral margin of the basal tubera and the basipterygoid processes is extremely compressed anteroposteriorly. In this anteroposteriorly narrow space, there are two openings that lead to the pituitary fossa. The one located at the right side of the space is smaller (7 x 6 mm) than the one on the left side (15 x 6 mm). The two are separated from each other by a 2 mm thick wall, and the right foramen opens into the pituitary fossa dorsally. From the right margin of this opening, a groove extends ventrally, slightly posteriorly and rightward to the point between the base of the basipterygoid process and the ventrolateral end of the basal tubera.

At this point, this groove merges with a sulcus that extends dorsally to the ventral end of the fenestra metotica. The other larger opening on the space between the basal tubera and the basipterygoid process must have been formed by the coalescence of the originally separated central and left openings with the postmortem loss of the wall separating them. Weak constriction at the left margin of the opening indicates the former location of the wall, and from this constriction, a groove extends ventrally, slightly posteriorly and laterally, as the corresponding groove on the right side does. Judging from the extent of the damage of the bony surface, only a thin layer of the bone covering the bottom of the pituitary fossa and a thin wall separating the lateral foramen from the pituitary fossa were lost by the postmortem distortion, and therefore the central opening may have been very small or did not exist, whereas the size of the lateral two openings might have been approximately the same as preserved. Considering its location and connection to the pituitary fossa, the lateral two openings might have accommodated the cerebral branch of the internal carotid artery.

In most sauropods, including the basal titanosauriform *Phuwiangosaurus* from the Early Cretaceous Thailand (Suteethorn *et al.* 2009), the cerebral branch of the internal carotid artery enters the brain cavity via a foramen located on the dorsolateral surface of the base of the basipterygoid process and then reaches the ventral side of the pituitary fossa (*e.g., Spinophorosaurus* [Knoll *et al.* 2012: fig.3]; *Chebsaurus* [Läng and Mahammed 2010: p.148]; *Apatosaurus* [Balanoff *et al.* 2010: p.13]; *Phuwiangosaurus* [Suteethorn *et al.* 2009: fig. 9]; *Malawisaurus* [Gomani 2005: fig. 6]; *Jainosaurus* [Chatterjee and Rudra 1996: fig.11]; *Rapetosaurus* [Curry Rogers and Foster 2004: p.138]), as is usual in dinosauriforms generally (Nesbitt 2011). However, in *Tambatitanis*, the foramen is positioned on the ventromedial surface of the base of the basipterygoid process, as described above. A similar location of the entrance of the internal carotid artery is seen in several titanosaurs (Paulina Carabajal 2012: table 1) and possibly in *Mongolosaurus* (Mannion 2011). *Nemegtosaurus* and *Quaesitosaurus have* a single transversely elongate opening between the basipterygoid processes and Wilson (2005) interpreted it as an opening for the internal carotid artery, although this interpretation was not accepted by Paulina Carabajal (2012).

The anterior border of the basipterygoid process bifurcates dorsally into the ventral extension of the crista antotica (see below) and a thin ridge that runs dorsomedially to the preserved ventral edge of the cultriform process (=parasphenoid rostrum). Above the ventral edge of the cultriform process, the dorsal part of the pituitary fossa is exposed anteriorly by the loss of part of the cultriform process. The surface between the ventral extension of the crista antotica and the lateral margin of the exposed part of the pituitary fossa corresponds to the lateral surface of the parasphenoid. This surface is slightly concave and faces almost anteriorly in *Tambatitani*s, but in other sauropods, the corresponding surface faces anterolaterally. The peculiar orientation of this surface in *Tambatitanis* is obviously brought about by the strong anteroposterior shortening of this part of the braincase. On this surface, there is a pair of the small openings (VI in Fig. 4B). These openings appear to be connected with a pair of the foramina located on the posterior face of the dorsum sellae (see below), and canals connecting these openings appears to have accommodated cranial nerve VI. As there is no opening on the right wall of the exposed part of the pituitary fossa, the canal for cranial nerve VI does not communicate with the pituitary fossa on the right side whereas the left one communicates with pituitary fossa halfway along the canal via small oval opening that can be observed on the left side of the internal surface of the pituitary fossa. Therefore, the canal for cranial nerve VI passes basically lateral to the pituitary fossa, in contrast with the general condition in sauropods in which cranial nerve VI penetrates the pituitary fossa. This derived condition of the route of cranial nerve VI has been observed only in an unnamed titanosauriform from the Early Cretaceous of North America (TMM 40435, described by Tidwell and Carpenter 2003) and some titanosaurs (Paulina Carabajal 2012; Knoll *et al.* 2013).

About 15mm dorsal to the possible openings for cranial nerve VI, there are small notches on the anterior end of the preserved part of the endocranial cavity (III in Fig. 4B, E). These notches appear to represent the posterior border of the foramen for cranial nerve III. About 10 mm above it, there is a small opening on the right side of the skull, which can be identified as the foramen for cranial nerve IV (IV in Fig. 4B, E). A small notch on the broken anterior end of the left wall of the cranial cavity represents the posterior wall of the foramen for cranial nerve IV.

Dorsal to the probable foramen for cranial nerve IV, there is a small incision on the broken surface that might correspond to the fused suture between the orbitosphenoid and laterosphenoid (ocf in Fig. 4B, E). This incision appears to be the posterior half of an aperture for a vein, possibly the orbitocerebral vein (Witmer *et al.* 2008), because a shallow groove that extends from this incision dorsoposteriorly on the endocranial surface of the laterosphenoid appears to correspond to a venous sinus. If this identification is correct, the opening for cranial nerve IV is located more closely to the orbitocerebral foramen than to the foramen for cranial nerve III.

The laterosphenoid and orbitosphenoid are firmly co-ossified so that the suture between them is completely obliterated. On the other hand, the interdigitated suture between the prootic and laterosphenoid is clearly visible on the medial wall of the adductor chamber (spl in Fig. 4E, F). This suture runs vertically from the dorsal margin of the trigeminal foramen (V in Fig. 4E) to the point just posterior to the round incision on the posterior half of the dorsal surface of the laterosphenoid (see below). On the lateral wall of the endocranial cavity, the suture between the prootic and laterosphenoid is represented by a distinct sharp sulcus running vertically from the dorsal rim of the foramen for cranial nerve V to the anterior end of the lateral recess, which is located at the posterodorsal corner of the remaining part of the endocranial cavity (see below). The wall of endocranial cavity anterior to this sulcus is slightly elevated to form a vertical pillar (Fig. 4H). A similar pillar has been described in braincases of two indeterminate titanosaurs (MCF-PVPH-765 and MGPIFD-GR 118), *Bonatitan*, *Saltasaurus* (Paulina Carabajal *et al.* 2008) and *Jainosaurus* (Wilson *et al.* 2009). The dorsal surface of the laterosphenoid is trapezoidal in dorsal view (Fig. 4F). Its anterior half is a rugose triangular surface which represents the interdigitated suture between the laterosphenoid and frontal (Fig. 4F). On the lateral part of the posterior half of the dorsal surface of the laterosphenoid, there is a transversely oriented short groove (gr in Fig. 4F). Its posterior border is located just anterior to the suture between laterosphenoid and prootic (spl in Fig. 4 E, F, see above). This short groove might be the ventral half of an opening, but it does not extend medially, as it is blocked by an irregular rugose surface, which occupies the medial part of the posterior half of the dorsal surface of the laterosphenoid and may represent the suture between the laterosphenoid and the frontal or parietal. Therefore, the foramen represented by this short groove is blind, at least on the laterosphenoid. Nevertheless, there is a possibility that this foramen continued dorsomedially into the now missing frontal or parietal, and then opened into the endocranial cavity. If this is the case, it can be compared with a canal for the middle cerebral vein reported in *Bonatitan* (Paulina Carabajal 2012), *Apatosaurus* (Balanoff *et al.* 2010) and *Giraffatitan* (Knoll and Schwarz-Wings 2009).

The crista antotica extends ventrally from the lateral vertex of the triangular anterior half of the dorsal surface of the laterosphenoid (ca in Fig. 4F) to the anterior edge of the basipterygoid process. The capitate process and the most dorsolateral part of the crista antotica are missing. The dorsal third of the preserved portion of the crista antotica is anteroposteriorly thin, wing like and flares strongly dorsolaterally (ca in Fig. 4B). Approximately a third of the way down from its dorsal end, the crista antotica is interrupted by the trigeminal foramen (V in Fig. 4E). The trigeminal foramen is well preserved on the right side of the braincase. It is dorsoventrally oblong (ca. 1.5 x 0.8 cm) and cuts across the crista antotica. In lateral view, the foramen is divided into posteroventral and anterodorsal parts by a constriction at the intersection of the crista antotica and the exit of the trigeminal foramen, although its medial opening is not constricted on the wall of the endocranial cavity. The posteroventral part is two times larger than the anterodorsal parts, and may have accommodated the maxillomandibular nerve whereas the latter may have accommodated the ophthalmic nerve. *Shunosaurus* (Chatterjee and Zheng 2002) and at least one individual of *Camarasaurus* (Chatterjee and Zheng 2005) have a separate exit for the ophthalmic nerve.

A shallow groove, possibly for the mandibular nerve, extends ventrally from the ventral rim of the opening for cranial nerve V. This shallow groove is bounded posteriorly and anteriorly by the crista prootica (see above) and the ventral continuation of the crista antotica respectively. The ventral continuation of the crista antotica is sharp, thin and runs from the construction of the trigeminal foramen to the anterior edge of the basipterygoid process (Fig. 4B, E).

The crista antotica of some titanosaurs has been described as a structure that terminates at the dorsal rim of trigeminal foramen by some authors (*e.g.,* Díez Díaz *et al.* 2011; Paulina Carabajal *et al.* 2008). However, at least in some titanosaurs, the ventral continuation of the crista antotica runs ventroposteriorly from the ventral margin of the trigeminal foramen and merges with the crista prootica at different levels: these cristae sometimes merge at the level of the basal tubera (*e.g., Jainosaurus* [Wilson *et al.* 2009: fig.4]) or at the level of the ventral border of the occipital condyle (*e.g., Narambuenatitan* [Filippi *et al.* 2011: fig.3]; an indeterminate titanosaur, MML-194 [García *et al.* 2008: fig.1]) . On the other hand, the crista antotica does not merge with the crista prootica, but contacts a protuberance or rugose surface that is located at the ventral end of the crista prootica, in some non-titanosaur macronarians (*e.g., Camarasaurus* [White 1958: pl.70; GMNH-PV 101: HS pers. obs.]; *Europasaurus* [Marpman *et al.* 2014: fig.13]) and diplodocoids (*e.g., Diplodocus* [Berman and McIntosh 1978: fig.4]; *Apatosaurus* [Berman and McIntosh 1978: fig.11]). The loss of the protuberance or rugose surface from the ventral end of the crista prootica appears to be a derived feature shared between *Tambatitanis* and titanosaurs. However, the former differs from the latter in that the crista antotica does not merge with the main part of the crista prootica, but with a faint ridge that branches from the latter (see below). This feature could be an additional autapomorphy of *Tambatitanis*.

A faint elevation runs dorsoventrally on the center of the posterior wall of the right adductor chamber (speo in Fig. 4B, E). This elevation appears to correspond to the suture between the exoccipital-opisthotic complex and the prootic, because a faint zigzag line that is visible on this elevation appears to be the remnant of an interdigitating suture. The portion of the occiput medial to this elevation is anteroposteriorly thicker than the part lateral to it. This probable suture between the exoccipital-opisthotic complex and the prootic terminates at a point about 3 cm below the dorsal margin of the occiput. Just ventromedial to this terminal point of the probable suture between the exoccipital-opisthotic complex and the prootic, the crista prootica arises as a blunt elevation on the anterior face of the prootic. It becomes rapidly thin and sharp anteroposteriorly as it extends ventrally. The crista prootica is weaker than the crista antotica and lacks a rugose surface, which is seen in *Camarasaurus* [Madsen *et al.* 1995]), or a tab-like (leaf-like) process, which is well developed in dicraeosaurids (Salgado and Calvo 1992; Upchurch 1998; Wilson 2002; Upchurch *et al.* 2004a; Harris and Dodson 2004).

At the point about 4 cm below its origin, the crista prootica bifurcates into two ridges: one is a strong ridge that forms the posterolateral margin of the basipterygoid process, and the other is a faint ridge which runs anteroposteriorly on the lateral face of the basipterygoid process and merges with the ventral extension of the crista antotica at the distal end of the preserved part of the basipterygoid process. At the junction between the two ridges there is a minute foramen. As noted above, this arrangement of cristae antotica and prootica could be an autapomorphy of *Tambatitanis.*

The region between the crista prootica and crista tuberalis is depressed and subdivided into anterior and posterior sub-regions. The former sub-region is a dorsoventrally elongate and anteroposteriorly narrow shelf adjacent to the posterior side of the crista prootica and accommodates a foramen possibly for cranial nerve VII. The latter sub-region is a dorsoventrally elongated sub-triangular fossa, and accommodates the fenestra ovalis and fenestra metotica. The fenestra ovalis is an elliptical opening (right: 0.95 x 0.51 cm; left: 1.05 x 0.42 cm) bounded anteriorly by the posterior margin of the shelf shaped sub-region mentioned above. The fenestra metotica is an anteroposteriorly narrow (right: 0.36 cm; left: 0.46 cm) and ventrodorsally elongated (right: 1.26 cm; left: 1.57 cm) slit bounded posteriorly by the crista tuberalis. On the right side of the braincase, the fenestra metotica is separated from the fenestra ovalis by a thin but unbroken crista interfenestralis. On the left side of the braincase, however, the fenestra metotica communicates with the fenestra ovalis via a break on the crista interfenestralis. This break is not an artifact of postmortem distortion but an original feature because its surface is smooth without any trace of deformation.

On both sides of the basicranium, foramina possibly for cranial nerve XII are located about 3 mm dorsal to the point where the crista tuberalis changes its orientation from mediolateral to dorsoventral. At this point, an additional opening for cranial nerve XII is located on the crista tuberalis of the left side. Thus, the exit of the cranial nerve XII is bifurcated on the left side whereas it is single on the right side. Internally within the cranial cavity, the foramen for cranial nerve XII is a single opening on both sides. Basal sauropods and diplodocoids have one or two external openings for cranial nerve XII, whereas most titanosaurs have a single external opening for the nerve (Paulina Carabajal 2012).

The endocranial cavity can be observed through the anterodorsal breakage of the braincase. A small but distinct foramen (ba in Fig. 4G) pierces the basal part of the dorsum sellae (ds in Fig. 4G, H) in between and slightly above the twin of openings for the abducens nerves (VI in Fig. 4G). The dorsal rim of this transversely elongated opening is continuous with the faint depression on the anterior face of the dorsum sellae. On the other hand, the ventral margin of the opening is continuous with the shallow and very short depression running posteriorly on the median floor of the brain cavity. This opening can be compared with a foramen identified as the canal for the basilar artery described on the basicranium of *Giraffatitan* (Janensch 1935-36; Knoll and Schwarz-Wings 2009). A similar opening is also reported on the braincases of *Apatosaurus* (Balanoff *et al.* 2010), *Plateosaurus* (Balanoff *et al.* 2010) and *Chebsaurus* (Läng and Mahammed 2010: p.148), but in these cases, presumed soft tissue passing through the opening was not assumed.

The endocranial opening of the fenestra metotica is situated halfway between the dorsum sellae and foramen magnum (IX-XI in Fig. 4G). Just anterodorsal to this fissure, there is a bulge which may house the semicircular canals. On this bulge, there is a small short slit which may represent the endolymphatic openings. The exits for the facial and acoustic nerves (VII and VIII in Fig. 4H) lie next to each other in a small shallow depression that is located between the large opening for trigeminal nerve and the eminence which may accommodate the semicircular canals. This depression is the internal acoustic pore (*Porus acusticus internus*). A similar anatomical configuration

has been described in *Giraffatitan* (Knoll and Schwarz-Wings 2009) and figured for *Camarasaurus* by Osborn and Mook (1921: pls.63 and 64).

A shallow groove runs dorsally from the opening for the trigeminal nerve to a recess that is located just posterior to the suture between the laterosphenoid and prootic on the dorsal part of the wall of the endocranial cavity (re in Fig. 4F). As described above, this recess may have communicated with the dorsal ends of the occiput and the adductor chamber via small two canals. Therefore, the groove extending from this recess may have accommodated the middle cerebral vein.

A very shallow small circular depression (pa in Fig. 4H) is present on the posterior margin of the groove. This depression is situated, above the internal acoustic pore, posterodorsal to the openings for the trigeminal nerve and anterior to the eminence that may have accommodated the semicircular canals. The diameter of this circular depression is about 5 mm and its bottom is pierced by small foramina. This depression is closely similar to a circular area pierced by small foramina that is found on the medial surface of the prootic of an indeterminate and incomplete braincase (MCF-PVPH-756) from the lower Cretaceous of Argentina (Paulina Carabajal *et al.* 2008; Paulina Carabajal 2012). At this point, this peculiar structure is exclusive to *Tambatitanis* and MCF-PVPH-756, but its absence in other sauropods is possibly due to incomplete preparation, poor preservation or insufficient resolution of CT scans.

In sauropods, the floccular recess (=Fossa auriculae cerebelli) is absent (*e.g., Shunosaurus* [Chatterjee and Zheng 2002]; *Apatosaurus* [Balanoff *et al.* 2010]; *Spinophorosaurus* [Knoll *et al.* 2012]), or present as a very small depression located in the area where the pierced circular shallow depression is present in MCF-PVPH-756 and *Tambatitanis* (*e.g., Giraffatitan* [Janensch 1935-36; Knoll and Schwarz-Wings 2009]; an indeterminate North American titanosauriform [Tidwell and Carpenter 2003], *Nigersaurus* [Sereno *et al.* 2007]; *Cetiosaurus*? [Galton and Knoll 2006]).

Dentary. The posterior half of the right dentary is preserved (Fig. 5; Table 2). In dorsal view, it is almost straight mesiodistally without marked curvature. The distal seven tooth sockets are preserved but their medial walls, including nutrient foramina, and the dorsal margin of the lateral walls are missing. There are no teeth inside the completely exposed tooth sockets. The teeth, including unworn ones, were found scattered around the other skeletal elements of MNHAH D-1029280. The tooth sockets are nearly equal in size, suggesting that there was no large size difference between the most mesial and distal teeth. The dorsal margin of the dentary posterior to the last tooth socket is preserved but the distal tip of the posterodorsal processes is missing. The distal tip of the posteroventral process is also missing, but judging from the preserved part the posteroventral process is two times longer anteroposteriorly than the posterodorsal processes, and lacks the small accessory process seen in *Abydosaurus* and *Giraffatitan* (Chure *et al.* 2010). The missing anterior half of the dentary may have been gently curved mesially, not square shaped in dorsal view as in some titanosaurs (*e.g.*, *Antarctosaurus* [von Huene 1929], *Bonitasaura* [Gallina and Apesteguía 2011]) and diplodocoids, (*e.g., Nigersaurus* [Sereno *et al.* 2007]), judging from the preserved posterior portion of the dentary, which does not show marked curvature.

TABLE 2. Size measurements of (in mm) dentary of *Tambatitanis amicitiae* **gen. et sp. nov.**, holotype (MNHAH D-1029280).

mesial end of the preserved portion of the dentary to distal end of the distal dorsal process	145
mesial end of the preserved portion of the dentary to distal end of the distal ventral process	182
mesial end of the preserved portion of the dentary to distal end of the final alveolus	56
distal end of the final alveolus to distal end of the distal dorsal process	90
distal end of the distal dorsal process to the ventral margin of the dentary, measured perpendicular to the latter	59
maximum mediolateral width of the dentary measured at the mesial portion of the preserved part below the penultimate alveolus	15

Teeth. The teeth are peg like, straight along the long axis, with an average slenderness index of greater than 3. Marginal tooth denticles are absent on both anterior and posterior edges. The teeth of the MNHAH D-1029280 have been described by Saegusa *et al.* (2008) and Saegusa and Tomida (2011). They did not exclude the possibility that extreme size difference is present among the teeth of the same tooth row. With the finding of the nearly same sized tooth sockets on the dentary, however, this possibility is now refuted and worn small-sized sauropod teeth found together with the holotype skeleton of *Tambatitanis* are those of smaller, presumably younger individuals of *Tambatitanis* or a closely related species.

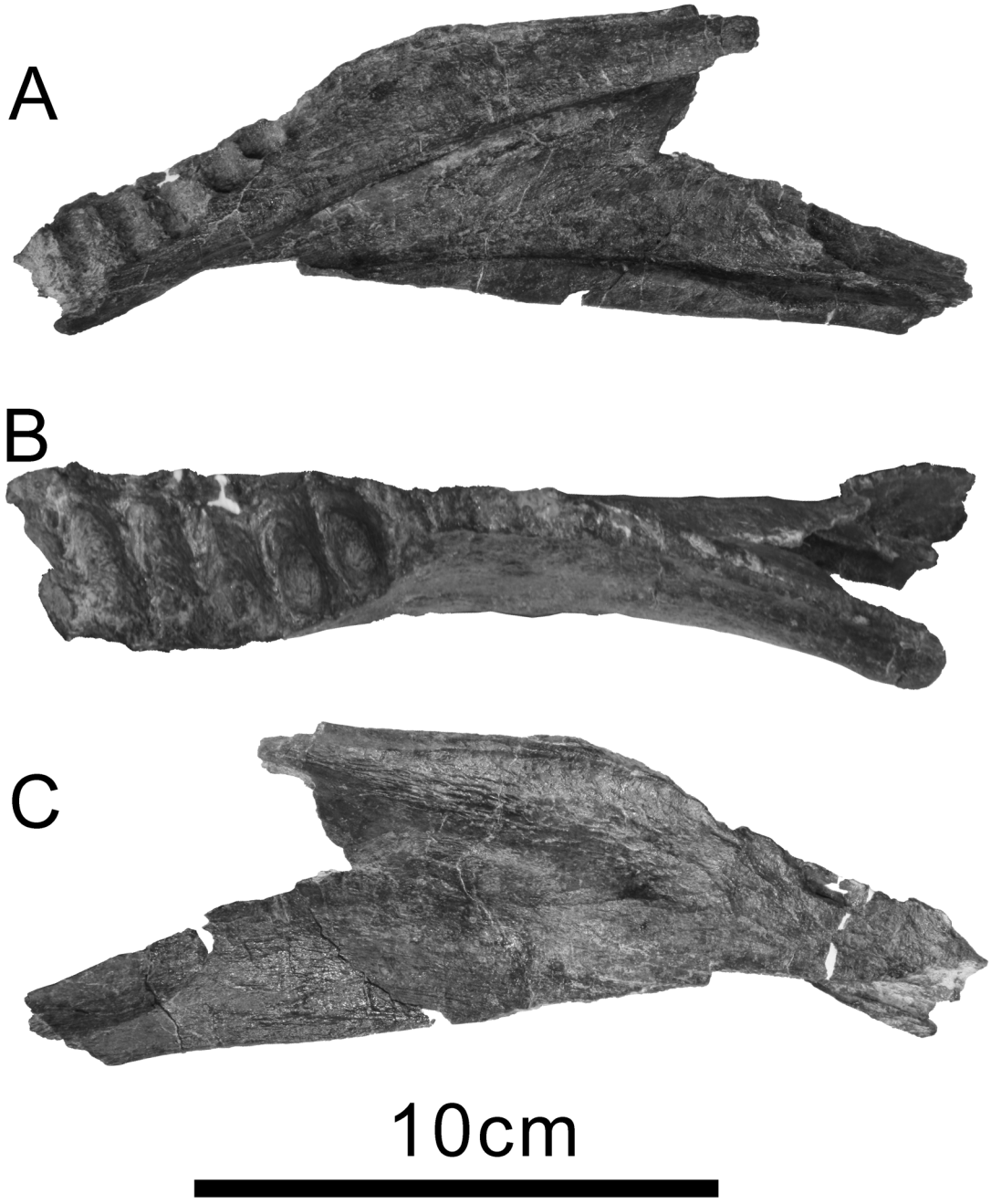

FIGURE 5. *Tambatitanis amicitiae* **gen. et sp. nov.**, holotype (MNHAH D-1029280). Fragment of right dentary. **A,** medial view, dorsal is to the top, and posterior is to the right of the page. **B,** dorsomedial view, lateral is to the top, and posterior is to the right of the page. **C,** lateral view, dorsal is to the top, and posterior is to the left of the page.

Atlas. The atlantal intercentrum is complete and crescentic in shape, with a dorsal excavation, and subrectangular in anterior and lateral views, respectively (Fig. 6A). The occipital facet of the intercentrum is concave for articulation with the occipital condyle and is higher than wide (Table 3). Its anterior margin is almost rectilinear in lateral view, although the anteroventral part of the facet projects slightly beyond the anterodorsal part of it. An anteroventral projection on the atlantal intercentrum has been noted as a synapomorphy uniting Diplodocidae + Dicraeosauridae (Wilson 2002; Upchurch *et al.* 2004a). A much weaker anteroventral projection of the atlas has been also described in *Mongolosaurus* (Mannion 2011) and *Rapetosaurus* (Curry Rogers 2009) and figured for *Erketu* (Ksepka and Norell 2006). An anteroventral projection on the atlantal intercentrum is almost absent in *Tambatitanis*. Just posterior to the anteroventral projection, a transversely elliptical depression is present centrally on the ventral surface of the intercentrum. Posterolateral to this depression, two small processes project

ventrolaterally. Comparable ventrolateral processes have been described or figured in *Apatosaurus*, *Diplodocus*, *Erketu* and *Suuwassea* (Marsh 1896; Hatcher 1901; Holland 1905; Gilmore 1936; Ksepka and Norell 2006; Harris 2006). These processes have been interpreted as articular facts for a single-headed cervical rib (Marsh 1896; Hatcher 1901; Holland 1905; Gilmore 1936). A distinct facet for a single-headed rib is present at the comparable location of the atlas as a pit or rugosity in *Camarasaurus* (Madsen *et al.* 1995; McIntosh *et al.* 1996a, Ikejiri *et al.* 2005), and a presumable atlantal rib is closely associated with an atlas in GMNH-PV 101 (McIntosh *et al.* 1996a). Gilmore (1933) and Mannion (2011) figured a similar flat surface on the posteroventral corner of the intercentrum of *Mongolosaurus* and the former author interpreted it as an articular facet for a cervical rib. Harris (2006), however, questioned the presence of atlantal ribs in sauropods, on the basis of the observation that in the holotype of *Suuwassea* (ANS21122) the ventrolateral processes of the atlas would articulate with the facet on the cranial side of the axial costolateral eminence. A rib facet is not present on an atlas of *Graffatitan* (Janensch 1950), but its absence could be due to its immature stage of development.

TABLE 3. Size measurements of (in mm) atlas of *Tambatitanis amicitiae* **gen. et sp. nov.**, holotype (MNHAH D-1029280).

Transverse width of anterior surface of intercentrum	56
Transverse width of posterior surface of intercentrum	58
Maximum anteroposterior length of intercentrum	32
Maximum dorsoventral height of anterior surface of intercentrum	53
Maximum dorsoventral height of posterior surface of intercentrum	50

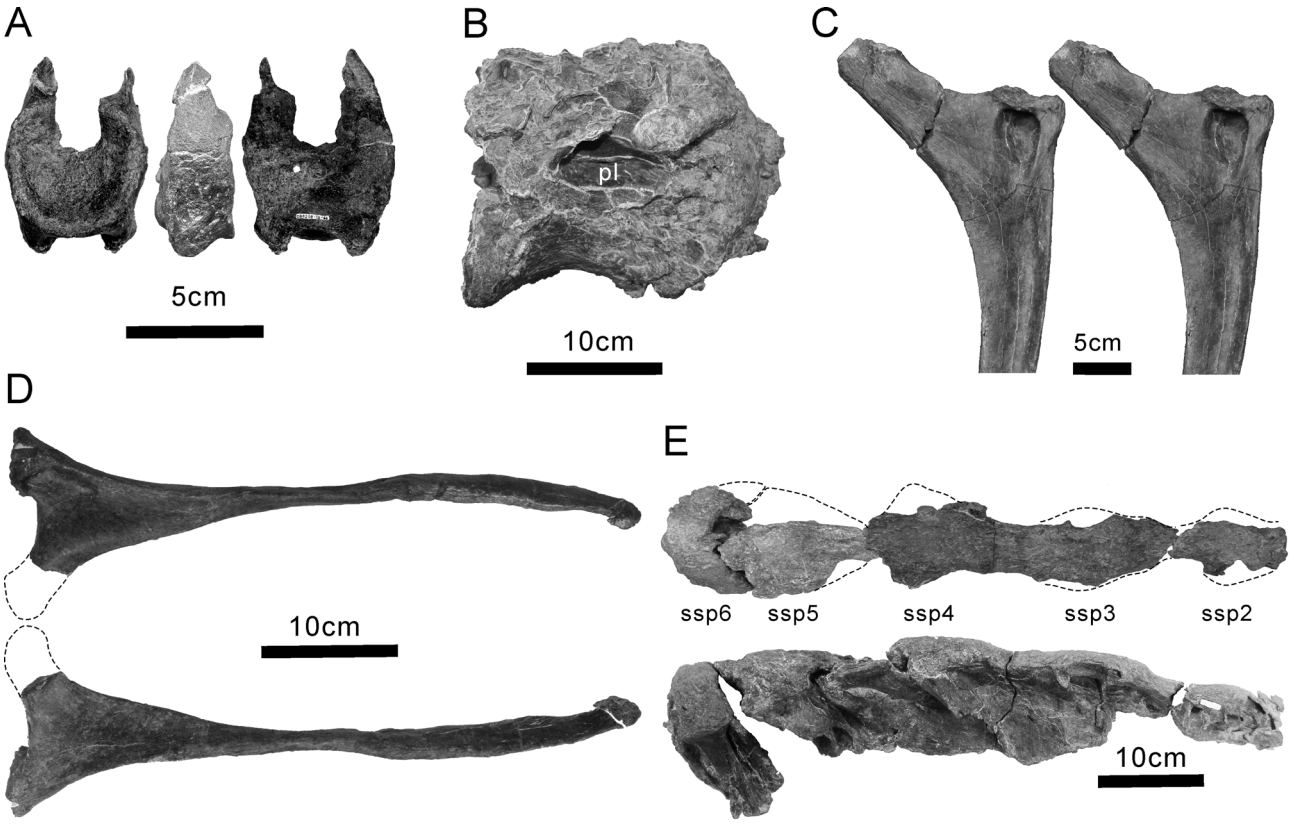

FIGURE 6. *Tambatitanis amicitiae* **gen. et sp. nov.**, holotype (MNHAH D-1029280). **A,** atlas in anterior, lateral, and posterior views. **B,** centrum of a dorsal vertebra in right lateral view. **C,** stereophotograph of proximal part of middle dorsal rib in posterior view. **D,** first sacral rib in posterior (top) and anterior (bottom) views. **E,** neural spine summits of the sacral vertebrae in dorsal (top) and right lateral (bottom) views. Dashed lines show areas of missing parts. See text for abbreviations.

The posterior surface of the intercentrum is flat as a whole, but a roughened and pendant small tubercle is present on the mid-dorsal part of the surface. The dorsal excavation of the surface in posterior view is considerably weaker than those of other known atlases of sauropods. The neuroapophyses are preserved only at their pedicels. Judging from the small size of the preserved part of the pedicel, the rest of the neuroapophyses may have been less developed than those of other known atlases of titanosauriforms. The neuroapophysis and the intercentrum are firmly fused.

Dorsal Vertebrae. The centra of two dorsal vertebrae are preserved (Fig. 6B). They have pneumatic foramina (pleurocoels), and their broken surfaces reveal camellae (the range of the diameter of the chambers=0.3 to 4 cm; the average of the diameter of the chambers=1.5 cm; the range of the thickness of the walls=0.5 to 3 mm; of the thickness of the walls =1.5 mm). Numerous irregular thin bone fragments found together with the skeletal elements of the sauropod may have been derived from breakage of the camellate presacral vertebra.

Presacral Ribs. At present, fragments of cervical ribs, 12 nearly complete dorsal ribs and one possible first sacral rib have been identified from the excavated specimens. Along with the prepared ribs, several additional dorsal ribs appear to be present in the unprepared excavated materials, and thus a complete series of dorsal ribs could possibly be reconstructed when preparation is completed. Pending the comprehensive description of the rib series in future work, we briefly mention some interesting features of the dorsal and first sacral ribs.

The shaft of the anterior dorsal rib is plank-like, as has been widely recognized in Titanosauriforms. All of the preserved proximal ends are deeply excavated (Fig. 6C). A similarly deep excavation is also seen on the posterior aspect of the proximal rib in *Giraffatitan brancai* and *Brachiosaurus altithorax*, though additional foramina are present on the anterior face of the tubercle and anterior surface of the proximal part of the rib shaft in the former and the latter, respectively (Janensch 1950: p.87; Taylor 2009). The proximal pneumatic openings do not lead distally into a pneumatic cavity that occupies the much of the shaft of the rib. A proximal extension of the pneumatic fossa into the internal cavity developed in the capitulum is reported in some Titanosauriformes (*e.g., Venenosaurus* [Tidwell *et al.* 2001]), but the dorsal rib of *Tambatitanis* lacks such an internal cavity in the capitulum.

Sacral Ribs. A pair of ribs that is shortest among the ribs recovered so far appears to represent the right and left first sacral ribs, judging from their shortness, the peculiar morphology of their proximal ends and their close association to the anterior margin of ilium in the quarry (Fig. 6D). They are not fused to the ilium but one of them was found closely appressed to the anterior margin of preacetabular process of the right ilium (Fig.2). These short ribs are similar to the first sacral ribs described in some titanosaurs (*e.g*., *Opisthocoelicaudia* [Borsuk−Białynicka 1977]; *Trigonosaurus* [Campos and Kellner 1999; Campos *et al.* 2005]), in their short length and the shape of the tubercle and head. A rib of *Brontomerus mcintoshi* described as first right dorsal rib (Taylor *et al.* 2011) is very similar to the first sacral ribs of MNHAH D-1029280 and is here interpreted as a first sacral rib.

The most notable feature of these possible first sacral ribs is an opening on the proximal surface of the tubercle. In the longer ribs of *Tambatitanis*, the proximal surface of the tubercle is rugose and there is neither an opening nor a depression, although the anterior surface of the tubercle is deeply excavated by a fossa as described above. On the other hand, the proximal surface of the tubercle of these presumable first sacral ribs is strongly rugose and pierced by a large opening leading to the deep fossa excavating the posterior surface of the tubercle. This may suggest this opening is connected to a foramen on the diapophysis of a vertebra, and that an air-filled diverticulum passed through the tubercle of the rib on its way to the vertebra in life. The rest of the right sacral ribs are firmly fused to the ridges on the medial surface of the right ilium (see below).

Sacrum. Only the distal ends of the neural spines of five sacral vertebrae have been identified among the prepared specimens at this point (Fig. 6E). However, the vertebral count of the sacrum can be estimated from these sacral neural spines and the probable first sacral rib. The neural spines of four sacral vertebrae are firmly fused to each other. The fused spines appear to correspond to the primary sacrals I-III and the dorsosacral of *Camarasaurus* described in Osborn and Mook (1921). Posterior to these fused spines, a fragment of a sacral spine was found isolated in the quarry (Fig. 2). This fragment is very similar to those of the first and second caudal spines but differs in the stronger development of the PRSL, which protrudes anteriorly beyond the SPRL, and appears to have been connected to the strong POSL on the posterior surface of the spine corresponding to the primary sacral III of Osborn and Mook (1921) in life. Besides these fragments of the sacral neural spines, no further remains of the sacrum have yet been identified. However, on the anterodorsal surface of the sacral spine of the dorsosacral there is a marked sutural surface, indicating that one more spine of the sacrum was firmly attached to the anterior surface of

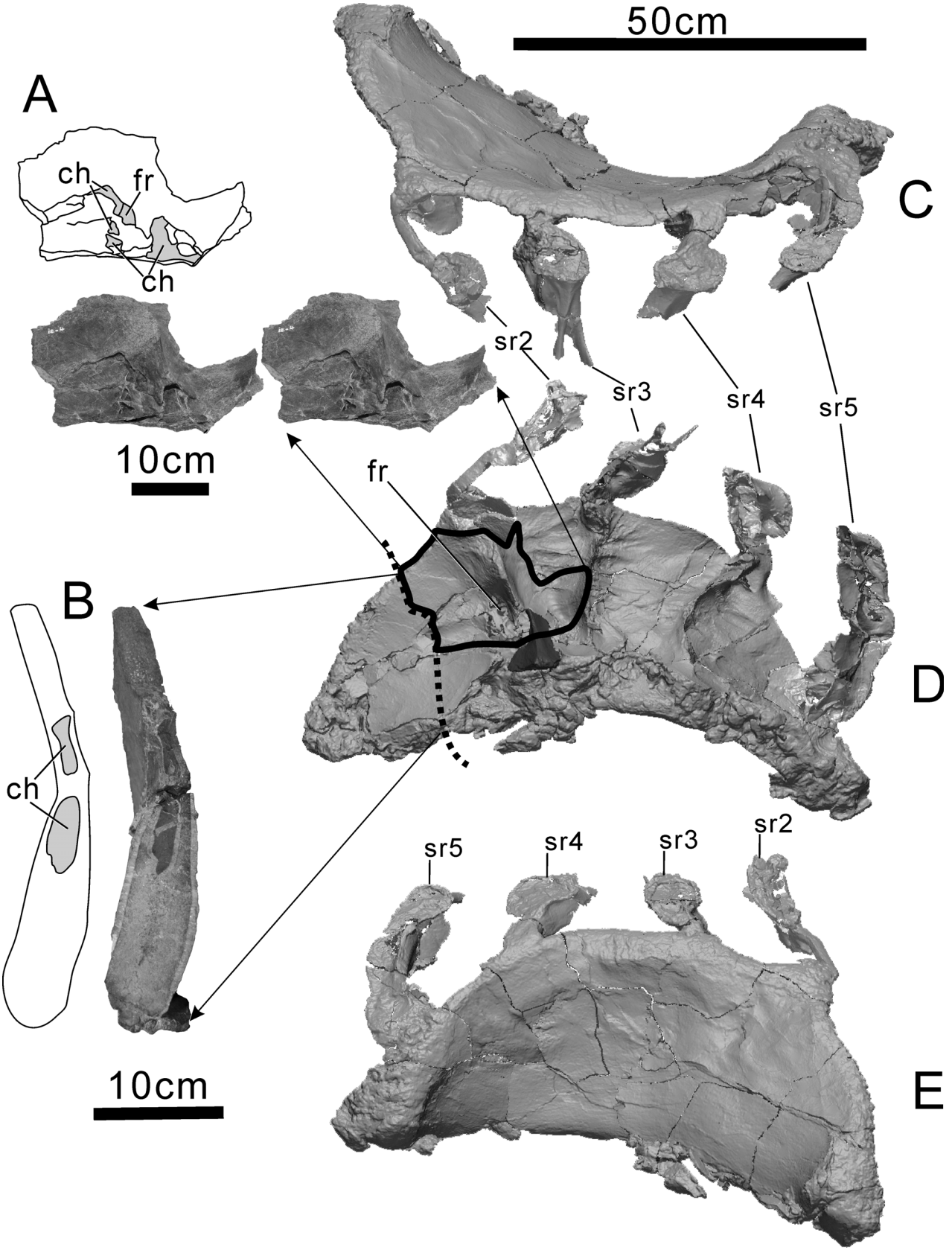

FIGURE 7. *Tambatitanis amicitiae* **gen. et sp. nov.**, holotype (MNHAH D-1029280). Ilium and sacral ribs. **A,** stereopair (bottom) of a fragment of ilium and its interpretative line drawing (top). **B,** fracture cross section of a fragment of ilium (right) and its interpretative line drawing (left). **C– E,** a virtual reconstruction of right ilium based on the 3D images of the 19 broken pieces of the ilium. **C,** dorsal view. **D,** medial view, showing the position of the fragments shown in **A** and **B**. **E,** lateral view. See text for abbreviations.

the fused sacral spines in life. In sum, the fragments of sacral spines identified so far suggest the presence of six sacral vertebrae. The presumable first sacral rib, which was found closely appressed to the anterior margin of the preacetabular process of the ilium, also supports the view that *Tambatitanis* had six sacral vertebrae.

Ilium. The right ilium is preserved (Fig. 7). Its dorsal border and medial and lateral surfaces are well preserved, but its ventral border is heavily damaged. The anterior tip of the preacetabular process is swollen as usual in sauropods, but deflected somewhat medially by postmortem distortion. The medial surface of the ilium exhibits a complicated morphology composed of the ridge of the medial surface of the ilium and four sacral ribs fused to it (Fig. 7C–E). During preparation, the ilium was separated into 19 parts along the fissures formed by preservational distortion in order to facilitate the preparation of this complicated and fragile bone. Internal pneumatic chambers are visible on the separated surfaces of the parts of ilium (ch in Fig. 7A–B). Pneumatic foramina connected to these internal chambers are present on the ridges that are fused with the sacral ribs (fr in Fig. 7A) (Saegusa *et al.* 2010). Although camellate internal architecture was described in the ilium of *Euhelopus* (Wiman 1929; Wilson and Upchurch 2009), *Epachthosaurus* (Martínez *et al.* 2004), *Lirainosaurus* (Sanz *et al.* 1999) and *Sonidosaurus* (Xu *et al.* 2006), and a single chamber was reported in the ilium of *Amazonsaurus* (Carvalho *et al.* 2003), the pneumatic foramen which led to the iliac chambers has only ever been previously described in the ilium of *Saltasaurus* (Cerda *et al.* 2012).

Caudal Vertebrae. Preservation. Twenty two caudal vertebrae have been collected from the Kamitaki Quarry (Fig. 8). These caudal vertebrae can be split into two groups according to the proportions of the centrum and by the presence or absence of the transverse process. The first group is composed of eleven caudal vertebrae which have transverse processes and the centra of which are higher dorsoventrally than they are anteroposteriorly long. Ten out of these eleven caudal vertebrae were found semi articulated and closely associated with the sacral and pelvic elements in the bed, while the eleventh was found about 5m apart from the others (Fig.2). However, the close similarity between the most posterior one of the articulated series and the isolated specimen suggests that they represent the first eleven caudal vertebrae in sequence. For ease of description, they will be referred to as Cd1–Cd11 according to their anatomical position in the body.

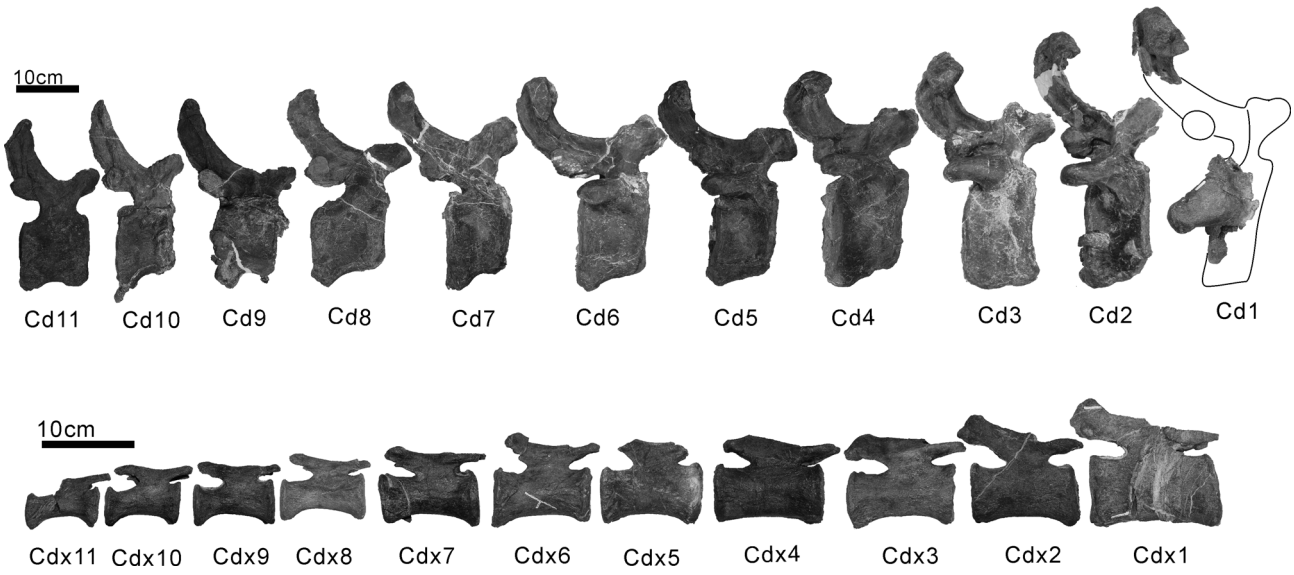

FIGURE 8. *Tambatitanis amicitiae* **gen. et sp. nov.**, holotype (MNHAH D-1029280). **A,** Cd2–Cd11 in right lateral view. **B,** Cdx1–Cdx2 in right lateral view.

The caudal vertebrae belonging to the second group lack transverse processes and their centra are anteroposteriorly longer than they are dorsoventrally high. They were found disarticulated and mingled with other skeletal elements of the same individual. There is a large gap between the first and second groups of the caudal vertebrae because the Kamitaki Quarry has not yielded any centra that show intermediate proportions between the two groups of caudal vertebrae. There are gaps also among the caudal vertebrae of the second group in terms of size and shape (Fig. 8). Thus the assignments of their position are necessarily approximate, although the relative order among them can be determined based on the size of the centrum. For ease of description, they will be called

Cdx1–Cdx11 according to their approximate anatomical order in life. In this numbering system, Cdxn is more anteriorly located than Cdxn+1, but none of these specimens ere necessarily consecutive in life.

Cd1–Cd11. The centra of caudal vertebrae lack pneumatic fossae (pleurocoelous fossae) and are internally solid without large internal cells. On the right side of the centrum of Cd2, there is an anteroposteriorly elongated, small oval depression (ca. 2cm long, ca. 1cm wide) 6 cm below the transverse process. This depression is only present on Cd2, and only on one side of the bone. (dp in Fig. 10A).

From Cd1 to Cd11, the centra become proportionally longer anteroposteriorly, although their length never exceeds their height(Fig. 8, Table 4). The centrum of Cd1 is represented only by the left side of the posterior end. Its articular surface is poorly preserved but its flatness suggests that Cd 1 was neither procoelous nor opisthocoelous (Fig. 9D and I). In Cd3–Cd10, as preserved, the anterior articular surfaces of the centra are nearly flat, whereas the posterior articular surfaces of the centra are relatively strongly concave (Figs. 11–18). On the other hand, the articular surfaces of the centra show a weak concavity in Cd2 and Cd11 (Figs. 10, 19). Judging from the extent of the postmortem lateral compression mentioned above, the concavity of the posterior articular facets of the centra is exaggerated by postmortem distortion in Cd3–Cd10 (Figs. 11–18), whereas in Cd2 and Cd11 they preserve the original concavity (Figs. 10, 19). The posterior articular surface is most strongly concave than anterior one also in Cd11, which is almost free from the postmortem lateral compression. Therefore, the stronger concavity of the posterior articular surface compared to the anterior surface in Cd3–Cd10 is not entirely due to the postmortem distortion, but is an original feature of the bone. The caudal vertebrae of most of basal titanosauriforms are mildly amphicoelous to amphiplatyan, with the exception of some East Asian titanosauriforms that exhibit procoelous anterior caudal vertebrae (*e.g., Daxiatitan* [You *et al.* 2008], *Dongbeititan* [Wang *et al.* 2007]). In *Borealosaurus* (You *et al.* 2004) and *Fukuititan* (Azuma and Shibata 2010), some mid-distal caudal vertebrae are opisthocoelous. *Gobititan* (You *et al.* 2003) and an Australian taxon, *Wintonotitan* (Hocknull *et al.* 2009), have incipient biconvexity of the posterior caudal vertebrae. In several other Cretaceous East Asian titanosauriforms, including *Huabeisaurus, Tangvayosaurus* and *Phuwiangosaurus,* the concavity of posterior articular surfaces of the caudal centrum is deeper than that of the anterior articular surfaces (D'Emic *et al.* 2013), as in *Tambatitanis*.

The centra of Cd4 to Cd10 are rhombus-shaped in lateral view, with the articular surfaces weakly angled anterodorsal when the ventral border of the centrum is held horizontally (Fig. 8). The orientation of the caudal vertebrae in the bed, and the mode of the deformation of the other bones found close to the caudal vertebrae, suggests that the rhombus-shape of these centra is original rather than a product of postmortem distortion. A rhombic outline of the centrum in lateral view has been reported in some basal titanosauriforms (*e.g.*, *Paluxysaurus* [=*Sauroposeidon*, according to D'Emic 2013] [Rose 2007]; *Cedarosaurus* [Tidwell *et al.* 1999]).

In Cd2 and Cd3, the ventral surface is poorly preserved (Figs. 10, 11), but weak elevations, which can be considered as remnants of the articular facets, are preserved on the anteroventral and posteroventral corner of the right side of the centra. The elevations on the anteroventral corner of the centra face lateroventrally, as the anterior chevron facets of Cd4 to Cd11 do (see below). However, those on the posteroventral corner of the centra lack distinct posteroventrally facing surfaces, which can be seen from Cd4 onwards. In Cd 4 and 5, the anterior one third of the left side of the ventral surface is missing, and the bony surface of the remaining ventral surface is roughened by postmortem distortion except for the lateral margin of the right anterior chevron facet in Cd5 (afc in Fig. 13). However, their overall configuration indicates the structure of the chevron facet is basically the same as that of Cd6 to Cd11 mentioned below. The swellings on the right anteroventral corners of the centra, which correspond to the anterior articular facets for the chevrons (hereafter referred to as anterior chevron facets), face lateroventrally and are flat, whereas those on the right posteroventral corners of the centra, which correspond to articular facets for the chevrons (hereafter referred to as posterior chevron facets), protrude ventrally and face posteroventrally (afc and pfc in Figs. 12, 13).

In Cd6 to Cd11, there are well defined posterior chevron facets at the posterior end of the ventral face of the centrum. These facets are slightly concave (From Cd6 to 8) or flat (From Cd9 to 11) and steeply inclined posteroventrally so that they meet the posterior articular surface of the centrum at an angle of about 20 degrees (pfc in Figs. 14–19). This facet is fairly well preserved on both sides of Cd8 to Cd10, but those of the left side of Cd6, 7 and that of right side of Cd11 have been subject to postmortem damage. On the other hand, the anterior chevron facets are seen on the right sides of Cd6 to Cd10 and the left side of Cd11 (afc in Figs. 14–19). They are slightly convex and face lateroventrally. On the left sides of Cd6 to Cd10 and on the right side of Cd11, these facets are represented by poorly preserved swellings. Differences in orientation between the anterior and posterior chevron facets clearly match the orientation of chevrons in life (see description of the chevrons below).

TABLE 4. Measurements of (in mm) caudal vertebrae of *Tambatitanis amicitiae* gen. et sp. nov., holotype (MNHAH D-1029280) from the Lower Cretaceous of Japan. For an explanation of the measured parameters see Fig. 3.

position	Lc	Wmin	Wca	Wcp	Hca	Hcp	Lzz	Hsp	Wpr	Wpo	Wpomin	Hcd	Wsps	Dpa	Dpm	Dpp	Aprc	Aspc	Apr	Apo
Cd1	-	-	-	-	-	-	-	-	-	-	-	-	53x2	-	-	-	-	-	-	-
Cd2	100	-	-	174	172	179	172	232	-	77	20	415	93+	17	48	28	38	40	80	71
Cd3	101	-	-	151	170	170	183	205	61	57	7	360	50x2	16	52	42	39	36	70	65
Cd4	112	-	-	134	160	167	184	193	81	41	0		42x2	14.5	55	39	35	47	65	62
Cd5	89	-	-	128	149	157	180	171	45	34	9	325	61	10	50	32	32	50	64	40
Cd6	99	91	117+	127	144	148	180	177	32	33	7	327	67	10	54	32	32	50	41	42
Cd7	91	81	117	122	-	127	170	197	44	-	11	-	58	7.5	53.5	20	17	46	51	50
Cd8	110	84	109	116	121	120	176	178	-	51	7	295	-	6	61	30	35	42	-	68
Cd9	100	87	111	139	-	117	155	168	59	51	0	286	32	14	47	24	26	46	90	73
Cd10	94	76	105	101	104	115	137	189	50	53	13	318	24	8	50	27	27	30	76	65
Cd11	109	93	117	106	115	107	142	170	50	53	16	277	18	15	54	29	38	34	60	62
Cdx1	ca 120	57	85	80	77	76	-	64	-	-	-	140	-	-	-	-	-	-	-	-
Cdx2	112	54	78	73.6	68	65	138	55	24	15	-	119	-	24	44	35	-	-	-	-
Cdx3	112	58	85	82	65	61	118	42	26	26	-	102	-	24	42	40	-	-	-	-
Cdx4	113	52	73	71	56	56	105	36	18	19	-	90	-	23	47	35	-	-	-	-
Cdx5	105	48	70	70	63	58	-	-	-	-	-	-	-	23	46	32	-	-	-	-
Cdx6	101	46	62	70	56	60	101	ca 35	18	17	-	ca 92	-	22	40	30	-	-	-	-
Cdx7	103	43	62	62	57	53	100	30	27	18	-	83	-	20	41	35	-	-	-	-
Cdx8	89	36	59	57	46	44	89	29	-	-	-		-	13	36	32	-	-	-	-
Cdx9	84	29	50	50	46	44	75	25	11	14	-	69	-	13	36	29	-	-	-	-
Cdx10	77	27	49	46	42	40	69	23	9	13	-	62	-	13	29	29	-	-	-	-
Cdx11	75	25	44	43	39	37	-	-	-	-	-	-	-	10	32	25	-	-	-	-

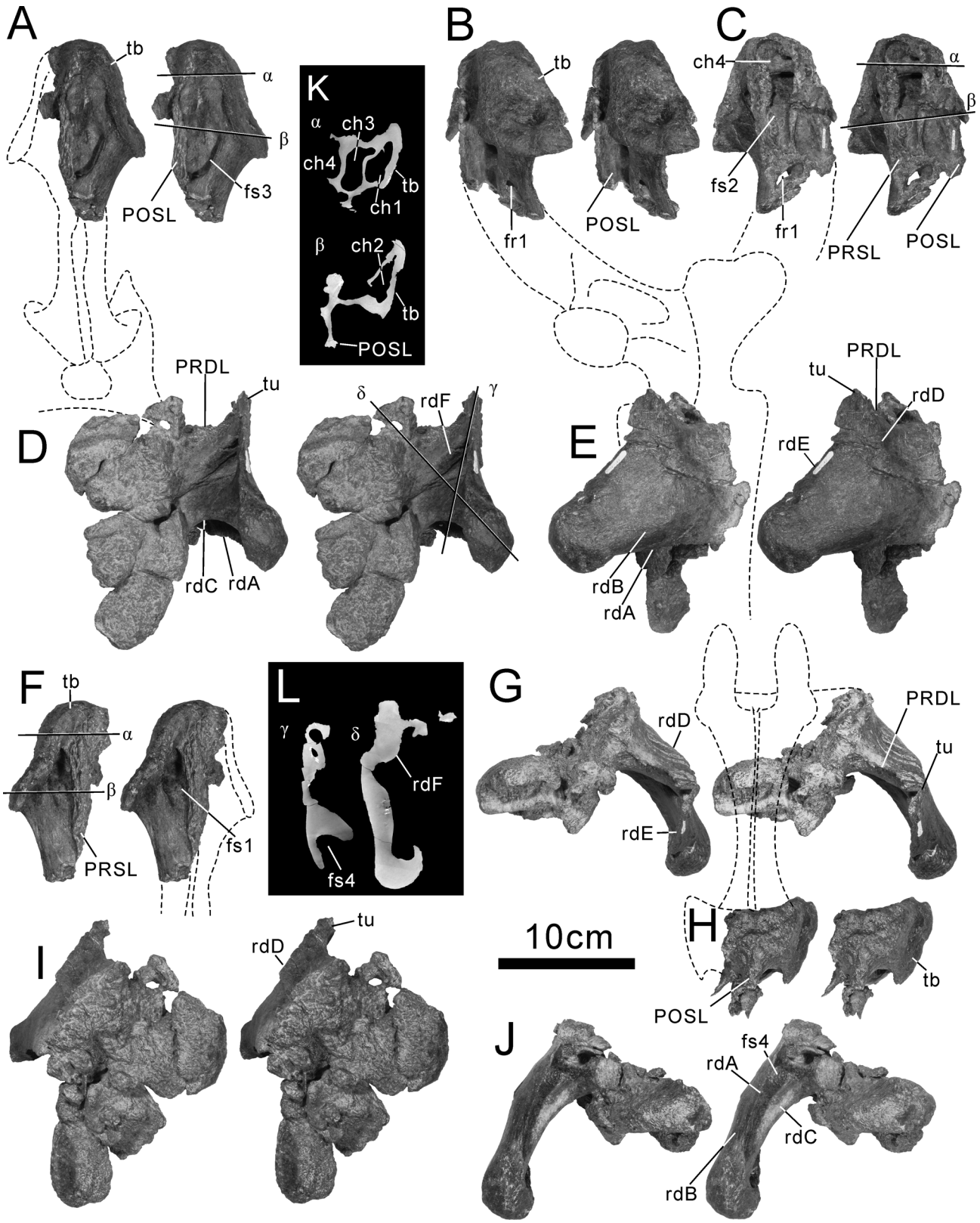

FIGURE 9. *Tambatitanis amicitiae* **gen. et sp. nov.**, holotype (MNHAH D-1029280). Cd1. **A–C, F** and **H**, fragment of distal end of neural spine, stereopairs. **A,** posterior view. **B,** right lateral view. **C,** left lateral view. **F,** anterior view. **H,** dorsal view. **D, E, G, I** and **J,** fragment of right transverse process and centrum, stereopairs. **D,** posterior view. **E,** right lateral view. **G,** dorsal view. **I,** anterior view. **J,** ventral view. **K** and **L,** CT slices through the neural spine of Cd1, part corresponding to the matrix that filling the internal chamber is removed from the CT image. Greek letters in **A, C, D** and **F** indicate the position of CT slices shown in **K** and **L**. Dashed lines indicate areas of missing parts. Scale bar = 10mm. See text for abbreviations.

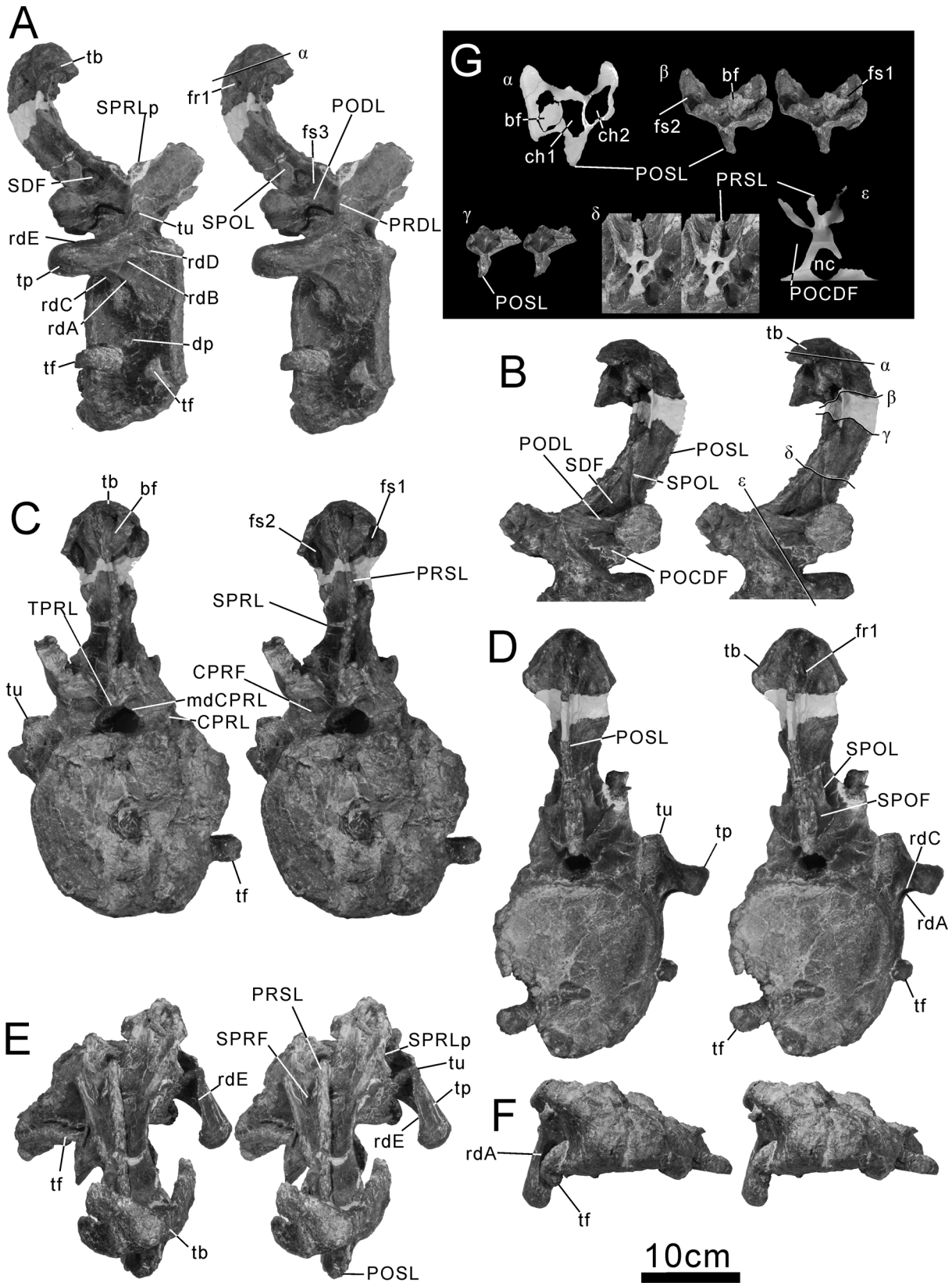

FIGURE 10. *Tambatitanis amicitiae* **gen. et sp. nov.**, holotype (MNHAH D-1029280). **A–F,** stereopairs of Cd2. **A,** right lateral view. **B,** left lateral view of the neural spine. **C,** anterior view. **D,** posterior view. **E,** dorsal view. **F,** ventral view. **G,** CT slices and stereopairs of the breakage section of the neural spine of Cd2, part corresponding to the matrix that filling the internal chamber is removed from the CT image. Greek letters in **A** and **B** indicate the position of CT slices and the stereopairs of the breakage surface of the spine shown in **G**. Scale bar = 10 cm. See text for abbreviations

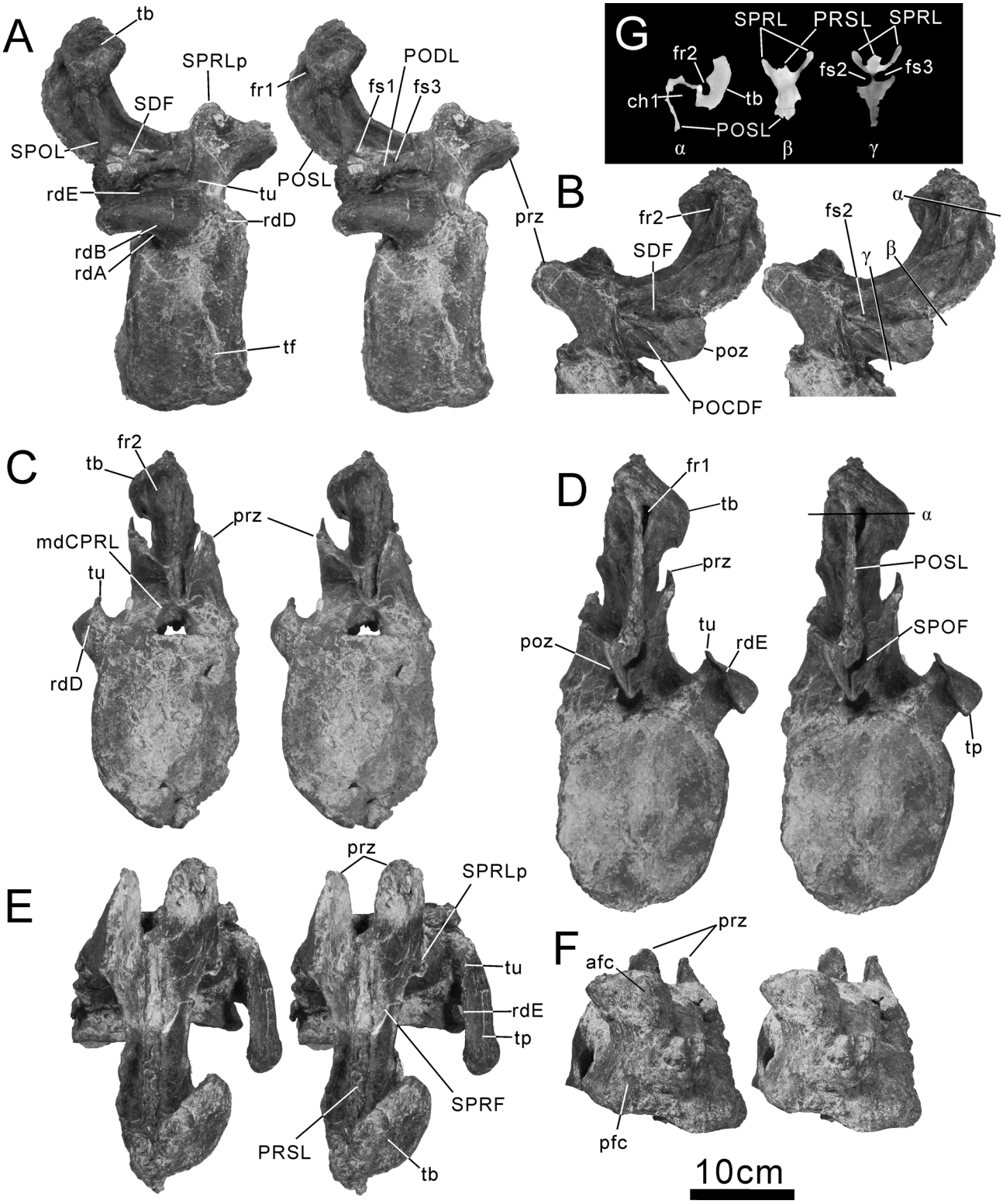

FIGURE 11. *Tambatitanis amicitiae* **gen. et sp. nov.**, holotype (MNHAH D-1029280). **A–F,** stereopairs of Cd3. **A,** right lateral view. **B,** left lateral view of the neural spine. **C,** anterior view. **D,** posterior view. **E,** dorsal view. **F,** ventral view. **G,** CT slices through the neural spine of Cd3, part corresponding to the matrix that filling the internal chamber is removed from the image. Greek letters in **B** and **D** indicate the position of CT slices shown in **G**. Scale bar = 10cm. See text for abbreviations

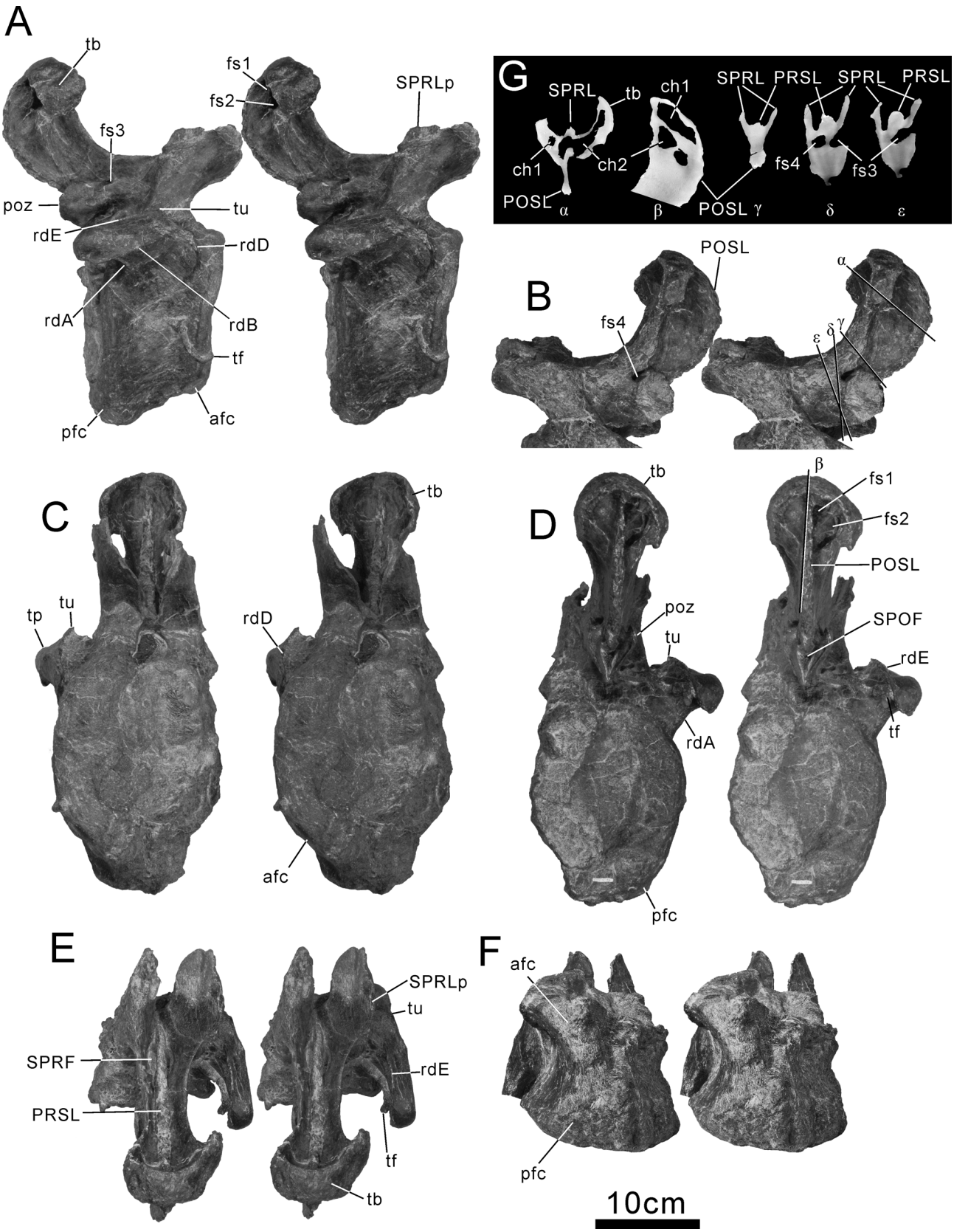

FIGURE 12. *Tambatitanis amicitiae* **gen. et sp. nov.**, holotype (MNHAH D-1029280). **A–F,** stereopairs of Cd4. **A,** right lateral view. **B,** left lateral view of the neural spine. **C,** anterior view. **D,** posterior view. **E,** dorsal view. **F,** ventral view. **G,** CT slices through the neural spine of Cd4, part corresponding to the matrix that filling the internal chamber is removed from the image. Greek letters in **B** and **D** indicate the position of CT slices shown in **G**. Scale bar = 10cm. See text for abbreviations.

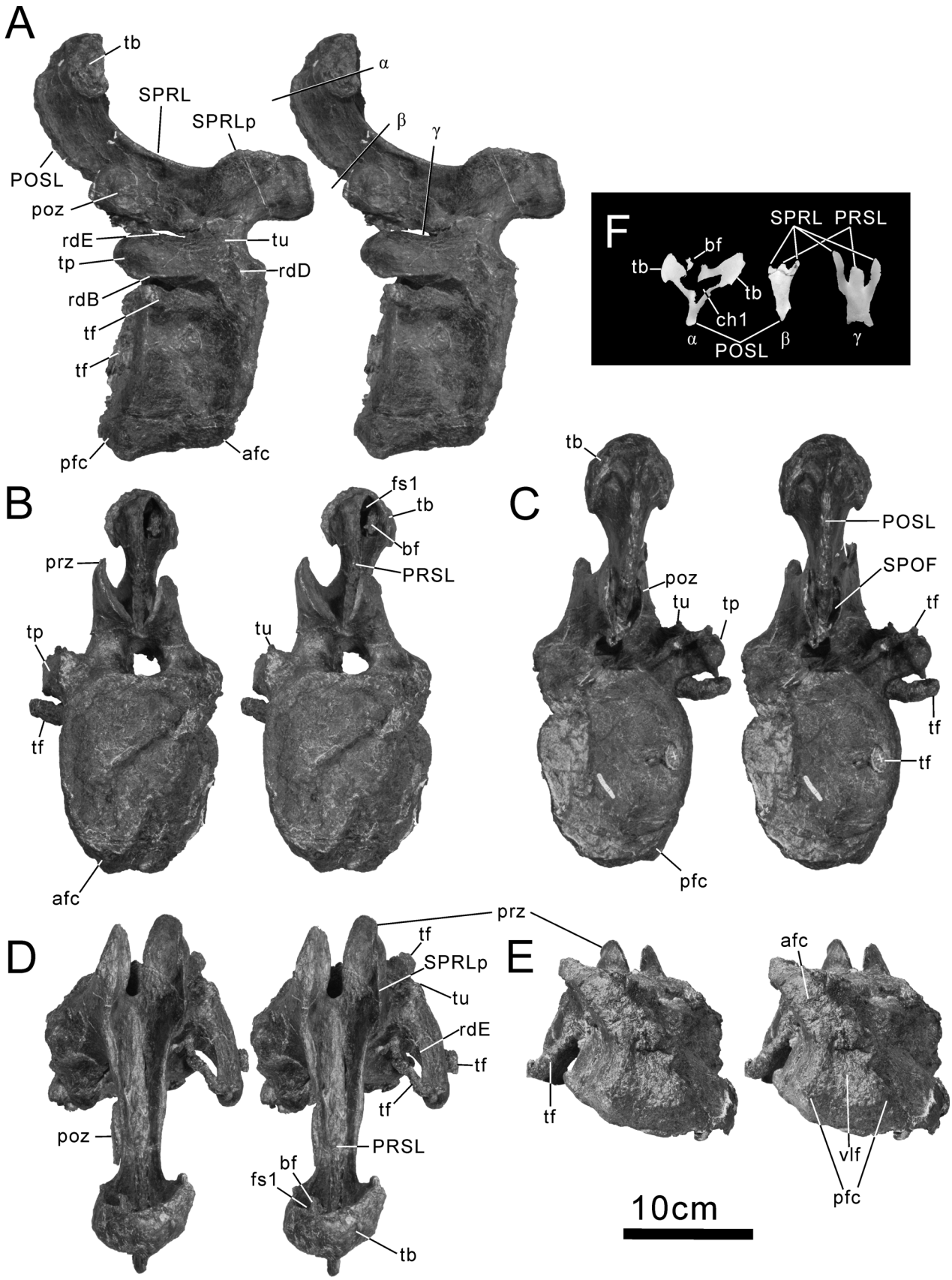

FIGURE 13. *Tambatitanis amicitiae* **gen. et sp. nov.**, holotype (MNHAH D-1029280). **A–E,** stereopairs of Cd5. **A,** right lateral view. **B,** anterior view. **C,** posterior view. **D,** dorsal view. **E,** ventral view. **F,** CT slices through the neural spine of Cd5, part corresponding to the matrix that filling the internal chamber is removed from the image. Greek letters in **A** indicate the position of CT slices shown in **F**. Scale bar = 10cm. See text for abbreviations.

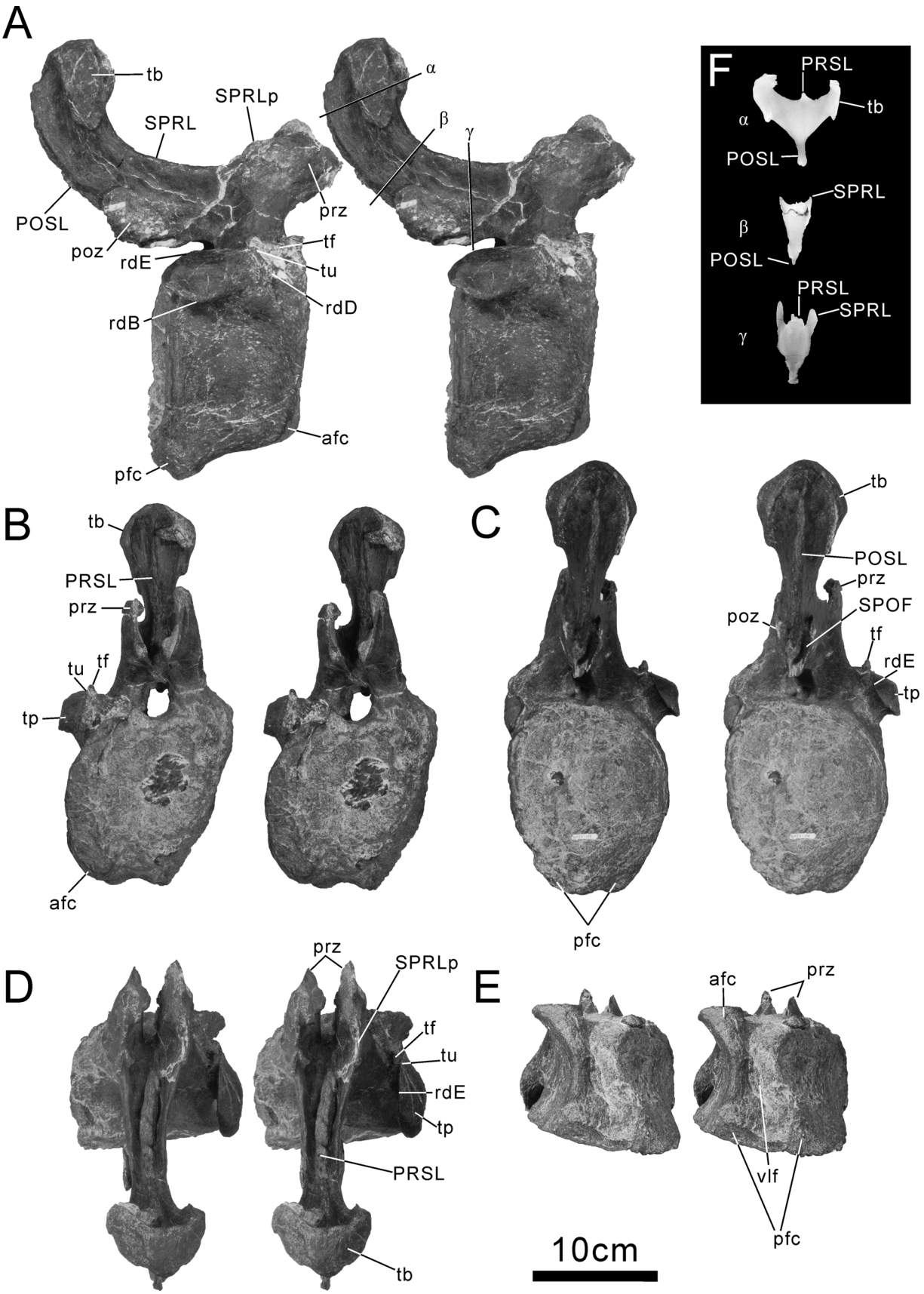

FIGURE 14. *Tambatitanis amicitiae* **gen. et sp. nov.**, holotype (MNHAH D-1029280). **A–E,** stereopairs of Cd6. **A,** right lateral view. **B,** anterior view. **C,** posterior view. **D,** dorsal view. **E,** ventral view. **F,** CT slices through the neural spine of Cd6, part corresponding to the matrix that filling the internal chamber is removed from the image. Greek letters in **A** indicate the position of CT slices shown in **F**. Scale bar = 10cm. See text for abbreviations.

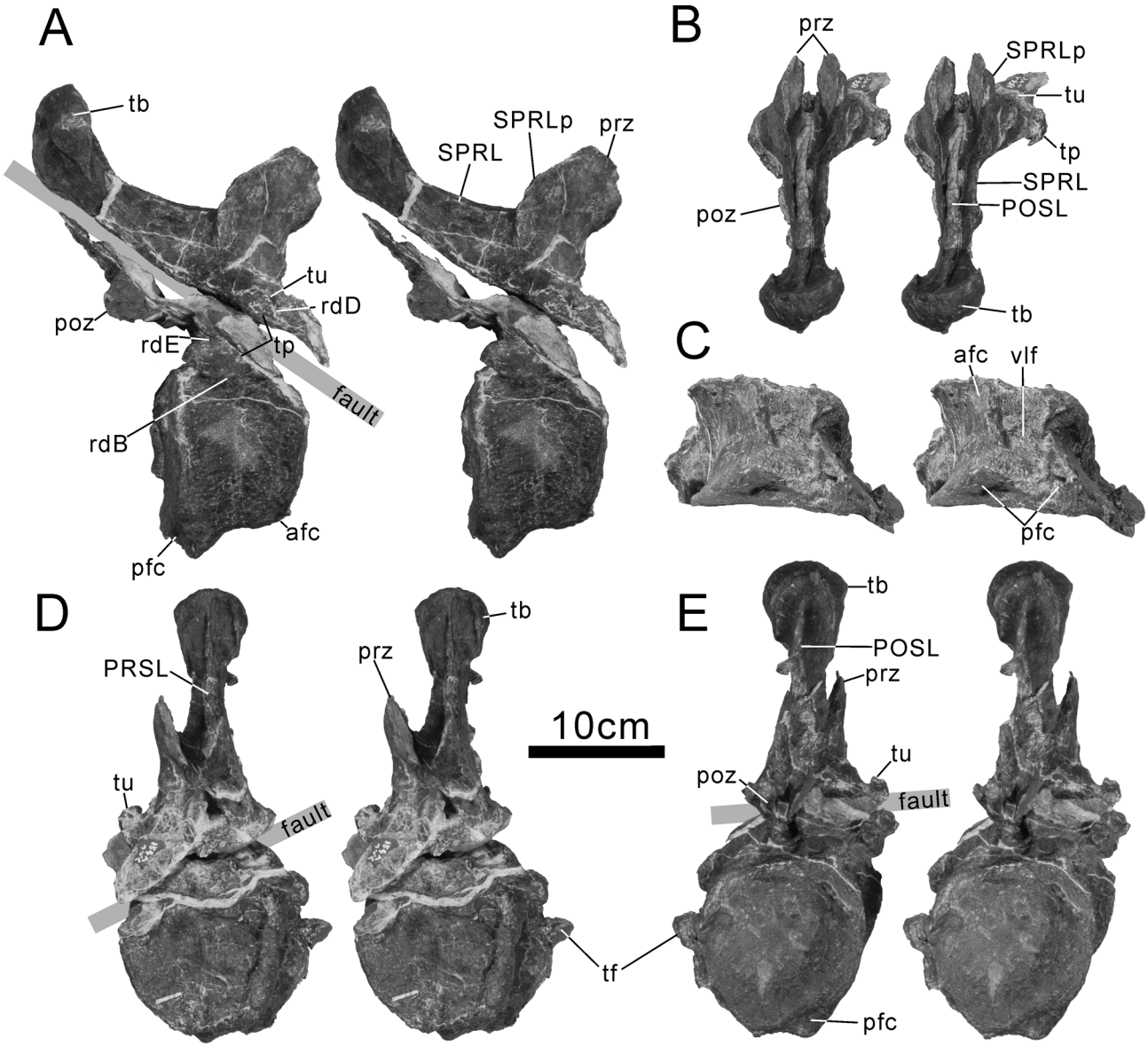

FIGURE 15. *Tambatitanis amicitiae* **gen. et sp. nov.**, holotype (MNHAH D-1029280). Stereopairs of Cd7. **A,** right lateral view. **B,** dorsal view. **C,** ventral view. **D,** anterior view. **E,** posterior view. Oblique gray bars in **A, D** and **E** indicates a fault along which the bones are mashed up and replaced by calcite veins. Scale bar = 10cm. See text for abbreviations.

As mentioned above, the ventral surface is badly preserved in Cd2 and Cd3. However, the preserved parts suggest that the ventral hollow, which is distinct in Cd6 to Cd11, is absent on Cd2 whereas it is absent or very rudimentary on Cd3. In Cd2, the left and right swellings on the posteroventral centrum, which can be considered as remnants of the articular facets, are very closely appressed to each other and there is no room for the ventral hollow. On Cd3, only the right swelling on the posteroventral centrum is preserved, but the groove separating it from its counterpart might have been very weak or absent because the most medial part of the remaining elevation is not depressed markedly. In Cd4 and 5, the anterior one third of the left side of the ventral surface is missing, but the posterior part of the ventral hollow is preserved (Figs. 12E, 13D). The remaining part of the hollow is a faint depression in Cd4, whereas that of Cd5 is a shallow depression bordered by a low longitudinally ridge. In Cd6–Cd11, the ventral surfaces of the centra are excavated to form a distinct double-keeled structure (vlf in Figs. 14–19), which becomes deeper posteriorly across the vertebral series, attaining its maximum depth at Cd10. The ventral hollow of the centrum is also seen in derived diplodocids (Hatcher 1901; Lull 1919; McIntosh 2005; Gillette 1991; Remes 2006; Upchurch and Mannion 2009), saltasaurid titanosaurs (Powell 1992; Wilson 2002; Upchurch *et al.* 2004a; Curry Rogers 2005), and basal titanosaurs, including *Andesaurus delgadoi* (Mannion and

Calvo 2011), but absent (Suteethorn *et al.* 2010; D'Emic 2012) or very shallow (*e.g.*, *Huabeisaurus* [D'Emic *et al.* 2013]) in other basal titanosauriforms.

From Cd2 to Cd6, the ventral margin of the centrum is very weakly arched dorsally in lateral view, whereas from Cd7 onward, it is arched markedly (Fig. 8). This trend is obviously related to the stronger development of the posterior chevron facets in Cd7–Cd11. In these caudal vertebrae, the dorsoventral dimension of the posterior chevron facet is almost the same as that of the neural canal, as in *Huabeisaurus, Phuwiangosaurus* and *Tangvayosaurus* (D'Emic *et al.* 2013).

The neural arches and transverse processes are firmly fused to the centra. In Cd2–Cd11, the neural arches are situated closer to the anterior than posterior end as is the case in other titanosauriforms (Calvo and Salgado 1995; Upchurch 1995; Salgado *et al.* 1997). The pedicle of the neural arch occupies the anterior two thirds of the dorsal margin of the centrum, with its anterior end located about a fifth to a tenth of the way back from the anterior margin of the centrum and its posterior end situated approximately 28 to 40% of the distance from the posterior margin of the centrum (Fig. 8, Table 4). At the same time, the pedicle of the neural arch of the anterior caudal of *Tambatitanis* is more posteriorly located, anteroposteriorly longer and dorsoventrally shorter than those of most other titanosauriforms (Table 4).

In Cd2, there is a pair of shallow CPRF on the anterior border of the pedicle of the neural arch (Fig. 10). The CPRF is bordered by the CPRL laterally, the mdCPRL medially and the TPRL dorsally. The mdCPRL extends dorsomedially from the medioventral corner of the CPRL and meets the TPRL at a point located ca. 0.5 cm away from the sagittal line. From this point, the medial part of the TPRL extends horizontally to the sagittal plane, and the lateral part of the TPRL runs dorsolaterally to the medioventral margin of the prezygapophysis. The configuration of these laminae and fossa is similar to that seen on the cervical vertebrae of some sauropods (*e.g.*, the anterior cervical of *Europasaurus,* [Carballido and Sander 2013]; 16th cervical of *Rapetosaurus* [Curry Rogers 2009]), although the columnar structure called the CPRL here may be too blunt to be called a lamina. By Cd3, only the very weak mdCPRL and subtle CPRF are present on the anterior border of the neural arch and (Fig. 11), from Cd4 onwards, both the mdCPRL and CPRF are absent (Fig.12C).

In Cd2–Cd11, the prezygapophysis is very thin transversely and has an oblong articular facet (Figs. 10–19). Both the prezygapophyseal and postzygapophyseal articular facets slope steeply and medioventrally. The angle between prezygapophyseal articular facets reaches its maximum at Cd2 (71 degrees), decreases in Cd3 and Cd4 (65 to 61 degrees), attains its minimum at Cd5 and Cd6 (65 to 61 degrees), increases again at Cd7, and from Cd8 onwards varies between 60 and 90 degrees. Matching with the angle between prezygapophyseal articular facets, that of postzygapophyseal articular facets is largest at Cd3, smallest at Cd6, and from Cd9 to Cd11 increases again. The ventral margins of the postzygapophyseal articular facets are very close together in Cd2–Cd11, except for in Cd4 and Cd9 where they contact each other (Figs. 12, 17; Table 4).

Less than half of the prezygapophyseal articular surface projects beyond the anterior articular surface of the centrum (Fig. 8). A similar posterior location of the prezygapophysis is seen in the anterior caudal vertebrae of some diplodocoids (*e.g.*, *Apatosaurus* [Upchurch *et al.* 2004b: pl. 5]; *Dicraeosaurus* [Janensch 1929: pl. 3]; *Tornieria* [Remes 2006: fig. 5]). In most titanosauriforms, however, the prezygapophysis protrudes strongly anteriorly, so that more than the half of its length is located beyond the anterior articular surface of the centrum (*e.g.*, *Giraffatitan* [Janensch 1950]; *Cedarosaurus* [Tidwell *et al.* 1999]; *Tastavinsaurus* [Royo-Torres 2009]; *Huanghetitan ruyangensis* [HS pers. obs.]; *Malarguesaurus* [González Riga *et al.* 2009]; *Andesaurus* [Mannion and Calvo 2011]; *Malawisaurus* [Gomani 2005]; Aeolosaurini [Santucci and Arruda-Campos 2011]). Therefore, the posterior location of the prezygapophyses in *Tambatitanis* is unique among titanosauriforms.

In concert with this peculiar location of the prezygapophyses, the postzygapophysis projects backwards strongly such that the anterior border of its articular surfaces is located just above the posterior end of the centrum (Fig. 8). Similar posterior locations of the postzygapophyses are also seen in anterior and middle caudal vertebrae of some diplodocoids (*e.g.*, *Tornieria* [Remes 2006: figs. 3, 5]; *Amazonsaurus* [Carvalho *et al.* 2003: figs. 8, 10, 11]; *Comahuesaurus* [Carballido *et al.* 2012: fig. 8]; *Dicraeosaurus* [Janensch 1929: pl. 3]; *Apatosaurus* [Osborn 1904: fig. 6; Gilmore 1936: pl. 33; Upchurch *et al.* 2004b: pl. 5]; *Barosaurus* [McIntosh 2005: fig. 2.6]. In a series of procoelous caudal vertebrae from site G of Tendaguru **(**HMN MB.R.2091.1-30**)**, the probable 10th caudal has a postzygapophysis protruding beyond the rim of the posterior articular surface, with the anterior margin of its articular facet in line with the posterior margin of the centrum (Bonaparte *et al.* 2000: pls. 4,5,11,12). According to Mannion *et al.* (2013), HMN MB.R.2091.1-30 is phylogenetically very close to *Mamenchisaurus.* In some of the

posterior-middle caudal vertebrae of *Mamenchisaurus*, the postzygapophyses are also located beyond the posterior end of the centrum (Young and Zhao 1972: pls.3 and 10; Ouyang and Ye 2002: pl. 15).

In all of the titanosaurs, including basal taxa (*e.g.*, *Andesaurus* [Mannion and Calvo 2011: figs. 5 to 7]; *Malawisaurus* [Gomani 2005: figs. 14 to 16]) and most basal titanosauriforms (*e.g.*, *Tastavinsaurus* [Royo-Torres 2009: figs 4.54–4.70]; *Giraffatitan* [Janensch 1950: pls. 1 and 2]; *Cedarosaurus* [Tidwell *et al.* 1999: figs. 3, 4]; *Malarguesaurus* [González Riga *et al.* 2009: fig. 5]; *Huanghetitan ruyangensis* [HS pers. obs.]), the postzygapophysis does not protrude beyond the rim of the posterior articular surface of the centrum. Therefore, *Tambatitanis* is the only titanosauriform in which the postzygapophysis extends beyond the posterior end of the centrum throughout the anterior caudal vertebrae. This peculiar feature is related to the posterior position of the prezygapophyses. The inclination of the prezygapophysis in lateral view (the angle between the axis of the prezygapophysis and the plane parallel to the articular surfaces of the centrum) fluctuates among Cd2–Cd11 from 39 (at Cd3) to 17 (at Cd7) degrees, with an average of 32 degrees (Fig. 3, 8, Table 4).

A very sharp and well developed SPRL runs from the prezygapophysis to the summit of the neural spine. A blade-like process (hereafter referred to as SPRL process following D'Emic *et al.* 2013) is present on the SPRL just behind the articular facet of the prezygapophysis (SPRLp in Figs. 8–19). The SPRL process is a transversely thin, delicate structure: its transverse thickness ranges from 0.1 cm in Cd5 to 0.5 cm in Cd4, with an average of 0.3 cm for Cd4 to Cd5. The SPRL process is most strongly developed in Cd3, and in more posterior caudal vertebrae it is less developed. On Cd2, only the basal part of the SPRL process is preserved but it may have been as large as or larger than that of Cd3 judging from the anteroposterior length of the preserved portion. The SPRL process has also been reported in *Graffatitan* (D'Emic 2012), *Phuwiangosaurus* (D'Emic and Wilson 2011), *Tangvayosaurus* (D'Emic 2012), *Adamantisaurus* (Santucci and Bertini 2006), *Mendozasaurus* (González Riga 2003), *Alamosaurus* (Gilmore 1946: plate 5), *Opisthocoelicaudia* (D'Emic 2012) and Saltasaurini (D'Emic 2012).

In Cd2–Cd11, the neural spines incline posterodorsally but their steepness varies; the angle between the plane parallel to the articular surface of the centrum and the line connecting the base (the most ventral point of SPRL just behind the SPRL process) and the most dorsal point of the spine ranges from 30 (at Cd10) to 50 (at Cds5 and 6) degrees, with an average of 42 degrees (Figs. 3, 8; Table 4). Because of this strong rear inclination of the spine, the anterior border of the summit of the neural spine is located beyond the posterior end of the centrum. This location is also the same level of the anterior margin of the postzygapophyseal articular facet. As a result, the neural spine summit is located above the anterior part of the succeeding centrum when these caudal vertebrae are articulated with one another.

The lateral profile of the spines also varies along Cd2–Cd11; the neural spine of Cd2 is almost straight like those of most other sauropods, whereas those of Cd3–Cd6 exhibit a strong curvature which distinguishes *Tambatitanis* from most other sauropods (Figs. 8–14). In Cd3–Cd6, the SPRL runs posteriorly and almost horizontally from the point just behind the SPRL process, which corresponds to the most ventral point of the dorsal margin of the SPRL, to the same level of the anterior margin of the postzygapophyseal articular facet, and from this point, it is directed posterodorsally and then sweeps dorsally. Thus, its anterior border has an anterodorsally concave arch, as is visible in lateral view. *Bonatitan* (Martinelli and Forasiepi 2004: fig. 16) and *Ferganasaurus* (Alifanov and Averianov 2003: fig. 3) are similar to *Tambatitanis* in exhibiting strong posterior inclination and strong curvature of the caudal neural spines, although they differ greatly from *Tambatitanis* in other aspect of the spine structure. From Cd7 onward, the SPRL rises just behind the SPRL process and runs posterodorsally at relatively steep angle (Fig. 8). In lateral view, its anterior border is steep and only slightly concave anteriorly. From Cd7 onward, the steepness of the SPRL increases posteriorly, and its maximum steepness is attained in Cd10.

The SPRL constitutes the thin wall laterally bounding the SPRF. The SPRF is deep along the length of the anterior face of the spine, including the distal part of the spine. A deep SPRF is also seen in derived titanosaurs, such as Saltasaurini, but in such forms, the anterior face of the distal part of the spine is occupied by a strongly protruding PRSL, leaving little or no room for a SPRF there. In Cd2–Cd11 of *Tambatitanis*, the PRSL originates from a point ca. 0.5 to 1.5 cm posterior from the anteromedial rim of the roof of the neural canal and runs upward along the median line on the bottom of the SPRF to the anteromedial corner of the hemispherical neural spine summit (Figs. 10–19). The PRSL is a very low rugose ridge, not protruding anteriorly, and obscured by the SPRL in lateral view even at the summit of the neural spine, except in Cd8 and Cd9, where the most dorsal part of the PRSL can be seen as a weak anterior protrusion in lateral view. However, even in those caudal vertebrae, the most distal part of the PRSL is transversely thin, so that a shallow but distinct SPRF extends dorsally along both sides of the PRSL.

In Cd2, the anteroventral part of the SPRF near the articular surface of the prezygapophysis is relatively wide and shallow, reflecting the wide angle between the articular surfaces of the prezygapophyses, which measures about 60 degrees (Fig. 10). Behind the SPRL process, the SPRF becomes narrower transversely towards the midheight of the spine. SPRLs bound the fossa, meeting at an angle of about 80 degrees. From the midheight of the spine, the SPRF becomes broader again toward the cup-shaped neural spine summit. The SPRF reaches its greatest depth at the point level with the SPRL process and its minimal depth is at the point where the SPRF becomes narrowest. Towards the summit of the neural spine, the depth of the SPRF slightly increases again. Although the basic structure of the SPRF and SPRL in Cd3–Cd7 is the same as that of Cd2, on the former caudal vertebrae the SPRF becomes narrower even at its most anteroventral part, reflecting the acute angle between the left and right articular surfaces of the prezygapophyses (Figs. 11–15). The angle between the left and right SPRLs decreases on more posterior caudal vertebrae; on Cd6, the right and left SPRLs meet at an angle of about 40 degrees and on Cd10, SPRLs are nearly parallel to the sagittal plane (Fig. 18).

In Cd1–Cd7, the summit of the neural spines is strongly expanded, giving it a semicircular outline in anterior view (Figs. 9–15). *Tambatitanis* shares this feature with *Tastavinsaurus* (Canudo *et al.* 2008; Royo-Torres 2009), *Huanghetitan ruyangensis* (HS pers. obs.), some specimens/species of *Camarasaurus* (*e.g.,* Osborn and Mook 1921: pls. 74–77; Ikejiri *et al.* 2005: figure 6.8), *Aragosaurus* (Sanz *et al.* 1987), and a series of indeterminate caudal vertebrae from site G of Tendaguru **(**HMN MB.R.2091.1-30**,** Bonaparte *et al.* 2000). However, unlike those other examples, the hemispherical summits of the neural spines of the *Tambatitanis* are excavated anteriorly by the dorsal extension of the SPRF, so that the anterodorsal surface of the spine summit forms a cup-shaped shallow depression. The dorsal extension of the PRSL separates this shallow depression into left and right halves, but it is very low and thin and thus fails to occupy the cup shaped shallow depression on the neural spine summit.

Tambatitanis is unique among sauropods in possessing a deep and narrow SPRF accompanied by its extension to the summit of the spine in the anterior caudal vertebrae. In saurischians in general, the spine of the anterior caudal vertebrae is a transversely compressed, short, plank-like structure, so that the room for the SPRF and SPOF is available only at the basal part of the spine (*e.g., Majungasaurus* [O'Connor 2007]; *Allosaurus* [Madsen 1976]). This plesiomorphic plank-like neural spine of the anterior caudal vertebrae is widely distributed in basal sauropods as well as basal macronarians and titanosauriforms such as *Europasaurus* (Carballido and Sander 2013), *Giraffatitan* (Janensch 1950), *Malarguesaurus* (González Riga *et al.* 2009) and *Epachthosaurus* (Martínez *et al.* 2004). However, associated with the lateral expansion of the neural spines, the SPRF and SPOF expand dorsally in various neosauropods (Wilson *et al.* 2011: figs. 11, 12, 13). The SPRF is enlarged in some basal titanosauriforms (*e.g., Huanghetitan ruyangensis* [HS pers. obs.]; *Huabeisaurus* [D'Emic *et al.* 2013]) , some titanosaurs (*e.g., Baurutitan* [Kellner *et al.* 2005]; *Trigonosaurus* [Campos *et al.* 2005]; *Rapetosaurus* [Curry Rogers 2009]; *Neuquensaurus* [Powell 2003; D'Emic and Wilson 2011; Salgado *et al.* 2005]; *Bonatitan* [Martinelli and Forasiepi 2004]; *Saltasaurus* [Powell 1992, 2003]) and taxonomically indeterminate articulated caudal vertebrae (HMN MB.R.2091.1-30) from site G of Tendaguru (Bonaparte *et al.* 2000: pls. 4-5,10-18). In most of these forms, the basal part of SPRF is wider than that of *Tambatitanis,* except in *Huanghetitan ruyangensis* and HMN MB.R.2091.1-30, which exhibit deep but relatively narrow SPRF as in *Tambatitanis*. In these forms, except for *Saltasaurus* and *Neuquensaurus,* however, the SPRF diminishes distally, and halfway up the spine becomes non-existent or only a faint streak located between a strongly developed PRSL and SPRL. On the other hand, in *Saltasaurus* and *Neuquensaurus*, the distal part of the PRSL is poorly developed even at the distal end of the spine and thus the PRSL is hidden by the SPRL in lateral view. In this respect, the neural spine of the anterior caudal vertebrae of *Saltasaurus* and *Neuquensaurus* is similar to that of *Tambatitanis* but it differs from the latter in the greater transverse width of the SPRF and the lack of the lateral expansion of the summit of the neural spine. The presence of small oval pneumatic openings on the bottom of SPRF of these titanosaurs, including *Saltasaurus* (D'Emic and Wilson 2011; Cerda *et al.* 2012) and *Neuquensaurus* (Salgado *et al.* 2005), also distinguish them from *Tambatitanis.* In Cd2 to Cd4 of *Tambatitanis,* the basal part of the spine is excavated by small deep fossae, but they are extending from the SDF, not from SPRF (see below).

From Cd1 to Cd7, the anterior half of the hemispherical spine summit is capped by a band-shaped tuberosity (tb in Figs. 9–15). This tuberosity is weakly rugose, elevated relative to the surface of the posterior half of the hemispherical spine summit, and demarcated posteriorly and ventrally by a sharp rim slightly overhanging the surface just posterior to the rim. The anterior border of this band-like tuberosity rims the cup-shaped dorsal-most part of the SPRF, and ventrally it meets the dorsal end of the SPRL. Where they meet, the anterior border of the

tuberosity is laterally located and slightly anteriorly protruding relative to the dorsal end of the SPRL, so that the latter abuts against the former medioventrally.

On Cd1, the summit of the neural spine is sub-triangular in anterior view (Fig. 9F). The tuberosity covering the two sides of this triangle is butterfly shaped in dorsal view; it is constricted medially (2.4 cm along median line), flares laterally (7 cm along lateral border) and in lateral view its anteroventral corner protrudes strongly beyond the dorsal end of the SPRL. In Cd2–Cd4, the tuberosity is still butterfly shaped but in more posterior caudal vertebrae the difference between the median and lateral parts of the tuberosity in anteroposterior width decreases as the neural spine summit becomes smaller, and in anterior view it becomes semicircular (Figs. 10–12). By Cd5, the anteroposterior width of the median part of the tuberosity is almost the same as that of the lateral part (ca. 3 cm along lateral border). From Cd6 onwards (Fig. 14), the tuberosity expands anteroposteriorly at the median part while it tapers lateroventrally. From Cd8 (Fig. 16) onward, the neural spine summit rapidly decreases in transverse width and by Cd10 (Fig. 18), its width is almost same as that of the basal part of the spine. In anterior view, the neural spine summit of Cd10 tapers and points dorsally but is still covered by the tuberosity.

In Cd2–Cd11 (Figs. 10–19), the posterior face of the spine is strongly convex posteriorly with a strongly protruding POSL in contrast to the anterior face of the spine. The POSL extends ventrally from the posteromedial end of the tuberosity and terminates in a SPOF that is bordered lateroventrally by the postzygapophysis and dorsolaterally by the SPOL. A SPOF is present only in Cd2–Cd11 as a deep small depression. In Cd2 to Cd8, the SPOF does not extend anteriorly beyond the anterior margin of the postzygapophysis. In Cd10 and Cd11, however, it does and consequently it hollows the wedge that bridges the postzygapophysis and the posterior end of the pedicle of the neural arch (see below).

The POSL is strongly bowed posteriorly in lateral view in Cd3–Cd8, while in Cd9–Cd10 its posterior curvature is weaker and, in Cd2, it is almost straight except for its most dorsal part (Fig. 8). The strong posterior protrusion of the POSL may correlate with the weak protrusion of the PRSL. The POSL does not fit into the SPRF when the successive caudal vertebrae are articulated with one another, but the distance between the posterior margin of the POSL and the anterior margin of the PRSL of successive caudal vertebrae is nearly constant along the length of spine and this may imply that the anteroposterior width of the ligament connecting them might have been also nearly constant over its dorsoventral length.

In contrast to the prominent SPRL and POSL, the SPOL is quite weak in *Tambatitanis.* In Cd2–Cd4 and Cd7, the SPOL is restricted to the ventral part, represented by a strut that extends nearly vertically from the dorsal corner of the postzygapophysis to the halfway point of the lateral face of the spine (Figs. 10–12, 15). In Cd2, the SPOL is bifurcated and a small fossa is present on the bifurcated portion of the lamina. In Cd5, it is totally absent. In Cd6, the SPOL is very small and almost hidden by the dorsal rim of the postzygapophysis in lateral view. In Cd8–Cd11, the SPOL is a weak ridge that connects the dorsal corner of the postzygapophysis and the ventral corner of the tuberosity capping the neural spine summit, and its middle part measuring ca. 1cm in length is particularly faint (Figs. 16–19). The variation of the angle of the pre- and postzygapophysis mentioned above closely correlates with the development of the SPOL; the angle between postzygapophyseal articular facets is most acute in Cd5 and Cd6, in which the SPOL is extremely reduced, while in other anterior caudal vertebrae, in which the SPOL is more developed, the angle between the postzygapophyseal articular facets is larger.

Besides the deep SPRF and minute SPOF, the spines of Cd1 to Cd4 have several external fossae and foramina as well as internal chambers (Figs. 9–12). These pneumatic structures are most strongly developed in Cd2 among the preserved portions of the caudal vertebrae, though they may have been strongest in Cd1, which is represented only by a few fragments. In Cd2, the strongly expanded summit of the neural spine contains large internal chambers extending from two asymmetrically developed fossae (fs1 and 2 in Fig. 10G) and a foramen (fr1 in Fig. 10D). The larger fossa (fs1 in Fig. 10C, G) excavates the entire left half of the anterior face of the spine summit and it invades the right half of the neural spine summit to form an internal chamber (ch1 in Fig. 10G). The smaller fossa (fs2 in Fig. 10C, G) deeply excavates the lateral margin of the right half of the anterior face of the spine summit. This fossa is dorsoventrally long, transversely narrow, sharply lipped medially, opens ventrolaterally and invades the bone posterodorsally and slightly medially (ch2 in Fig. 10G). Far behind the posterior border of the butterfly-shaped rugose surface and just lateral to the POSL, a small foramen (fr1 in Fig. 10A, D) pierces the right half of the posterior face of the spine summit. This foramen is sharply lipped except at the ventral end, opens ventrally, is deeper dorsally, and only slightly excavates the bone medially underneath the POSL. A CT scan revealed that these two fossae and the foramen do not communicate with each other via an internal chamber.

In Cd1 and Cd3 to Cd5, most of the volume of the summit of the neural spines is occupied by the fossae and

internal chambers, which are developed quite asymmetrically as in Cd2 (Figs. 9, 11–13). In Cd1, the medial half of the right anterior face of the spine summit is excavated by a deep fossa, which is dorsoventrally long and transversely narrow (fs1 in Fig. 9F). This fossa is delimited medially by the PRSL and sharply lipped laterally and dorsally, but opens ventrally. The matrix still fills the most lateral and the most dorsal parts of the fossa but a CT scan shows that the fossa extends laterally (ch2 in Fig. 9K) as well as dorsally (ch1 in Fig. 9K) under the sharp lip. The left half of the neural spine summit is mostly missing but the base of a wall left on the broken surface indicates the former presence of a fossa (fs2 in Fig. 9C) similar to that of the right side. This fossa was separated from that of the right side by the PRSL but a CT scan revealed that its dorsal extension, which is still filled with matrix, invades the right half of the neural spine summit and occupies the medial part of the most dorsal part of the summit (ch3 in Fig. 9K). A sub-chamber (ch4 in Fig. 9K) was present adjacent to chamber 3, judging from the remnants of the walls left of the broken surface of the spine summit. On the right side of the posterior surface of the spine summit is a dorsoventrally oblong depression below the level of the ventral margin of the butterfly-shaped tuberosity mentioned above. This fossa (fs3 in Fig. 9A) opens dorsally without a distinct border, whereas it is delimited medially by the POSL and lateroventrally by a sharp lip under which the fossa extends laterally as a slit shaped pocket. This slit is still filled with matrix but a CT scan shows that it is not continuous with the fossa on the anterior face. Just ventrolateral to the lip of the slit, a smaller foramen penetrates the POSL transversely (fr1 in Fig. 9 B–C). This foramen may suggest the presence of an internal chamber in the middle of the neural spine.

Two foramina are preserved on the neural spine summit of Cd3, one situated on the posterior surface (fr1 in Fig. 11A, D) and the other on the anterior surface of the right side of the summit (fr2 in Fig. 11B, C). The former foramen is dorsoventrally long, oval, sharply lipped laterally and dorsally, delimited medially by the most dorsal part of the POSL and located just behind the posterior end of the butterfly-shaped tuberosity mentioned above. This foramen is the window of a large internal chamber that occupies a large portion of the right side as well as the medial third of the left side of the spine summit (ch1 in Fig. G). A smaller foramen is located on the middle of the right side of the anterior face (fr2 in Fig. 11B, C, and G). It is small, dorsoventrally oblong, sharply lipped (except for the ventral border) and open ventrally. A CT scan revealed that this foramen does not communicate with the larger foramen on the posterior surface via an internal chamber (Fig. 11G). The lateral two thirds of the left side of the spine summit are missing. The ventral two thirds of the broken surface are smooth and represent a wall that separates the large chamber mentioned above and a smaller chamber which may have occupied the lateral two thirds of the left side of the spine summit.

In Cd4, two deep fossae occupy much of the space behind the butterfly-shaped tuberosity on the right half of the posterior surface of the neural spine summit (fs1 and 2 in Fig.8PA and D). These fossae are sharply lipped, arranged one above the other and separated from one another by a sub-horizontal septum. Each of these fossae invades the left half of the neural spine summit to form separate internal chambers (ch1 and 2 in Fig.8PG). In Cd5, a sharply lipped fossa occupies much of the left side of the anterior surface of the spine summit (fs1 in Fig. 13B). This fossa is oval, oblong dorsoventrally, delimited medially by the PRSL and excavates the median portion of the spine summit underneath the PRSL. A CT scan revealed that the fossa is continuous with an internal chamber that occupies both sides of the spine summit (ch1 in Fig. 13F). From Cd6 onwards, the spine summit lacks the internal chamber (Fig. 14F).

In Cd2, the middle portion of the neural spine has a tubular internal chamber extending along the axis of the spine. This chamber is closed dorsally but opens ventrally to the most dorsal corner of a triangular fossa located on the left side of the spine (Fig. 10). This fossa is one of a pair of fossae flanking the basal part of the spine laterally just above the postzygapophysis. We identify them as SDF because they are bounded posteriorly by a short SPOL, anterodorsally by a SPRL and ventrally by a horizontal short lamina which we identify as a PODL. The PODL extends from the anterior most corner of the postzygapophysis to the point just below the posterior end of the SPRL process, rather than to the upper part of the transverse process which is generally considered to be homologous to the diapophysis (*e.g.,* Whitlock *et al.* 2011). As will be shown later, Cd3 and Cd4 also have a similar short ridge, which does not contact the transverse process. A short ridge identifiable as a PODL may have been also present in the poorly preserved Cd1, which is represented by few fragments, but it would not contact directly with the transverse process because there is no elevation representing the anterolateral extension of PODL on the basal part of the fragment of the right transverse process of Cd1 (Fig. 9D). A similar short lamina that runs horizontally from the anterodorsal corner of the postzygapophysis to the basal part of the SPRL also occurs in anterior caudal vertebrae of other titanosauriforms (*e.g., Mendozasaurus* [González Riga 2003]; *Neuquensaurus* [Salgado *et al.*

2005; Wilson *et al.* 2011; Whitlock *et al.* 2011]). A similar short lamina that runs horizontally from the postzygapophysis to the basal part of the SPDL has been described in some rebacchisaurids (*e.g., Demandasaurus* [Torcida Fernández−Baldor *et al.* 2011]; a rebacchisaurid anterior caudal [MIWG5384, Mannion *et al.* 2011]). Though none of these examples of short laminae running horizontally from the postzygapophysis are directly connected to the transverse process, they are identified as a PODL by these authors and we accept their interpretation here because the position and the orientation of laminae in these examples is closely comparable with the PODL on the anterior caudal vertebrae of some diplodocids, in which the PODL is directly connected to the transverse process (*e.g.,* Wilson 1999). The only example that could contradict such an identification is an anterior caudal of an unidentified sauropod from the Early Cretaceous of China (PMU R263). This caudal has a short lamina extending horizontally from the postzygapophysis to the SPRL, as well as a lamina running anteroventrally from the postzygapophysis to the basal part of the transverse process. Upchurch and Mannion (2009) identified the latter as a PODL and left the former unnamed while Whitlock *et al.* (2011) identified the latter as CPOL and the former PODL. According to the strict definition of a PODL, the identification of Upchurch and Mannion (2009) might be justified, but if the overall arrangement of the fossae and laminae is taken into consideration, the identification made by Whitlock *et al.* (2011) might be more appropriate, and therefore, we adopt the latter author's interpretation here.

In Cd2, the anteroventral corner of the right SDF is pierced by a small tubular fossa, which extends anteriorly into the bone (fs3 in Fig. 10A) and is bordered dorsally by a strut running anterodorsally within the fossa. Within the left SDF, a triangular deep depression is present at the anteroventral corner of the fossa. Besides this depression, the bottom of the left SDF is flat without any sub-fossa or foramen (Fig. 10B). In Cd3, the structure of the right SDF is same as that of Cd2 except for the presence of a small deep fossa at the dorsal corner of SDF, instead of a foramen (fs1 in Fig. 11A). The dorsal border of the left SDF is not distinct and lacks foramina or sub-fossae. The rest of the left SDF is shallower than the right one and its floor is rippled by two low struts. Anterior to one of these struts is a small deep fossa (fs2 in Fig. 11B), which is sharply lipped anteriorly, extends anteromedially, and near the median plane approaches a similar small deep fossa extending from the right SDF (fs2 and f3 in Fig. 11Gγ). Anterior to this small deep fossa is a small depression, which marks the anterior-most corner of the left SDF. In Cd2 and Cd3, the SDF is represented by a shallow large depression which contains smaller pits or foramina. On the other hand, in Cd4, SDF is represented solely by small deep fossae. On the right side, the SDF is represented by an anteriorly extending small deep fossa which is located just anterodorsally to the postzygapophysis and which is anteriorly lipped but opens posteriorly (fs3 in Fig.12A, Gδ, ε). On the left side, the SDF is represented by an oblong small pit which is lipped in all directions and located just above the dorsal margin of the postzygapophysis (fs4 in Fig.12B, Gδ). Both of these fossae excavate the basal part of spine deeply, but those of the right side are deeper and invade the right side of the spine. In Cd5 and Cd6, the SDF is not present and the PODL is reduced to a faint ridge that runs horizontally from the anterior end of the postzygapophysis to the base of the prezygapophysis in parallel with the anterior portion of the SPRL, which also runs horizontally. In Cd7–Cd11, however, the SDF appears again as a small fossa (Figs. 15–19). This fossa is bordered posteriorly by the SPOL, whose ventral part is thin but distinct, and ventrally by an anteroposteriorly short PODL. Anterodorsally, it is not bordered and opens to the lateral face of the SPRL.

In *Tambatitanis,* all of the remains of centra, including the fragment of the centrum of Cd1, do not bear pneumatic internal structures, as described above, so that the development of the pneumatic structures is restricted to the spine of first to fifth caudal vertebrae. The combination of the pneumatic spine and apneumatic centrum is also known in the second caudal of *Malawisaurus* (Wedel 2009), but its neural arch is also pneumatic. Pneumatic internal cavities of the sacrum and the spine of Cd1 and Cd2 may suggest the presence of posterior compartment pneumaticity, widely recognized in Neosauropoda (Wedel 2009).

In Cd2–Cd11, the postzygapophysis is located posteriorly far beyond the posterior end of the centrum and consequently there is a large gap between the postzygapophysis and the posterior margin of the pedicle of the neural arch (Fig. 8). This gap is bridged by a wedge-like structure, which is dorsoventrally tall, transversely narrow, and tapers posteriorly. The structure is bordered posteriorly by the anterior margin of the postzygapophysis, dorsally by the PODL and ventrally by the posterior extension of the CPOL, which extends from the posterior border of the pedicle of the neural arch. It can be compared with a hyposphenal ridge, which is usually found in most sauropod anterior caudal vertebrae (Upchurch 1995, 1998), except for those of some titanosaurs (Upchurch and Martin 2003). On its lateral surface there is a shallow depression, which can be identified as a POCDF. The

POCDF is deepest in Cd2 among the well preserved anterior caudal vertebrae (Fig. 10B, G). It is most deeply hollowed out just anterior and just ventral to the postzygapophysis and PODL respectively. The POCDF and CPOL become shallower and blunter, respectively, on more posterior caudal vertebrae. The POCDF is shallower than the SDF in *Tambatitanis*, as in *Huabeisaurus* (D'Emic *et al.* 2013). This feature could be a synapomorphy uniting some East Asian titanosauriforms. In Cd10 and Cd11, the SPOF extends anteriorly beyond the anterior margin of the postzygapophysis and consequently it hollows the wedge that bridges the postzygapophysis and the posterior end of the pedicle of the neural arch (Figs. 18D, 19D).

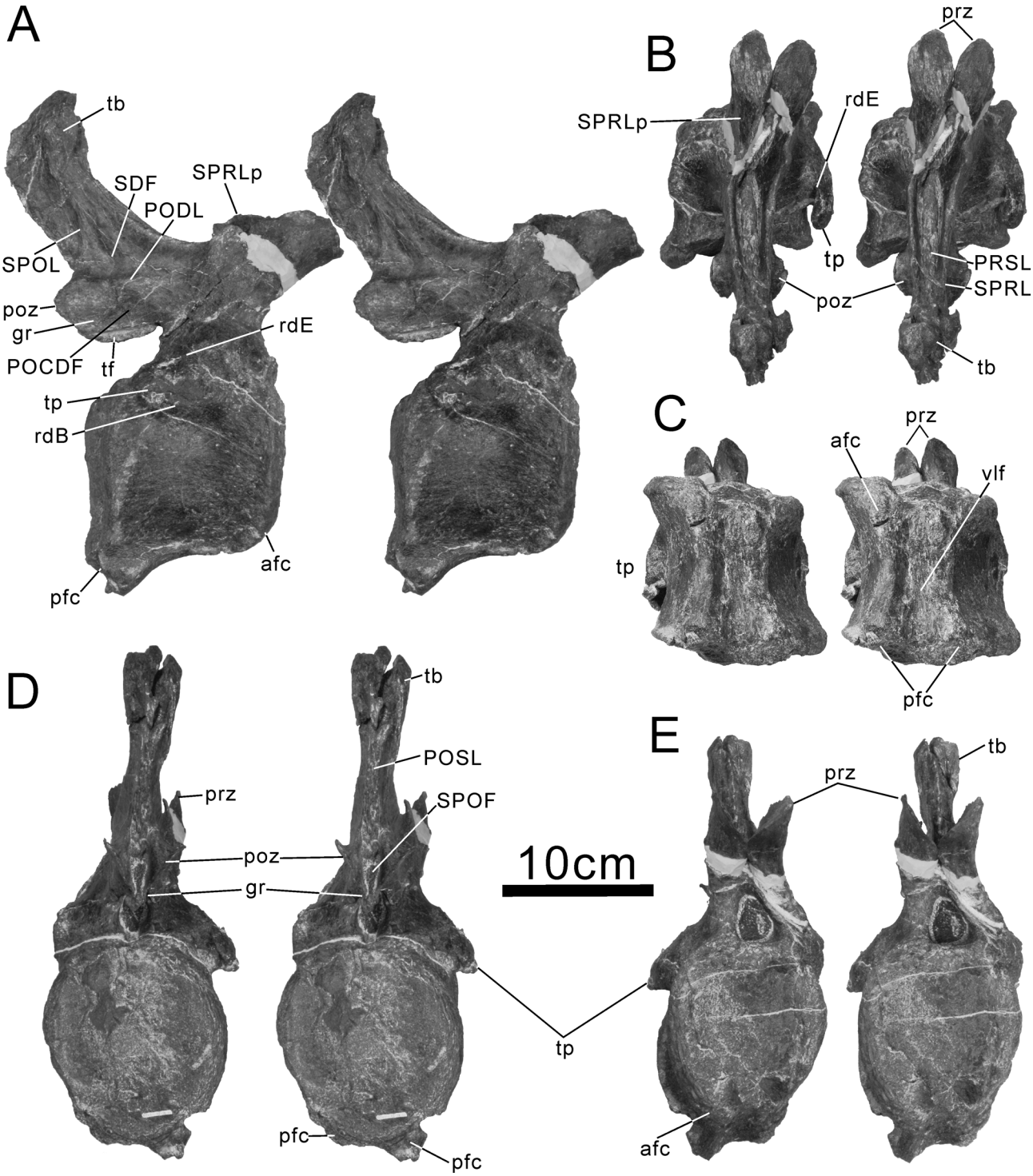

FIGURE 16. *Tambatitanis amicitiae* **gen. et sp. nov.**, holotype (MNHAH D-1029280). Stereopairs of Cd8. **A,** right lateral view. **B,** dorsal view. **C,** ventral view. **D,** posterior view. **E,** anterior view. Scale bar = 10cm. See text for abbreviations.

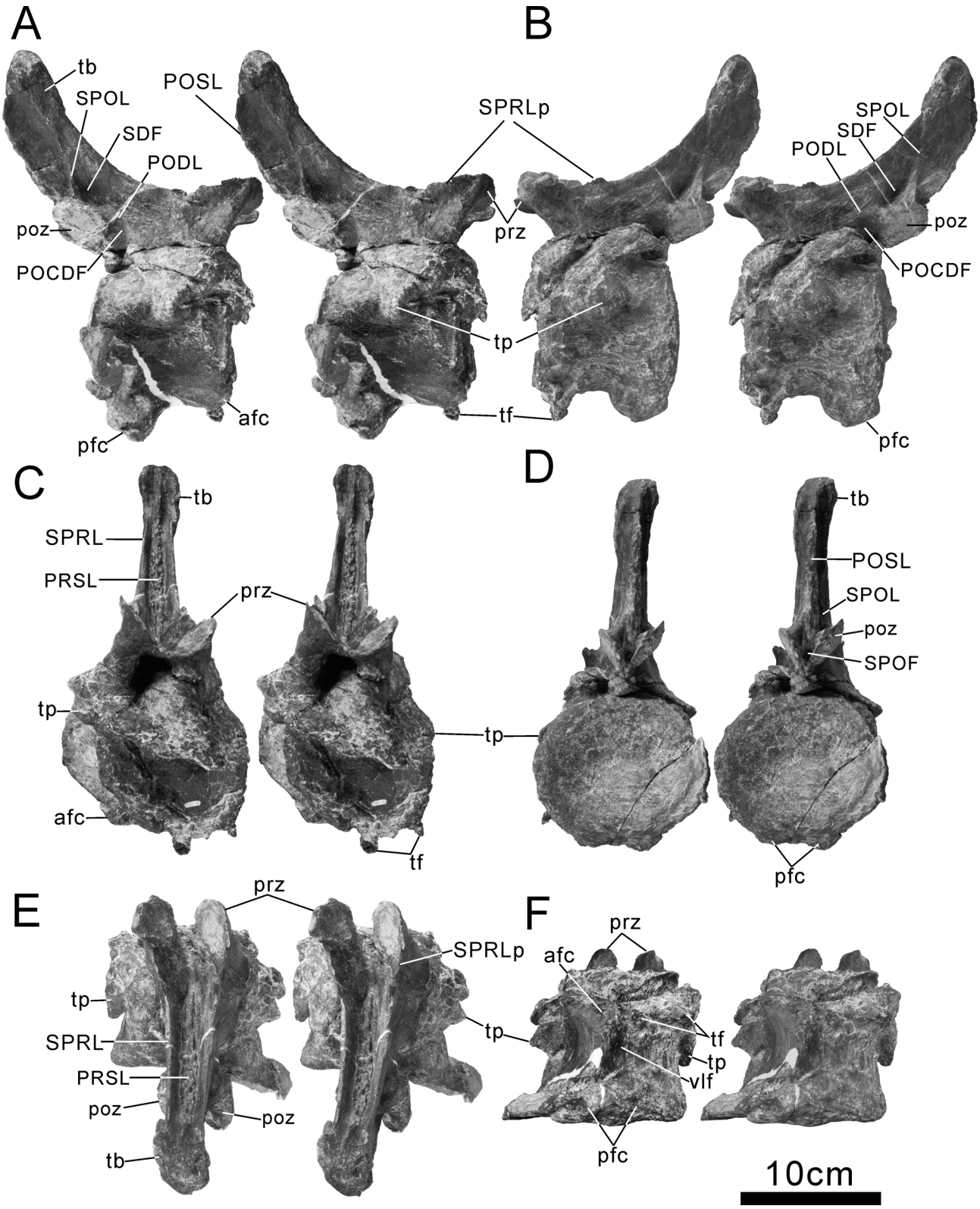

FIGURE 17. *Tambatitanis amicitiae* **gen. et sp. nov.**, holotype (MNHAH D-1029280). Stereopairs of Cd9. **A,** right lateral view. **B,** left lateral view. **C,** anterior view. **D,** posterior view. **E,** dorsal view. **F,** ventral view. Scale bar = 10cm. See text for abbreviations.

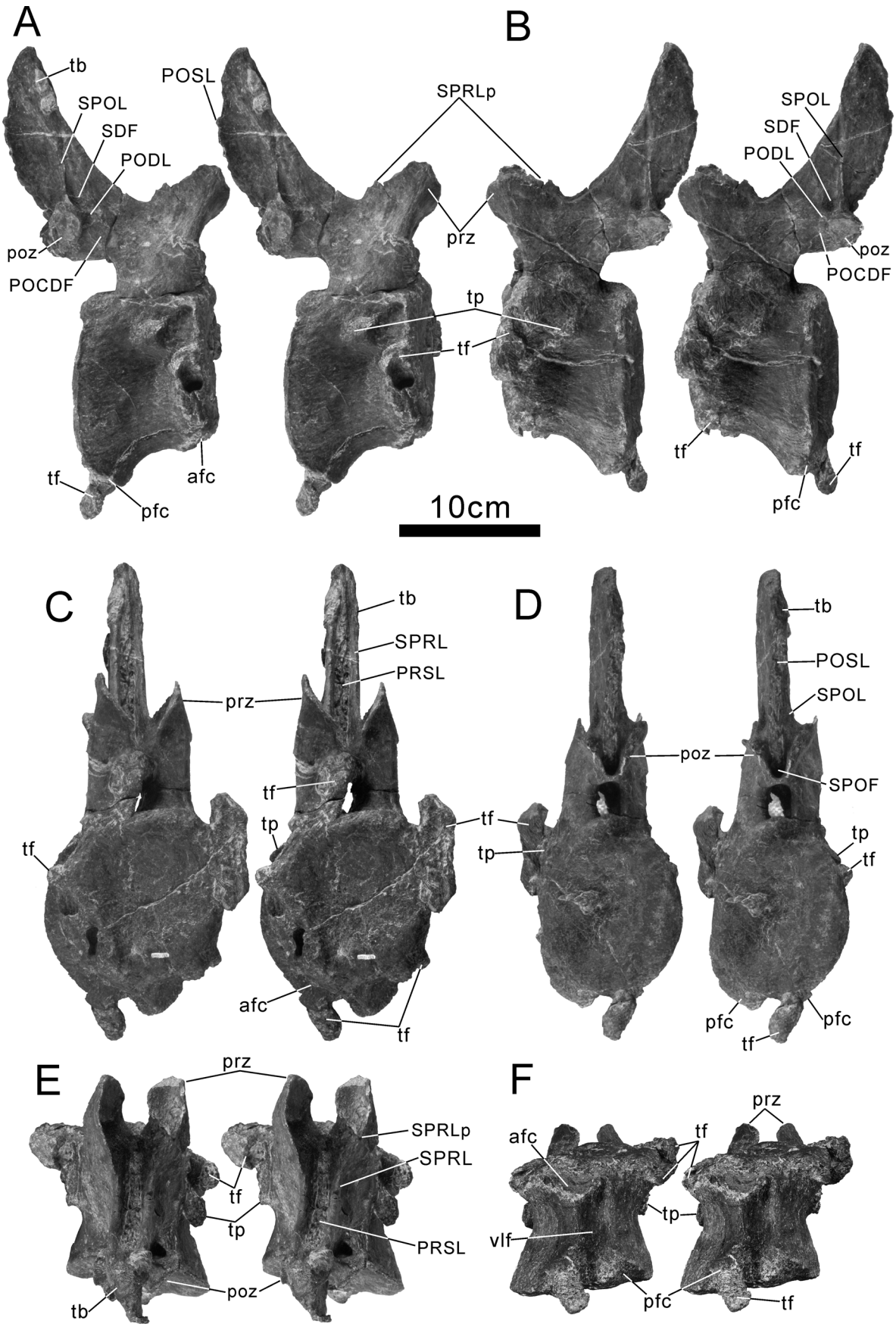

FIGURE 18. *Tambatitanis amicitiae* **gen. et sp. nov.**, holotype (MNHAH D-1029280). Stereopairs of Cd10. **A,** right lateral view. **B,** left lateral view. **C,** anterior view. **D,** posterior view. **E,** dorsal view. **F,** ventral view. Scale bar = 10cm. See text for abbreviations.

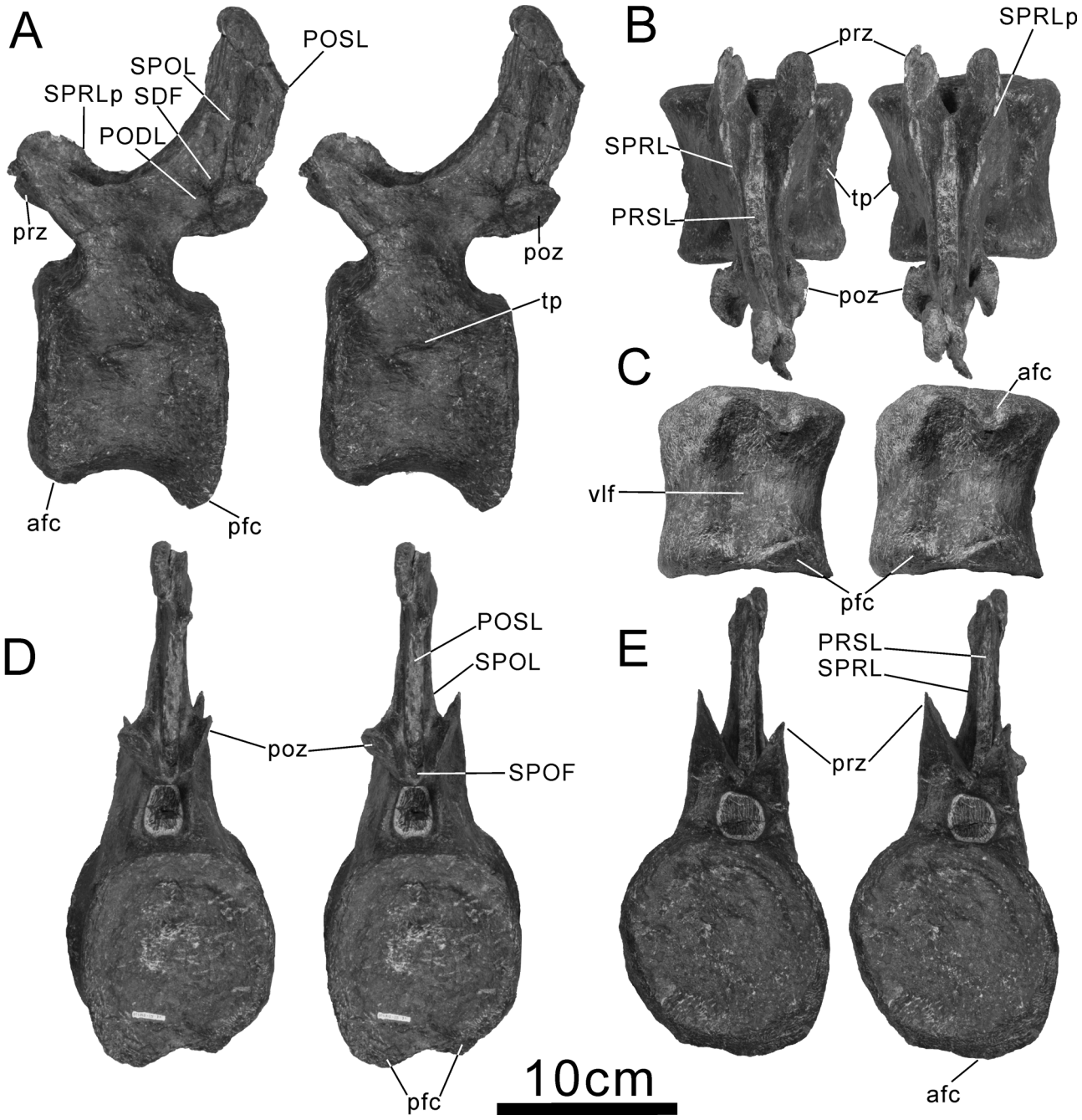

FIGURE 19. *Tambatitanis amicitiae* **gen. et sp. nov.**, holotype (MNHAH D-1029280). Stereopairs of Cd11. **A,** left lateral view. **B,** dorsal view. **C,** ventral view. **D,** posterior view. **E,** anterior view. Scale bar = 10cm. See text for abbreviations.

In Cd2–Cd11, the articular facets of the postzygapophyses are flat or weakly convex laterally, with the exception of Cd8, in which the facets are concave laterally at their most ventral part to form anteroposteriorly extending shallow grooves (gr in Fig. 16A, D). This shallow groove is continuous anteriorly with the POCDF, forming an anteroposteriorly elongate groove extending from the posterior border of the pedicle of the neural spine to the posteroventral corner of the postzygapophysis. Ventral to this groove, the ventral borders of the articular facets of the postzygapophyses and the CPOLs flare ventrally to form a structure comparable with a hyposphene. However, this structure is obviously functionless because the articular facet of the prezygapophysis of Cd9 is flat without the structure comparable with a hypantrum typically seen on the prezygapophysis of *Astrophocaudia* (D'Emic 2013).

The transverse process (or caudal rib) is posteriorly directed as a whole (Fig. 8), as is seen in other titanosauriforms (D'Emic 2012). From Cd1 to Cd6, it extends beyond the posterior end of the centrum (Figs.

9–14). However, the transverse process diminishes in size posteriorly so that by Cd7 (Fig. 15A) it no longer extends to the posterior end of the centrum and by Cd11 it is reduced to a rudimentary projection (Fig. 19A). The bases of the transverse processes of the anterior caudal vertebrae, including those of rudimentary ones, are located on the junction between the pedicle of the neural arch and the centrum, apart from those of Cd1, Cd10 and Cd11, which is situated just ventral to the junction.

In Cd1, the base of the transverse process is anteroposteriorly compressed, plate-shaped, dorsoventrally tall and rectangular in anterior view (Fig. 9). At the junction between the base and the body of the transverse process, the transverse process of Cd1 attains its maximum dorsoventral breadth because of the development of a prominent dorsally pointed projection at the junction (hereafter referred to as tubercle A for simplicity, tu in Fig. 9). The body of the transverse process is mediolaterally flattened, sub-triangular in lateral view, and from the junction between the base and body of the transverse process decreases in dorsoventral breadth toward its distal end. In Cd2–Cd8, the transverse process is L-shaped (Figs. 10–16). The basal part of the transverse process projects outward, perpendicular to the lateral surface of the centrum. It is short mediolaterally and wider anteroposteriorly than dorsoventrally, and constitutes one fifth of the total length of the process. On the other hand, the body (or shaft) of the transverse process is anteroposteriorly elongated, mediolaterally compressed, and extends posteriorly from the junction between the base and body of the process.

The base and body of the transverse process bisect each other at right angles in Cd3–Cd8, so that the body runs nearly parallel to the lateral surface of the centrum (Figs. 11–16). In Cd1 and Cd2, the basal part of the transverse process projects outward perpendicular to the lateral surface of the centrum as in Cd3–Cd8, but it meets the body of the transverse process at an angle of about 135 and 120 degrees in Cd1 and Cd2 respectively, so that the body runs about 45 and 30 degrees to the lateral surface of the centrum in Cd1 and Cd2, respectively (Figs. 9G, 10E).

On the dorsal border of the transverse process of Cd1–Cd7, there is a tubercle A at the junction between the base and body of the transverse process (tu in Fig. 9–15). A similar tubercle on the transverse process has been reported in some titanosauriforms such as *Huabeisaurus* and *Mendozasaurus* (D'Emic *et al.* 2013) and *Baurutitan* (Kellner *et al.* 2005). This process or tubercle could be also homologous with a shoulder or angle that is frequently seen on the dorsal margin of the basal part of the caudal transverse processes of other sauropods (*e.g., Apatosaurus* [Ostrom and McIntosh 1966: pl.32]; *Haplocanthosaurus* [Hatcher 1903: pl.3]; and *Camarasaurus* [Osborn and Mook 1921: pl.76]); it may demarcate the part corresponding to the diapophysis laterally.

In Cd2, a sharp PRDL runs medially from the tubercle A to the lateral face of the pedicle of the neural arch, and then continues dorsally to join the posterior end of the SPRL process (Fig. 10A). The PRDL extends medially from the tubercle A also in Cd1, but its dorsomedial part is missing (Fig. 9). In Cd3, a thin ridge extends posteroventrally from the posterior end of the SPRL process (Fig. 11). This ridge might correspond to a PRDL but it ends at the midpoint of the pedicle of the neural arch. The arrangement of the PRDL and SPRL seen in Cd2 of *Tambatitanis* is similar to that in an anterior caudal vertebra of *Phuwiangosaurus* (Suteethorn *et al.* 2010). In the latter taxon, the PRDL runs dorsomedially from the transverse process and meets the SPRL just posterior to the prezygapophysis. Their junction is not swollen but slightly elevated. The above examples are similar to the arrangement of the PRDL, SPRL and prezygapophyseal tuberosity seen in the first caudal of *Baurutitan* (Kellner *et al.* 2005), as well as those seen just posterior to the prezygapophysis in most anterior caudal vertebrae of *Trigonosaurus* (Campos *et al.* 2005: figs. 31, 32) and *Opisthocoelicaudia* (HS pers. obs.).

Beside the PRDL, two ridges arise from the tubercle A in Cd1–Cd7; one is a short ridge which runs ventrally to demarcate the anterior end of the basal part of the transverse process (rdD in Figs. 9–15) and the other is the dorsal margin of the body of the transverse process which forms an extremely sharp ridge running distally from the tubercle A to the distal end of the transverse process (rdE in Figs. 9–15). The distal end of the transverse process is round in lateral view, capped with a weak and small tuberosity, flat or slightly concave medially and swollen laterally. Although the lateral surface of the body of the transverse process is dorsoventrally convex as a whole, the medial surface of the body is concave dorsoventrally, so that dorsal margin of the body gently overhangs the latter surface. In Cd1, the dorsal margin of the body is inclined posteriorly about 45 degrees in lateral view (Fig. 9E), whereas those of Cd2 to Cd7 are oriented almost parallel to the dorsal border of the centrum in lateral view (Figs. 10–15).

In Cd1 and Cd2, a very blunt ridge (or bulge, hereafter referred to as ridge B for simplicity) arises from the sharp ventral margin of the distal tip of the transverse process. The ridge B extends anteriorly almost parallel to the posteriorly inclining dorsal margin of the body of the transverse process, and then fades out at the level of the

tubercle A (Figs. 9E, 10A). In Cd1, a sharp ridge (hereafter referred to as ridge A for simplicity) extends horizontally from the anteroventral end of a sharp rim, which is located about 2 cm anterior to the distal margin of the transverse process on the medial surface of the process (see below), to the broken anterior end of the transverse process along the ventral border of the body of the process (Fig. 9D, E and J). In Cd2, the ridge A extends nearly horizontally and anteriorly also from the rim on the medial surface of the distal tip of the transverse process about a half the length of the body and then veers ventrally to connect with the posterior border of the base of the transverse process, which is located about a half of the length of the centrum from the distal end (Fig. 10A, D, F).

The medial faces of the transverse processes of Cd1–Cd2 bear fossae and ridges. A blunt ridge (hereafter, ridge C) runs nearly parallel to the ridge A from the lateral face of the centum to the medial surface of the distal end of the transverse process (rdC in Figs. 9, 10). Ridges A and C bound a deep, elongated, mediolaterally narrow and ventrally open fossa (fs4 In Fig. 9J and L). In Cd1, the most medial part of this fossa bears two circular sub-fossae, which are separated from one another by a short, low, and transversely oriented strut that arises from the basal part of the lateral face of the ridge C within the fossa. On the posteromedial surface of the transverse process of Cd1, there is an additional blunt ridge (hereafter, ridge F) extending from the posteromedial face of the tubercle A to the lateral face of the centrum. Between ridges C and F, there are two deep fossae. One of them is ca. 3 cm long oval depression, oriented dorsolaterally, located about 3 cm below the spinous projection, bounded dorsolaterally by ridge F, sharply lipped lateroventrally, and open medioventrally. From this fossa, a slit-shaped fossa extends distally underneath the lip. The other is a 2.5cm long oval fossa, located about 2cm from the distal tip of the process, bounded dorsolaterally and ventrally by the dorsal margin of the body of the transverse process and ridge C respectively, and open medially. These fossae present on the transverse process of Cd1 and Cd2 are possibly pneumatic. On the other hand, ridges C and F may be comparable with the ventral and dorsal bars of the anterior transverse process, both of which are most developed in Diplodocoidea, whereas the latter is reduced in titanosauriforms (Gallina and Otero 2009).

In Cd2, the distal end of the transverse process is globular and wider than dorsoventrally high, whereas in Cd1 it is transversely compressed and round in lateral view. In both caudal vertebrae, the weak rugosity capping the distal end of the transverse process is bordered by a sharp rim about 2 cm anterior to the distal margin of the transverse process. This sharp rim connects the ridge A and the sharp dorsal border of the body of the transverse process in Cd1 and Cd2 (Figs. 9, 10D). On the transverse process of Cd3, the ridge A is moderately sharp, runs nearly horizontally and connects with the sharp dorsal margin of the body via a blunt margin of the transverse process (Fig. 11A, D).

From Cd4 to Cd7, the ridge B becomes prominent and constitutes the ventral margin of the posterior half of the body, which is sharp and bowed ventrally in lateral view (rdB in Figs. 12–15). In these caudal vertebrae, the ridge B connects to the dorsal margin of the body via the margin of the distal end of transverse process instead of the ridge A, which becomes blunt, short and abuts the medial face of ridge B. In Cd4 and Cd5, the margin of the distal end of the transverse process that connects the ridge B and the dorsal margin of the body is blunt. In Cd6 and Cd7, however, the margin is sharp, so that it forms a U-shaped sharp ridge with the ridge B and the dorsal margin of the body.

The transverse process of the Cd8 is basically the same as that of Cd7, aside from its smaller size, the posteroventral orientation of the dorsal margin of its body and the absence of the tubercle A on its dorsal border (Fig. 16A). From Cd9 to Cd11, the transverse process becomes increasingly small and simple. In Cd9 and Cd10, the transverse process is a posteroventrally directed simple projection composed of two parts; one is a flat lateral surface, which faces posterodorsally and laterally, and is bordered by a U shaped ridge, and the other is a short and saddle shaped ventral part of the process, which supports the lateral surface medioventrally (Figs. 17–19). By Cd11, the transverse process is reduced to a low bulge demarcated ventrally by a horizontal short ridge which corresponds to the U shaped ridge seen in Cd6–Cd10.

Cdx1–Cdx11. In Cdx1–Cdx11, the centra are sub-square shaped in anterior and posterior view, being slightly transversely wider than dorsoventrally tall (Table 4, Figs. 20, 21). This shape of the centrum might be the original morphology rather than the result of the postmortem distortion, because the centra found lying on their lateral side (see Cdx1 and Cdx2 in Fig.2) also exhibit the same shape. The subtle dorsoventral compression of the centrum in *Tambatitanis* is not comparable with the more extreme dorsoventral compression of the centrum seen in titanosaurs and some basal titanosauriforms (*e.g.,* the middle-posterior caudal vertebrae of *Lusotitan* [Mannion *et al.* 2013]).

In Cdx1–Cdx11, the centrum is approximately 1.5 to 1.7 times as long anteroposteriorly as transversely wide

(Table 4). These caudal vertebrae of *Tambatitanis* are proportionally more elongated anteroposteriorly than the corresponding caudal vertebrae of other Asian titanosauriforms, such as *Gobititan* (You *et al.* 2003: fig.1), *Phuwiangosaurus* (HS pers. obs.), and *Tangvayosaurus* (HS pers. obs.).

In Cdx1 to Cdx6, there are round small bumps on the anterior and posterior articular facets of the centrum, and on Cdx7 only on the anterior facet (bm in Fig. 20C). A similar bump has been reported in *Tastavinsaurus* (Canudo *et al.* 2008; Royo-Torres 2009). In Cdx1 to Cdx11, the ventral surface of the centrum is flat transversely and set off from the lateral faces by well defined corners (Figs. 20E, 21E). The ventral surface of the centrum of the distal caudal is flat also in *Phuwiangosaurus* (HS pers. obs.). On both ventral ends of the centrum of these caudal vertebrae, there is a pair of weak elevations which corresponds to the articular surfaces for the chevron. In addition to the corners that border the flat ventral surface, a faint ridge occasionally runs anteroposteriorly on the mid height of the flank of the centrum (*e.g.,* Cdx3, Cdx6) and in some cases the ridge is stronger than the ventral corner (*e.g.,* Cdx8). Similar but stronger ridges are developed on the flank of the centum of anterior-middle caudal vertebrae in *Huabeisaurus* (D'Emic *et al.* 2013).

In Cdx1–Cdx11, the pedicles of the neural arch are anteroposteriorly long and dorsoventrally very low (Figs. 8, 20A, 21A, Table 4). In contrast, the pedicles of the middle caudal vertebrae are extremely anteroposteriorly short and dorsoventrally high in some titanosauriforms (*e.g., Malarguesaurus* [González Riga *et al.* 2009: fig.6]; *Tangvayosaurus,* [HS pers. obs.]). In Cdx1, the pedicles are almost centrally located but in more posterior caudal vertebrae they become progressively more anteriorly located, and by Cdx11 the pedicle is situated on the anterior half of the centrum. There is no bulge or ridge at the junction between the centrum and the pedicle of the neural arch, except for in Cdx9, in which a faint anteroposteriorly running ridge is developed on the most ventral part of the lateral flank of the pedicle of neural arch. This faint ridge on Cdx9 is similar to a structure seen in some titanosaurs (*e.g., Baurutitan* [Kellner *et al.* 2005]; *Andesaurus* [Mannion and Calvo 2011] and *Phuwiangosaurus* [HS pers. obs.])

In Cdx1–Cdx11, the prezygapophyses project anteriorly and almost horizontally beyond the anterior end of the centum, are rod shaped, taper anteriorly and are mildly bowed laterally (Fig. 8). In Cdx1 to 6, posterior half of prezygapophysis is convex lateroventrally and concave dorsomedially in cross section. Toward their anterior tips, the right and left prezygapophyses twist clockwise and counterclockwise, respectively, in anterior view, and their tips are concave medially and convex laterally in cross section. On the other hand, from Cdx7 onwards, the prezygapophysis is convex dorsolaterally and weakly concave or flat medioventrally throughout its length. In most titanosauriforms, the prezygapophyses of middle and posterior caudal vertebrae are more robust than in *Tambatitanis,* and their cross sections are frequently circular.

From Cdx1 to Cdx8, the prezygapophyses are linked to each other by a TPRL that forms the roof of the anterior-most part of neural canal (Figs. 20D, 21D). The anterior border of the TPRL is situated at the level of the midpoint between the anterior margin of the pedicle of the neural arch and the anterior end of the centrum from Cdx1 to Cdx6. In Cdx7 and 8, the TPRL is reduced to the extent that its anterior border is located a third of the way back from the anterior margin of the centrum to the anterior border of the pedicle of the neural spine. From Cdx1 to Cdx6, the dorsal surface of the TPRL forms a shallow trough that is posteriorly continuous with a cave-like fossa located just below the anterior end of the neural spine. This fossa is anteroposteriorly deep and transversely narrow, and its roof and floor are covered by a strong rugosity which is comprised of anteriorly projecting spines (rg1 in Figs. 20, 21). The posterior two thirds of the shallow trough on the TPRL is bordered laterally by a thin but distinct ridge, which posteriorly contacts the rugosity associated with the cave-like fossa, but anteriorly is not continuous with the dorsal border of prezygapophysis. This ridge, the combination of the trough on the TPRL and the cave-like fossa (fs in Figs. 20, 21), and the rugosity covering the roof and the floor of the cave-like fossa seem to correspond to the SPRL, SPRF, and PRSL, respectively. In Cdx7 and Cdx8, the dorsal trough on the TPRL is reduced to a small and faint triangular depression, and both the cave-like fossa located behind the depression and the rugosity associated with the fossa also become very rudimentary. From Cdx9 onward, both the depression and the fossa are absent and only the rudimentary rugosity remains at the junction between the prezygapophyses.

In Cdx1–Cdx11, the neural spine is very short dorsoventrally (Figs. 8, 20, 21). From the point just behind the rugosity that covers the roof of the cave-like fossa mentioned above, the anterodorsal border of the neural spine extends posterodorsally to the summit of the spine. The neural spine is transversely narrow and lacks the rugosity along its anterodorsal border, and inclines more gently in more posterior caudal vertebrae (in Cdx1 and Cdx10 it inclines posteriorly 20 and 5 degrees, respectively). The neural spine summit is sub-triangular in lateral view,

transversely flat, and capped by a slightly swollen weak rugose surface. From Cdx1 to Cdx6, the posterior end of the neural spine beneath the neural spine summit flares ventrally toward the laterally projecting postzygapophysis. In Cdx1 and Cdx2, the postzygapophysis is a laterally projecting knob (Fig. 8). From Cdx3 to Cdx6, it is a horizontally projecting wing, the ventral surface of which is somewhat irregular and continuous with the surface of the posterior roof of the neural canal. From Cdx7 onward, the postzygapophysis is thinner and more anteriorly located than the level of the summit of the neural spine (Fig. 8).

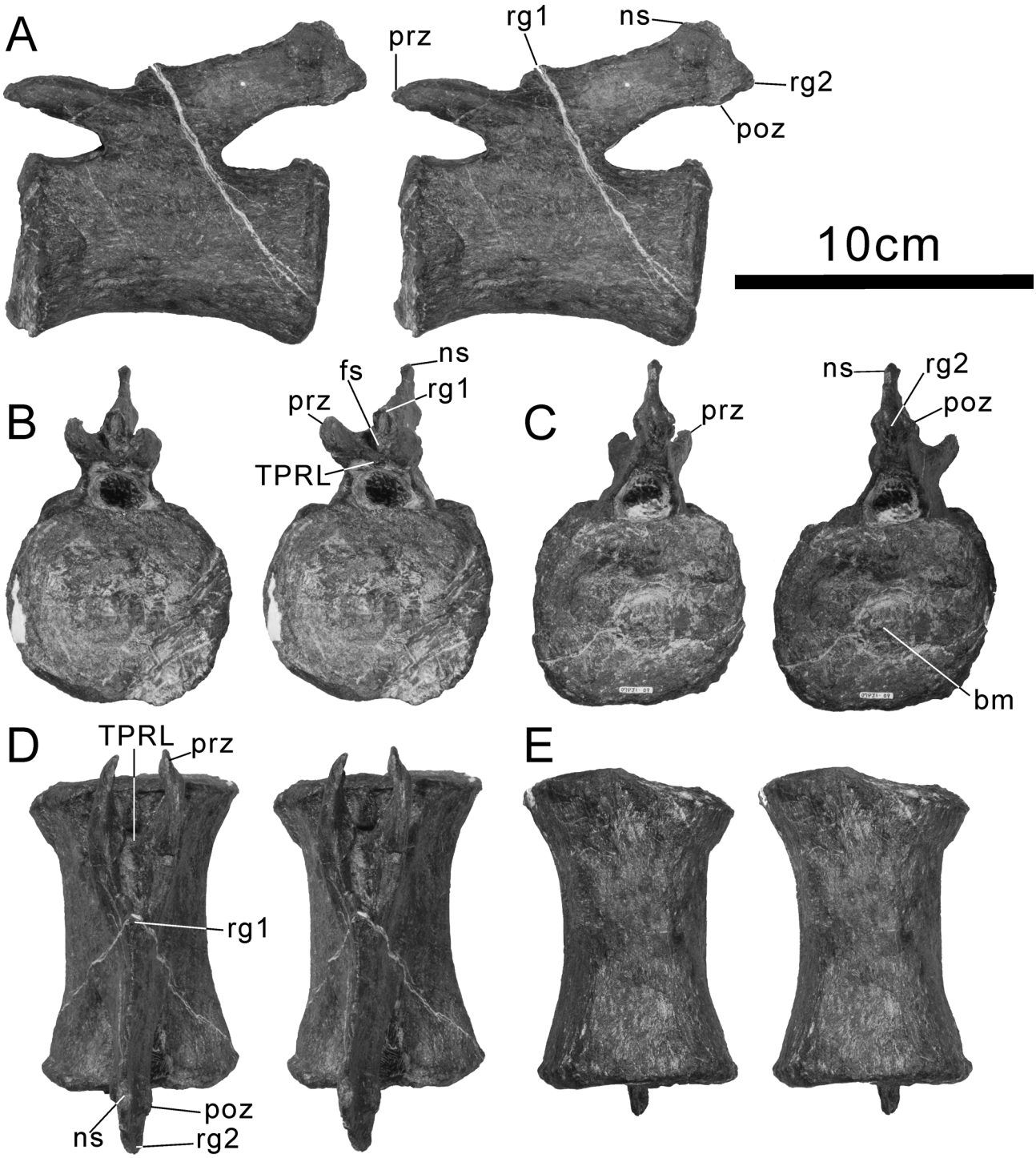

FIGURE 20. *Tambatitanis amicitiae* **gen. et sp. nov.**, holotype (MNHAH D-1029280). Stereopairs of Cdx2. **A,** left lateral view. **B,** anterior view. **C,** posterior view. **D,** dorsal view. **E,** ventral view. Scale bar = 10cm. See text for abbreviations.

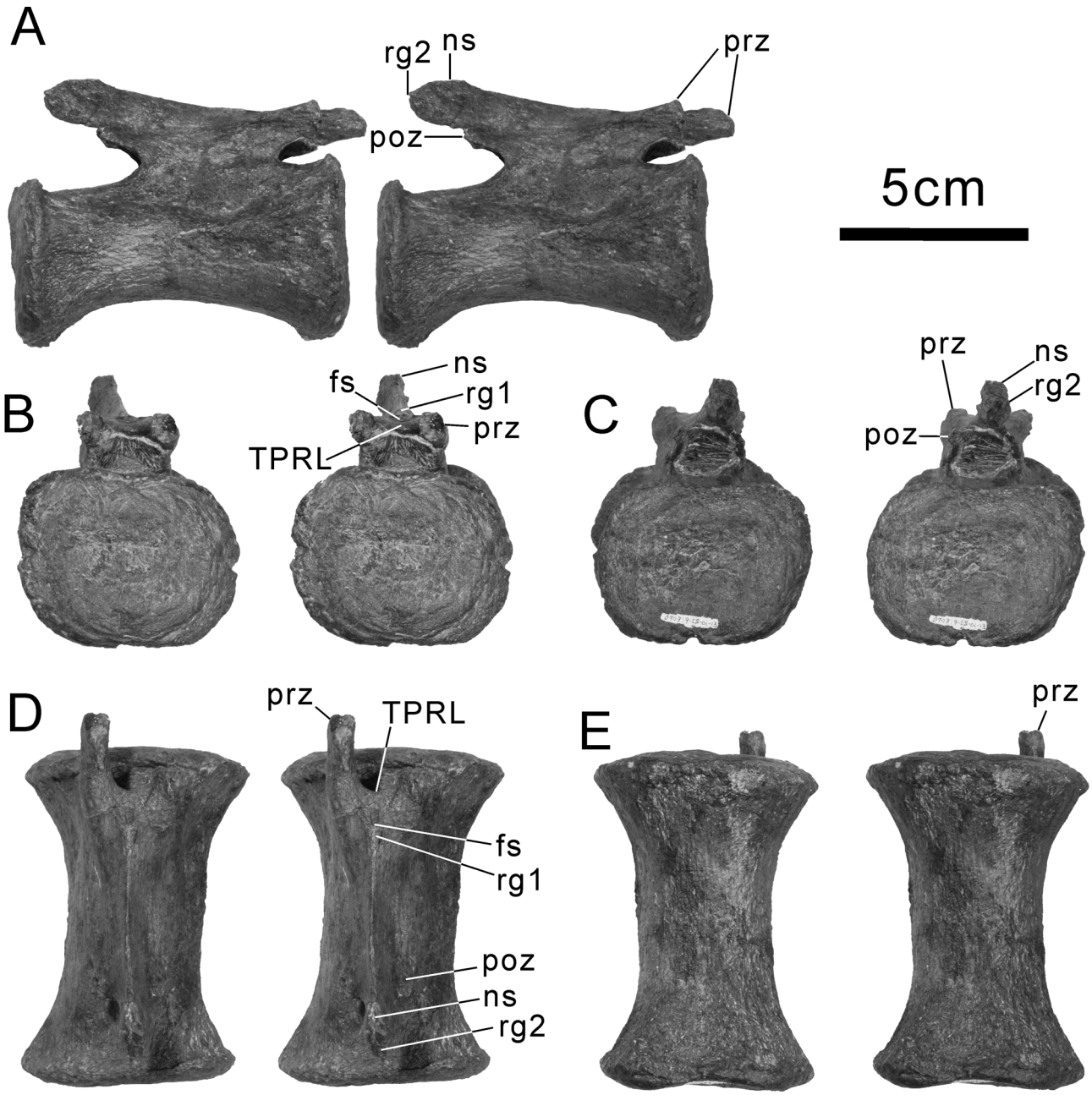

FIGURE 21. *Tambatitanis amicitiae* **gen. et sp. nov.**, holotype (MNHAH D-1029280). Stereopairs of Cdx8. **A,** right lateral view. **B,** anterior view. **C,** posterior view. **D,** dorsal view. **E,** ventral view. Scale bar = 10cm. See text for abbreviations.

Posterior to the postzygapophysis and posteroventral to the neural spine summit, there is rugosity composed of minute posteriorly projecting spines, marking the posterior end of the neural spine (rg2 in Figs. 20, 21). In life this rugosity would have been connected with the rugosity located on the anterior end of the neural spine of the succeeding caudal by the interspinous ligament. In Cdx1, the posterior end of the neural spine is located about 3 cm beyond the posterior articular surface of the centrum, but on more posterior caudal vertebrae it is situated more anteriorly: by Cdx3 it is situated almost even with the posterior end of the centrum, whereas it is located about a ninth of the way forward from the posterior end of the centrum in Cdx10 (Fig. 8).

Among Cdx1–Cdx11, what can be called an articular surface is present only on the right prezygapophysis of Cdx2 and the left postzygapophysis of Cdx3. From Cdx1 to Cdx4, however, the tips of the prezygapophysis and postzygapophysis appear to come close the tips of their counterparts on adjacent caudal vertebrae when succeeding caudal vertebrae are articulated with one another, judging from the position of these caudal vertebrae. From Cdx6 onward, and possibly in Cdx5, however, the prezygapophysis is too short and the postzygapophysis is too

anteriorly situated to contact with their counterparts on the adjacent caudal vertebrae when caudal vertebrae are articulated (Fig. 8) .

Chevrons. Seventeen chevrons are preserved. None of them were found articulated with caudal vertebrae, but based on their position in the quarry (Fig.2), their dimensions, and their serial change in morphology, their proximodistal order in the tail can be reasonably reconstructed. For ease of description, they will be called Ha1–Ha17 according to their presumed anatomical order in the tail. In this numbering system, Hn is more anteriorly located than Hn+1, but none of these chevrons are necessarily consecutive in life.

Ha1 is a simple rod-shaped bone that was found on the right ventral surface of the centrum of Cd3 (Fig. 22A, B). Because of its location in the quarry and its shape, it is considered to be the most anterior chevron among the preserved specimens. This bone is laterally compressed and twisted distally. At its proximal end, it has a sub-circular and weakly concave articular facet, which faces posteriorly and dorsomedially when the shaft of the bone is held vertical. The plane of this facet intersects the longitudinal axis of the bone at an angle of approximately 30 degrees. Below the articular facet, the shaft of the bone is composed of three faces, medial, lateral, and posterior, and thus its horizontal section cross section is triangular. However, the posterior face rapidly diminishes toward the distal tip of the bone, so that the distal half of the rod is mediolaterally flattened with only lateral and medial faces, and slightly twisted. Based on its position in the quarry and the direction of its articular facet, this bone is considered to be the right half of an unfused chevron. Another rod-like chevron was found a few meters away from this bone and is considered to be its counterpart. This is the left half of an unfused chevron; compare to its counterparts it is shorter with a thicker proximal part and has slightly more convex and mediolaterally narrower proximal articular facet.

Unfused anterior-most chevrons have been reported in *Opisthocoelicaudia* (Borsuk−Białynicka 1977) and *Camarasaurus* (Maltese 2002), and those of the former also exhibit a triangular cross section in their proximal part (HS pers. obs.). Unfused chevrons have been also reported in *Alamosaurus* (Gilmore 1946), *Malawisaurus* (Gomani 2005), *Mendozasaurus* (González Riga 2003), *Tastavinsaurus* (Royo-Torres 2009), but they are distal chevrons which are shorter than the anterior unfused chevrons of *Tambatitanis* and *Opisthocoelicaudia*.

Except for these presumable anterior-most chevrons (Ha1), all of the chevrons retrieved from the Kamitaki Quarry are Y-shaped or V-shaped with a ventrally directed ventral ramus (referred to as spine, shaft, blade, or ventral process in previous papers) and dorsal rami (referred to as arms in some previous papers) which bound the haemal canal laterally (Fig. 22). Ha16 and Ha17 are classified as V-shaped chevrons here because their ramus is very short. In both Y-shaped and V-shaped chevrons, the haemal canal is not dorsally closed by crus bridging the dorsal ends of the dorsal rami, and this is a feature broadly shared by macronarian sauropods (Upchurch 1995; Wilson 2002), with the exception of *Dongbeititan* (Wang *et al.* 2007), *Daxiatitan* (You *et al.* 2008) and *Xianshanosaurus* (Lü *et al.* 2009b). As preserved, Ha5 is the dorsoventrally longest among the preserved chevrons (Table 5). However, Ha2 could be originally the longest the chevron series, because the ventral end of the ventral ramus is damaged on most of the preserved chevrons, with the exception of Ha1, 11, 13, 14, and 16. The preserved dorsoventral length of Ha2, 4 and 5 exceeds 40 cm, although the maximum original dorsoventral length of the chevron is not known in MNHAH D-1029280. A chevron longer than 40 cm has been reported in *Alamosaurus* (Gilmore 1946) and *Camarasaurus* (McIntosh *et al.* 1996b), but these exceptionally long chevrons are those of very large individuals. Based on the ratio of the maximum length of the chevron to the maximum height of the centrum, the chevron of *Tambatitanis* is proportionately longer than in *Alamosaurus* and *Camarasaurus*. This ratio is about 2.29 in MNHAH D-1029280, whereas those in *Alamosaurus* and *Camarasaurus* are 1.85 and 1.70, respectively. The same ratio in other sauropods is also less than that of MNHAH D-1029280 (Table 6). Thus the longest chevron of *Tambatitanis* is proportionately the longest known sauropod chevron.

From Ha2 to Ha10, the depth of the haemal canal is on average 25% of the total length of the chevron and never exceeds 30% (Table 5). The dorsoventral depth of the haemal canal of these chevrons is fairly small compared to other titanosauriforms. This small proportion of the depth of the haemal canal is mostly due to the greater development of the ventral ramus in *Tambatitanis* than in other sauropods. From Ha11 onwards, however, the proportional depth of the haemal canal increases posteriorly, starting at more than the 30 % the total length of the chevron, and attaining its maximum (about 60 %) at Ha17 (Table 5).

From Ha2 to 17, the dorsal rami are transversely compressed with a moderately convex lateral surface, which continues onto the lateral surface of the ventral ramus without interruption. On the other hand, the medial surfaces of the dorsal rami are weakly concave to flat, with the exception of those of Ha16 and Ha17, which are flat to weakly convex. In *Apatosaurus*, both the lateral and medial surfaces of the rami of the chevrons are convex

(Upchurch *et al.* 2004b). Anterior and posterior borders separating the lateral and medial surfaces of the dorsal rami are very sharp except for the ventral half of the posterior border of the dorsal rami of Ha2.

TABLE 5. Measurements of (in mm) chevrons of *Tambatitanis amicitiae* **gen. et sp. nov.**, holotype (MNHAH D-1029280). For an explanation of the measured parameters see Fig. 3.

	Wha	Hha	Dhc	Whabc	Whafap	Whafaml
Ha-1(right half)	-	194	-	-	-	-
Ha-1(left half)	-	153	-	-	-	-
Ha-2	114	403+	117	36	51	51
Ha-3	105	342+	80	49	56	43
Ha-4	88	405+	97	42	45	40
Ha-5	80	410+	93	32	47	41
Ha-6	81	352+	88	38	44	33
Ha-7	67	345+	86	37	46	32
Ha-8	75	326+	83	33	49	34
Ha-9	96	252+	76	26	37	36
Ha-10	82	270+	69	25	44	36
Ha-11	72	243	76	23	41	26
Ha-12	82	197+	66	22	46	26
Ha-13	61	165	55	22	45	24
Ha-14	53	158	64	22	41	21
Ha-15	51	99+	66	15	34	18
Ha-16	28*2	102	51	15	27	14
Ha-17	53	82+	49	16	28	15

TABLE 6. The ratio of the maximum length of the chevron to the maximum height of the centrum in various sauropods.

taxon	maximum length of chevron	maximum height of centrum	maximum length of chevron/maximum height of centrum	ref.
Tambatitanis amicitiae	410	179	2.29	this work
Alamosaurus sanjuanensis	403	218	1.85	Gilmore 1946
Opisthocoelicaudia skarzynskii	340	240	1.42	Borsuk−Białynicka1977
Tastavinsaurus sanzi	245	202	1.21	Royo Torres 2009
Camarasaurus lewisi	402	236	1.70	McInthosh *et al.* 1997b
Camarasaurus grandis	360	245	1.25	McInthosh *et al.* 1996a
Dicraeosaurus hansemanni	319	208	1.53	Janensch 1929
Mamenchisaurus hochuanensis	335	350	0.95	Young and Chao 1972
Omeisaurus jiaoi	325	280	1.16	Jiang *et al.* 2011
Omeisaurus tianfuensis	380	260	1.46	He *et al.* 1988

The shape and length of the ventral ramus varies among specimens, whereas that of the dorsal ramus does not. In lateral view, the ventral rami in Ha2, Ha4–Ha7, Ha8–Ha10, Ha11–Ha13 and Ha14 are dorsoventrally straight, slightly curved posteriorly, moderately curved posteriorly, strongly curved posteriorly and straight dorsoventrally, respectively. From Ha11 to Ha14, the ventral part of the ventral ramus forms the anteroposteriorly long and transversely thin blade, whereas it is rod-shaped and anteroposteriorly compressed in Ha3–Ha10 and Ha2, respectively.

The ventral ramus is composed of four surfaces, namely anterior, posterior and left and right lateral surfaces. The lateral surface of the ventral ramus is continuous with those of the dorsal rami, whereas the anterior and posterior surfaces of the ventral ramus are connected to the medial surfaces of the dorsal rami. Lateral surfaces are separated from the anterior and posterior surfaces by anterior and posterior borders, respectively, and those borders are continuous with the anterior and posterior borders of the dorsal rami respectively. In addition to these borders, a bulge runs dorsoventrally on the distal half of the lateral surface. The location and the size of these features vary in the ventral ramus of Ha2–Ha14.

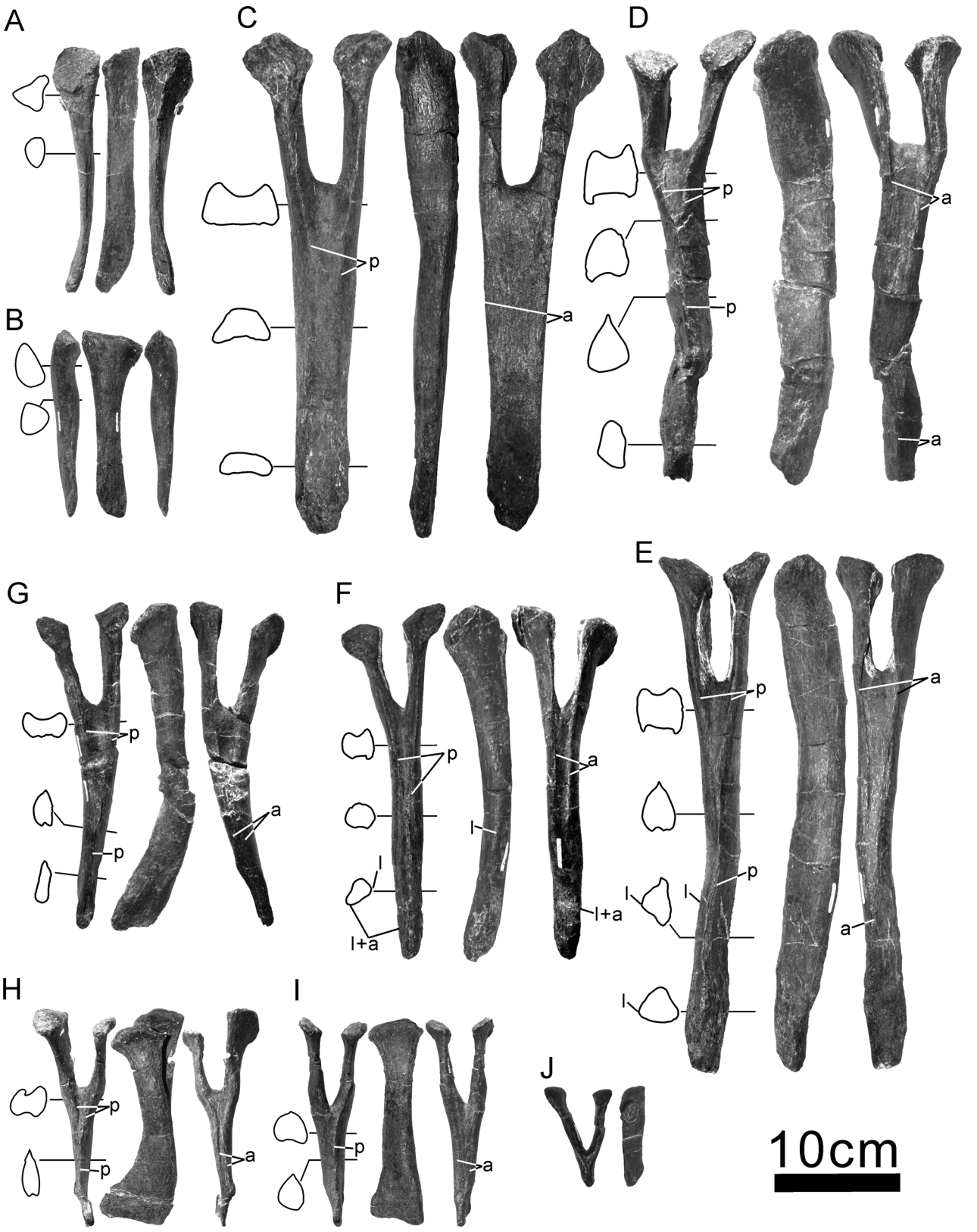

FIGURE 22. *Tambatitanis amicitiae* **gen. et sp. nov.**, holotype (MNHAH D-1029280). Chevrons. **A,** right half of Ha1. **B,** left half of Ha1. **C,** Ha2. **D,** Ha3. **E,** Ha4. **F,** Ha10. **G,** Ha11. **H,** Ha13. **I,** Ha14. **J,** Ha17. In **A** through **I**, three photos from left to right are in posterior, lateral, and anterior views, respectively. In **J**, the two photos from left to right are in posterior and lateral views, respectively. In **A** to **I**, silhouettes arranged from top to bottom on the left side are horizontal cross sections of the chevron, and their positions are indicated by horizontal lines. In horizontal cross sections of **A** to **I**, posterior is to the top, and right lateral is to the right of the page. Letters "a", "p", "l" and "l+a" indicate the anterior and posterior borders, the lateral bulge and fused lateral bulge and anterior border, respectively.

On Ha2, all four surfaces continue to the distal tip of the ventral end of the preserved portion of the ventral ramus, with sharp anterior borders and blunt right and left posterior borders whose distal parts are indistinct. Thus, the lateral surfaces are incompletely separated from the anterior surface at the most distal part of the ventral ramus. The anterior, lateral and posterior surfaces of the ventral ramus are the broadest, medium-breadthed and the narrowest surfaces, respectively. The transverse section of the ventral ramus is trapezoidal and its longer base, legs, and shorter base correspond to the anterior, lateral and posterior surfaces, respectively (Fig. 22C). The anterior surface is flat to slightly concave. The proximal half of the lateral surface is weakly convex, whereas a shallow dorsoventrally elongated groove is present on the distal part of the surface. The dorsal one third of the posterior surface (about 5 cm below the ventral margin of the haemal canal) is concave transversely, forming a shallow dorsoventrally extending groove. On the middle of the ventral ramus, the posterior surface becomes weakly convex both transversely and longitudinally. On the ventral one third of the ventral ramus, the posterior surface becomes slightly concave transversely.

The ventral ramus of Ha2 is compressed anteroposteriorly rather than laterally, in contrast to those of other chevrons of MNHAH D-1029280. However, the anteroposteriorly compressed morphology of the ventral ramus of the first or second chevron appears to be not uncommon in Titanosauriforms. The ventral ramus is anteroposteriorly compressed on the first chevron of *Graffatitan* (Janensch 1950), *Andesaurus, Muyelensaurus, Rinconsaurus* (Mannion and Calvo 2011), *Malawisaurus* (Gomani 2005: fig. 17a), *Chubutisaurus* (Carballido *et al.* 2011), and *Neuquensaurus* (Salgado *et al.* 2005). A chevron of *Phuwiangosaurus* (SM PW5-56) described as the first chevron by Martin *et al.* (1999) could be also of this type, having an anteroposteriorly compressed ventral ramus. The second chevron of *Epachthosaurus* may also exhibit a comparable condition with it in its transversely widened ventral ramus (Martínez *et al.* 2004).

Ha3–Ha11 were found scattered in an area ventral to the articulated series of Cd5–Cd8 (Fig.2). They are completely disarticulated from the caudal vertebrae but their relative position in the quarry roughly corresponds to their serial order in the body. Judging from this order and their morphology, these specimens seem to represent a consecutive series of chevrons.

Ha3 is intermediate in morphology between the more posterior chevrons and Ha2 (Fig. 22D). In anterior and posterior views, the haemal canal is U-shaped on Ha2 and 3, whereas it is V-shaped on more posterior chevrons, with the exception of Ha13, in which it is U-shaped (to be exact, the bottom of the canal is almost flat transversely). On Ha3, the anterior surface continues from the ventral margin of the haemal canal to the ventral end of the ventral ramus, as on Ha2. The dorsal one third of the surface is gently concave transversely and bordered laterally by thin and sharp anterior borders. The rest of the surface is flat and bordered laterally by blunt anterior borders. The posterior surface of Ha3 is similar to that of more posterior chevrons. It is transversely concave and triangular in posterior view and restricted to the most dorsal part of the ventral ramus. The posterior borders delimiting the surface laterally become blunt and indistinct ventrally as they approach each other and then they conjoin to form a single sharp medially running border (hereafter referred to as single posterior border for simplicity) at the point about 6 cm below the ventral margin of the haemal canal. Below this point, the single posterior border continues ventrally to the ventral tip of the ventral ramus. The dorsal half of this border is very sharp, whereas its ventral half is dull. The ventral two third of the ventral ramus forms an isosceles triangle in cross section, with the short base and the longer two equal sides representing the posterior and lateral surfaces, respectively. Thus the ventral ramus is transversely compressed rather than anteroposteriorly as in Ha2.

From Ha4 to Ha8, the structure of the posterior surface and the posterior borders is basically the same as that of Ha3, except for the level at which the posterior borders merge with each other to form a single posterior border (Fig. 22E). The posterior borders are conjoined more ventrally than in Ha3; they are conjoined 7, 10, 9, 10, and 8 cm below the ventral margin of the haemal canal on Ha4, Ha5, Ha6, Ha7, and Ha8 respectively. In other sauropods, the extent of development of the anterior and posterior surfaces on the ventral ramus is not clear because they have only ever been described in *Apatosaurus* as posterior grooves (Upchurch *et al.* 2004b). However, judging from the published figures of some specimens, the posterior surface is less developed in forms exhibiting a deep haemal canal (*e.g.,* Santucci and Arruda-Campos 2011: fig. 7).

From Ha4 to Ha8, the structure of the dorsal half of the lateral and anterior surfaces is uniform whereas that of their distal half varies. The anterior surface is shallowly concave transversely, and extends only to the midpoint of the ventral ramus (Fig. 22E). The anterior borders are thin and sharp, gradually approach each other towards the midpoint of the ventral ramus and become very weak just before they conjoin to form a single sharp medially

running border (hereafter referred to as single anterior border for simplicity). Thus the level where the anterior borders merge with each other to form single anterior border is lower than the comparable level on the posterior surface where the posterior borders conjoin. Additionally, the single posterior border is always sharper than the single anterior border on the same chevron. On Ha4 and Ha5, the single anterior border is indistinct approximately halfway down the ventral ramus. At the point about three quarters of the way down the ventral ramus, it is moderately sharp but soon becomes indistinct ventrally and then fades out. On Ha6 and 7, the single anterior border is sharp at the point where it emerges but becomes gradually less sharp distally from the point about two thirds of the way down the ventral ramus. On Ha8, the single anterior border is indistinct along the length of the ventral ramus.

From Ha3 to Ha8, the lateral surface is the widest surface of the bone and its dorsal half is gently convex transversely (Fig. 22D, E). From Ha5 to Ha8, both the left and right lateral surfaces are divided into anterior and posterior halves by the lateral bulge that extends from the midway point to the distal end of the distal ramus. About 2 to 3 cm above the distal end of the ventral ramus, the lateral bulge bears a small swelling, making the transverse width of the ramus of this level slightly greater than the adjacent parts of the ramus. On Ha5 and Ha8, the ventral parts of the anterior halves of the lateral surfaces twist anteriorly and merge with each other to form an anteriorly facing surface at the level where the single anterior border fades out. This surface does not correspond to the anterior surface mentioned above because it is delimited not by the anterior borders but by the lateral bulges. Ha4 also has an anteriorly facing surface at the most ventral part of the ventral ramus. It is continuous only with the anterior part of the left lateral surface, bordered by the left lateral bulge and the most distal part of the single anterior border, which is off to the right side distally.

The structure of Ha10 is basically same as that of Ha8, except for the bluntness of the single posterior and anterior borders on the ventral half of the ventral ramus (Fig. 22F). Lateral bulges are also present on the both sides but they develop asymmetrically. On the left side of the ventral ramus, the lateral bulge twists anteriorly and merges with the blunt single anterior border (l+a in Fig. 22F), so that the anterior and posterior halves of the lateral surface diminish and expand ventrally, respectively. On the contrary, on the right side the lateral bulge twists posteriorly and merges with the blunt posterior ridge at the ventral apex of the ventral ramus, so that the posterior and anterior halves of the lateral surface diminish and expand ventrally, respectively. The dorsal half of Ha9 is fairly well preserved and structurally identical to that of Ha10. The ventral half of Ha9 is poorly preserved, but appears to be identical to that of Ha10 in basic structure, because the preserved portions of the single posterior and anterior borders are as indistinct as those of Ha10.

On Ha11, Ha13 and Ha14, the single posterior and anterior borders are very sharp and clearly separate the lateral faces of the ventral part of the ventral ramus, which forms an anteroposteriorly long and transversely thin blade (Fig. 22G–I). The anteroposterior width of this blade increases towards its ventral end, where its sharp ventral border runs anteroposteriorly. The anterior and posterior ends of this ventral border meet the ventral ends of the single anterior and posterior border of the ventral ramus to form distinct angles, in contrast to the round or rectangular ventral end of the other chevrons. The blade of the distal ramus is widest anteroposteriorly on Ha13. The anteroventral corner of the blade is situated even with (in Ha14) or posterior to (in Ha12 and 13) the single anterior border of the ramus. Therefore, the blade totally lacks a cranial process that is present on the asymmetric chevrons, including that of *Andesaurus* (Otero *et al.* 2012), and the anteroposteriorly expanded shape of the most ventral part of the blade is created solely by the posterior extension of the ventral part of the ventral ramus. The ventral ramus decreases posteriorly in dorsoventral length, and by Ha14 the depth of the haemal canal becomes almost the same as the dorsoventral length of the ventral ramus (Fig. 22I). Though its distal end is missing, Ha12 may also have had an anteroposteriorly long and transversely thin distal end judging from the remaining part of the ventral ramus.

On Ha11 and 12, the structure of the posterior surface and border of the dorsal half of the chevron are basically identical to those of Ha4–Ha8. However, the anterior surfaces are different; the anterior surface forms a very narrow groove with a small swelling, which occupies the most dorsal part of the groove. On Ha13, the anterior surface is also transversely very narrow ventrally but lacks a swelling on its most dorsal part (Fig. 22H). Unlike in Ha3–Ha12, the posterior border of Ha13 remains sharp event at the point where they unite with each other. Ha13 has a swelling on its lateral surface at the junction between the dorsal and ventral ramus. A similar protuberance has been reported in *Aeolosaurus* but in that taxon it is located on the ventral half of the dorsal ramus (Santucci and Arruda-Campos 2011). Ha14 has also similar but weaker swelling on the ventral end of its dorsal ramus (Fig. 22I).

On Ha14, the left posterior border is blunt, whereas the right one is fairly sharp. They are united to form a sharp single posterior border about 2cm below the ventral border of the haemal canal, which extends to the posteroventral corner of the ventral ramus. On the other hand the anterior borders are relatively dull and meet each other at the anteroventral corner of the blade. The anterior border is only slightly convex at the most dorsal part and the rest of it is entirely flat. On Ha15 to 17, the posterior and anterior surfaces and borders are basically identical to those of Ha14, but the ventral ramus itself is extremely shortened, so that in anteroposterior view Ha17 is V shaped rather than Y shaped (Fig. 22J).

The shape of the ventral ramus is unique for *Tambatitanis* among sauropods. In sauropods in general, the ventral rami of the anterior chevrons are compressed transversely, blade-like and have ventral margins that are rounded in lateral view, with the exception of *Cetiosaurus* (Upchurch and Martin 2002, 2003). From Ha3 to Ha10, however, the ventral rami are rod-shaped rather than blade shaped. Among the retrieved chevrons of *Tambatitanis*, Ha11 and possibly Ha12 are most similar to this general shape of the ventral ramus of other sauropod chevrons, but their distal ends are anteroposteriorly nearly straight rather than round in lateral view.

The ventral ends of Ha14 and Ha13, especially that of Ha13, are somewhat similar to those of the asymmetric chevrons of other sauropods (Otero *et al.* 2012), in that ventral end of the ventral ramus is fairly longer anterior posteriorly than the dorsal parts. However, the asymmetric chevrons are V-shaped, having a reduced ventral ramus. Otero *et al.* (2012) also classified a chevron of *Andesaurus* figured in Mannion and Calvo (2011: fig. 8D) as an asymmetric chevron, although it has a moderately developed ventral ramus. It is most similar to Ha14 and 13 of *Tambatitanis* among known sauropod chevrons because the latter also have a moderately developed ventral ramus. However, as mentioned above, Ha14 and 13 of *Tambatitanis* are distinguished from the asymmetric chevrons of *Andesaurus* and diplodocoids in they lack cranial processes on their distal end, and thus represent a type of chevron hitherto unknown in sauropods, except for in *Gobititan*. Three of the five chevrons known for *Gobititan* are similar to Ha13 and Ha14 in having an anteroposteriorly long and transversely thin blade without cranial processes, but which are more robust than Ha13 and Ha14 of *Tambatitanis* (HS pers. obs.). The last two preserved elements in the chevron series of *Huabeisaurus* (HS pers.obs.) and the 8th chevron of *Tastavinsaurus* (Royo-Torres 2009) are also somewhat similar to Ha13 and 14 in the distal anteroposterior expansion of the blade but differ from those of the *Tambatitanis* in their round ventral border of the blade in lateral view.

On Ha1–Ha2 and Ha9–Ha17, the proximal articular surface faces posterodorsally and slightly medially and is not divided (Fig. 22). On the other hand, the proximal articular surface is divided into anterior and posterior facets by a bulge running mediolaterally on both dorsal rami on Ha4 to Ha8, and only on the right ramus on Ha3. The anterior facets face anterodorsally, whereas the posterior ones face posterodorsally and slightly medially, and the angle between them ranges between 100 and 130 degrees. The ratio of the area of anterior facet to that of the posterior facet is about one fifth on Ha4 and 5, one third to one fourth on Ha6 and 7 and one sixth on Ha8. When articulated with the centrum, these chevrons slope posteroventrally at about 45 degrees to the plane parallel to the articular facet of the centrum, because the anterior half of the proximal articular surface of the chevron articulates with the steeply inclined and posteroventrally sloping posterior chevron facets of the centrum, whereas the posterior half of the proximal articular surface of the chevron articulates with the anterior chevron facet of the succeeding centrum that is lateroventrally facing but extends almost parallel to the ventral border of the centrum.

The subdivision of the proximal articular surface, namely the double articular facet, is present in *Aeolosaurus* (Salgado & Coria 1993; Bonaparte 1996; Powell 2003; Casal *et al.* 2007; Santucci and Arruda-Campos 2011), *Neuquensaurus* (Mannion and Calvo 2011), *Rapetosaurus* (Curry Rogers 2009), *Isisaurus* (Jain and Bandyopadhyay 1997), *Maxakalisaurus* (Kellner *et al.* 2006), *Mendozasaurus* (González Riga 2003), *Tastavinsaurus* (Canudo *et al.* 2008), *Lusotitan* (Mannion *et al.* 2013) and *Phuwiangosaurus* (HS pers. obs.). Anterior and posterior subdivision of the proximal articular surface of the chevron is also known in those having the crus bridging the left and right dorsal rami of the chevron: *e.g., Apatosaurus* (Upchurch *et al.* 2004b), *Cetiosaurus* (Upchurch and Martin 2002, 2003) and *Tazoudasaurus* (Allain and Aquesbi 2008). In *Maxakalisaurus*, *Aeolosaurus* and *Mendozasaurus*, the posterior facet is concave and faces posteriorly (Kellner *et al.* 2006; Santucci and Arruda-Campos 2011). In *Tambatitanis,* the posterior facet is flat to weakly concave and has a shallow incision at its posteromedial corner. This incision appears to be identical to a transversely running furrow on the proximal articular facet of the chevron of *Phuwiangosaurus* (D'Emic 2012). As has been noted by Mannion and Calvo (2011), the distribution of the double articular proximal facet of chevron in sauropods is currently not clear and consequently its taxonomic value is not certain. It should be also noted, however, that the subdivision of

the proximal articular surface could be restricted to a certain part of the chevron series of a given species or individual, as exemplified by the case of *Tambatitanis*.

Taxonomic remarks and phylogenetic analysis

Generic and specific status of *Tambatitanis amicitiae.* All of the sauropods for which overlapping elements with *Tambatitanis* are known are not congeneric and/or conspecific with *Tambatitanis amicitiae*, based on the comparison of such elements.

The combination of mildly amphicoelous centra and unique features of the neural arch and spine of the anterior caudal vertebrae distinguishes *Tambatitanis amicitiae* from most of the sauropods for which the caudal vertebrae are known. Mamenchisaurids, some diplodocoids, some basal titanosauriforms and most titanosaurs are distinguished from *Tambatitanis amicitiae* in having procoelous or opisthocoelous caudal centra. Among the East Asian titanosauriforms, *Daxiatitan* (You *et al.* 2008), *Dongbeititan* (Wang *et al.* 2007), and *Xianshanosaurus* (Lü *et al.* 2009b) are distinguished from *Tambatitanis amicitiae* by having procoelous caudal vertebral centra, whereas *Opisthocoelicaudia* (Borsuk-Białynicka 1977), *Borealosaurus* (You *et al.* 2004) and *Sonidosaurus* (Xu *et al.* 2006) possess opisthocoelous centra. *Tambatitanis* is distinguished from all of the sauropods for which the neural spines of the anterior caudal vertebrae are known by its very unique morphology of the anterior neural spine. The following East Asian titanosauriforms that have amphicoelous or amphiplatyan caudal centra lack this unique morphology of the anterior neural spine: *Dongyangosaurus* (Lü *et al.* 2008); *Fusuisaurus* (Mo *et al.* 2006); *Huabeisaurus* (Pang and Cheng 2000); *Huanghetitan liujiaxiaensis* (You *et al.* 2006); "*Huanghetitan" ruyangensis* (Lü *et al.* 2007); *Phuwiangosaurus* (Martin *et al.*1999; Suteethorn *et al.* 2009), and *Yunmenglong* (Lü *et al.* 2013). A fragment of the neural spine of an anterior caudal is the only the caudal element known for *Qingxiusaurus* (Mo *et al.* 2008), but the spine differs from that of *Tambatitanis* in being anteroposteriorly flat and transversely wide.

Some East Asian titanosauriforms can be compared directly with *Tambatitanis* in caudal vertebral characters other than the shape of articular surface of the centrum and the shape of the anterior neural spine. *Baotianmansaurus* (Zhang *et al.* 2009) differs from *Tambatitanis* in having a pear-shaped neural canal that is seen on a poorly preserved anterior caudal vertebra from which the neural spine is missing. A series of 41 caudal vertebrae are known for *Gobititan* but the most proximal caudal vertebra among them lacks transverse processes (You *et al.* 2003). Therefore, the caudal elements preserved both in *Tambatitanis* and *Gobititan* are the middle caudal vertebrae and chevrons. The basic configuration of these elements of *Gobititan* is very similar to that of *Tambatitanis* but differs in that the posterior middle caudal vertebrae are proportionally shorter anteroposteriorly, the caudal prezygapophyses are robust and the chevron is robust. *Jiutaisaurus* (Wu *et al.* 2006) is also known from a series of disarticulated middle and distal caudal vertebrae. This taxon differs from *Tambatitanis* in having anteroposteriorly shorter posterior middle caudal vertebrae and chevrons with a deeper haemal canal. In *Jiangshanosaurus,* the presumed first caudal vertebra is slightly procoelous (Tang *et al.* 2001), but the anterior articular surface of Cd1 of *Tambatitanis* is not preserved. However, the neural spine of the posterior anterior caudal appears to be different from that of *Tambatitanis*. Judging from the description and figures in Tang *et al.* (2001), the caudal vertebra identified as the 13th or 14th caudal by the authors appears to be comparable with Cd10 or Cd11 of *Tambatitanis* in the size of the transverse process and the proportion of the centrum. The ventral half of the neural spine of this caudal is similar to that of Cd10 or Cd11 of *Tambatitanis*, but its dorsal half differs in its greater anteroposterior width and the stronger development of the dorsal half of PRSL.

Tambatitanis can be distinguished from some titanosauriform sauropods for which no caudal elements are known by the features of the teeth, ribs, ilium or braincase. *Tambatitanis amicitiae* is clearly not congeneric or conspecific with any sauropods having a tooth slenderness index of <3, including the East Asian titanosauriforms *Euhelopus* (Wiman 1929; Wilson and Upchurch 2009), *Fukuititan* (Azuma and Shibata 2010) and *Yongjinglong* (Li *et al.* 2014). *Ruyangosaurus* differs from *Tambatitanis* in having a dorsal rib that lacks pneumatic fossa on the tuberculum (Lü *et al.* 2009a). *Qiaowanglong* (You and Li 2009) is distinguished from *Tambatitanis* by the lack of the pneumatic foramen connected to the internal chamber on the medial surface of the ilium (HS pers. obs.). The low occiput distinguishes *Tambatitanis* from *Nemegtosaurus* (Wilson 2005), *Tapuiasaurus* (Zaher *et al.* 2011), *Antarctosaurus wichmannianus* (Wilson *et al.* 2009) and *Jainosaurus* (Wilson *et al.* 2009).

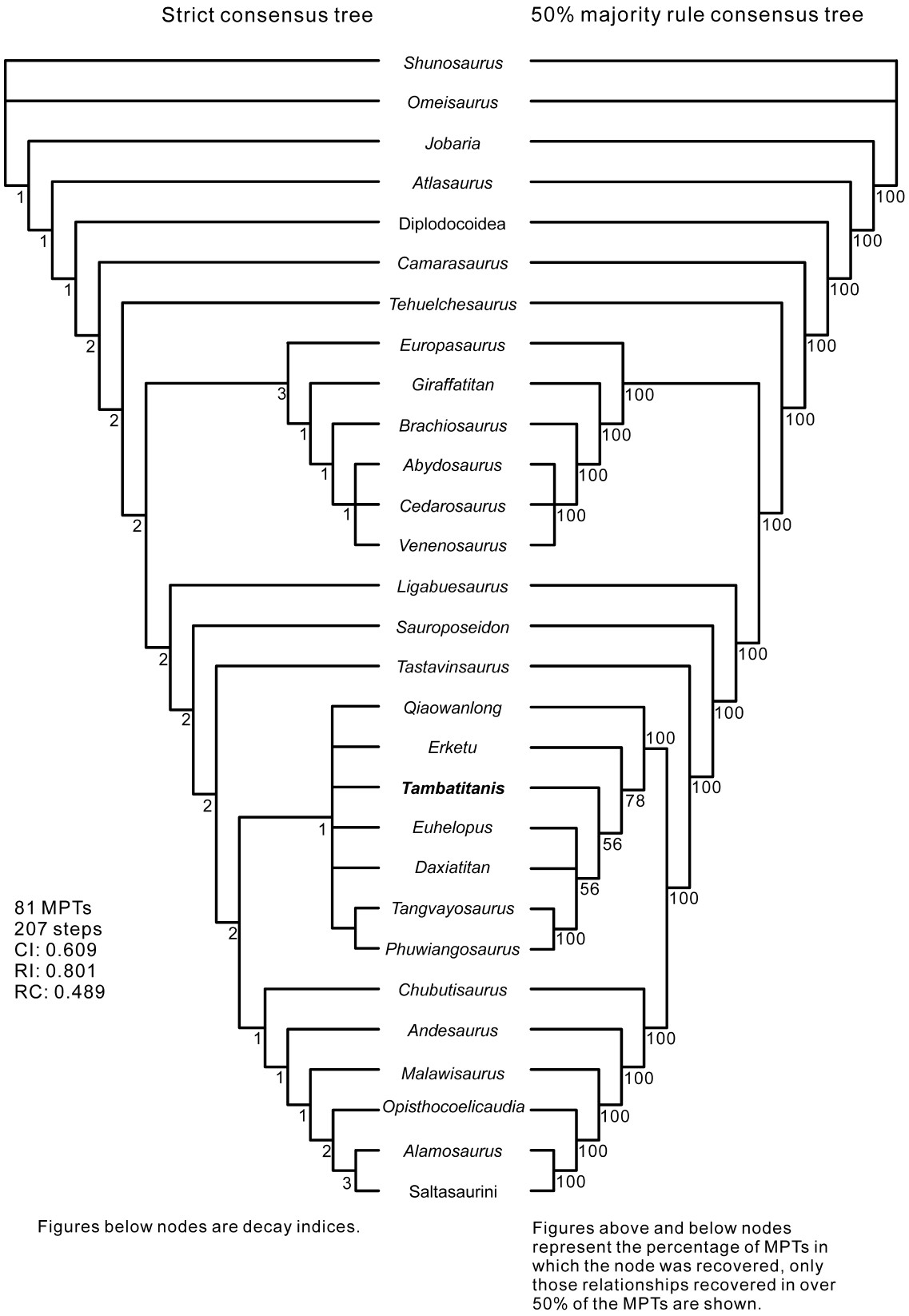

FIGURE 23. Phylogenetic relationships of the titanosauriform sauropod *Tambatitanis amicitiae* **gen. et sp. nov.** from the Lower Cretaceous Sasayama Group of Tamba, Hyogo, Japan produced using the matrix of D'Emic (2012) with the addition of *Tambatitanis*. The final matrix, including 29 taxa and 119 characters, was analyzed in PAUP* 4.0b10. Left side, strict consensus of 81 most parsimonious trees (length = 207; CI = 0.609; RI = 0.8010; RC = 0.489), figures below nodes are decay indices. Right side, 50% majority rule consensus, figures above and below nodes represents the percentage of MPTs in which the node was recovered (only those relationships recovered in over 50% of the MPTs are shown).

Almost of all of the sauropods that cannot be compared directly with *Tambatitanis* due to the absence of overlapping and well preserved material are known from different ages and/or continents, so that there is little possibility that they are congeneric and/or conspecific with *Tambatitanis amicitiae*. The only exception is a basal titanosauriform, *Liubangosaurus,* which is known from the Early Cretaceous of Guangxi, China (Mo *et al.* 2010). *Liubangosaurus* is known only from five articulated dorsal vertebrae, whereas the two poorly preserved centra currently represent the only known dorsal vertebrae of *Tambatitanis*. Therefore, there is no well-preserved overlapping material between these taxa, and we do not have means to refute the synonymy between these two taxa. Thus, *Liubangosaurus* remains as the only potential sauropod taxon that could be the senior synonym of *Tambatitanis*.

Phylogenetic analysis. The phylogenetic relationships of *Tambatitanis* were analyzed using the matrix of D'Emic (2012), with addition of a further character state (state 2 herein) for character 55. This character state is "anterior articular faces flat, posterior faces concave", and *Phuwiangosaurus, Tangvayosaurus,* and *Tambatitanis* are scored for this condition. The scores of *Tambatitanis* (Table 7) were added to this modified matrix of D'Emic (2012) to yield a matrix of 29 taxa (26 ingroups and three outgroups) and 119 characters. *Tambatitanis* could be scored for 23 of the 119 characters, 19.3% of the total (Table 7). Following D'Emic (2012), PAUP* 4.0b10 (Swofford 2002) was used to perform a heuristic branch-and-bound search. The analysis yielded 81 most parsimonious trees (MPTs) with length = 207, consistency index (CI) = 0.609, retention index (RI) = 0.801, and rescaled consistency index (RC) = 0.489. These trees were combined into a strict consensus, and a 50% majority rule consensus tree was also constructed (Fig. 23).

TABLE 7. Character scoring for *Tambatitanis amicitiae* **gen. et sp. nov.** based on character list of D'Emic (2012).

?????00??0 ???2011??? ?????????? ?????????? ?????????1 ?0?1201110
0001100??? ?????????? ?????????? ?????????? ?????????? ?????????

In the strict consensus tree (Fig. 23) all the standard titanosauriform clades are recovered and the clade composed of titanosaurs more derived than *Andesaurus* is fully differentiated. This strict consensus tree sufficiently indicates that *Tambatitanis* is a member of Euhelopodidae, but within this clade the taxa other than *Tangvayosaurus* and *Phuwiangosaurus* form a polytomy. This represents a loss of resolution compared to the original results without *Tambatitanis* presented by D'Emic (2012: fig.5) and it likely owes to the addition of a phylogenetically less informative taxon to the analysis. Nevertheless, the 50% majority rule tree (Fig. 19) shows the position of *Tambatitanis* as a basal euhelopodid. *Tambatitanis* is located in the clade containing most East Asian basal titanosauriforms included in the analysis. In this clade *Tambatitanis* is the sister group of the sub-clade composed of *Euhelopus, Daxiatitan, Tangvayosaurus and Phuwiangosaurus*. The basal phylogenetic position of *Tambatitanis* relative to *Euhelopus* raises the intriguing possibility that the narrow tooth crown breadth shared between *Phuwiangosaurus* and *Tambatitanis* is a homoplastic character, and may have evolved at least two times within Euhelopodidae, because *Euhelopus,* which is positioned in between the former two taxa in the tree, has low slenderness indices of the teeth. However, it should be noted that the support for this tree topology is still very low, as indicated by the relatively low percentage of MPTs in which the basal node of Euhelopodidae was recovered.

Discussion

The low resolution and clade support in the present phylogenetic analysis is partly caused by the fact that *Tambatitanis* is not scored for the characters of some skeletal elements that have yet to be prepared, such as cervical and dorsal vertebrae, which bear a large amount of phylogenetic signal. Unfortunately, the cervical and dorsal vertebrae of the *Tambatitanis* holotype were found in a highly fragmented state, but there remains some possibility that at least a cervical and a dorsal can be reconstructed from the fragments, though it will be a formidable task. Apart from the preservational condition of the specimens of *Tambatitanis*, the lack of detailed descriptions of other East Asian Cretaceous sauropods also hampers the phylogenetic analysis. There are some potentially phylogenetically informative characters, including those of the caudal vertebrae, that have yet to be adequately documented in most East Asian titanosauriform specimens, and this hinders the further analysis of the

titanosauriform relationships, as suggested by D'Emic *et al.* (2013). We do not, therefore, further address the phylogenetic position of *Tambatitanis* in this paper, awaiting the completion of the preparation of the rest of the specimen. The present state of knowledge of the systematic position of *Tambatitanis* is thus still limited, but even within such limitations, it can safely be said that *Tambatitanis* is a basal titanosauriform from East Asia, possibly within Euhelopodidae.

The derived features of the braincase which are shared with titanosaurs appear to contradict the result of the present phylogenetic analysis. The braincase of *Tambatitanis* exhibits the following derived features which are currently almost exclusively known in titanosaurs (Wilson *et al.* 2009; Paulina Carabajal 2012): basal tubera that are sheet-like, an abducens nerve that does not penetrate the pituitary fossa, and an internal carotid artery that enters the medial aspect of the basipterygoid process. The presence of such derived features of the braincase may seemingly suggest that *Tambatitanis* is a titanosaur rather than a member of the East Asian basal titanosauriform clade Euhelopodidae, and recalls the case of recently described *Yongjinglong* which exhibits a peculiar combination of a *Euhelopus*-like axial skeleton and teeth and an *Opisthocoelicaudia*-like antebrachium (Li *et al.* 2014). However, two pitfalls complicate things: one is the possibility that some specimens are a chimera brought about by the mixture of skeletal elements of more than one individual or taxon, and the other is the uneven distribution of known anatomical parts among the taxa in question.

The coexistence of the titanosaurs and basal titanosaurs seems to be not uncommon in Cretaceous formations (*e.g.,* Hocknull *et al.* 2009). Thus, there is always some chance skeletal elements of more than one species have been confused at a site. Only the collection of detailed field data including the precise records of the special distribution and orientation of the fossils and the taphonomy based on such data prevent the creation of a chimera, and such task can be done only by those who excavate the fossils. In the present case, it can be safely said that the braincase belongs to the same individual as the postcranial skeleton, because it is closely associated with the caudal elements as shown in the map of Kamitaki quarry (Fig. 2), and preliminary taphonomic analysis (Appendix) suggests that only a single sauropod died and decomposed during the deposition of the fossil bed.

As noted above, the braincase of *Tambatitanis* exhibits features which have been almost exclusively known in titanosaurs (Paulina Carabajal 2012). However it should be noted that few braincases of basal titanosauriforms have been found and studied thus far, and there is some possibility that the features in question may have been distributed widely among the non-titanosaur titanosauriforms. An indeterminate titanosauriform braincase from the North America (TMM40435) has been described as possessing a derived route of cranial nerve VI, whereas the location of the entrance of the internal carotid artery is not clear (Paulina Carabajal 2012). In *Mongolosaurus,* on the other hand, three openings between the basal tubera and the basipterygoid processes are identified as "the foramina for cranial nerve VI and for the internal carotid artery" (Mannion 2011).

The original arrangement and size of the openings on the space between the basal tubera and the basipterygoid process in *Tambatitanis* is apparently similar to that of *Mongolosaurus*, and judging from this similarity, the cranial nerve VI of *Mongolosaurus* also passed lateral to the pituitary fossa like that of *Tambatitanis*. However, the identification of the foramen for nerve VI in *Mongolosaurus* is problematic because the dorsal aspect of AMNH 6710, which might give a clue to the identification of the foramen for nerve VI, has never been described in detail. If cranial nerve VI of *Mongolosaurus* also passed lateral to the pituitary fossa, it may support the result of the phylogenetic analysis of *Mongolosaurus* by Mannion *et al.* (2013) which places this taxon within Titanosauria. However, TMM40435 is not likely to be a titanosaur (Tidwell and Carpenter 2003). This may mean that at least some North American non-titanosaur titanosauriforms share derived route of the cranial nerve VI with titanosaurs and *Tambatitanis.*

Compared to the braincase, the morphological diversity of the postcranial skeleton is much better known in sauropods, including in the East Asian titanosauriforms. *Tambatitanis* exhibits a peculiar set of autapomorphies in the caudal elements that are not known in any other sauropods. As described above, the pre- and postzygapophyses are located rather posteriorly relative to the centrum in the anterior caudal vertebrae of *Tambatitanis.* This unusual positioning of the pre and postzygapophyses contrasts with the anterior positioning of these structures in titanosaurs, especially the condition culminating in Aeolosaurini where the postzygapophysis is located above or anteriorly to the anterior end of the centrum (Casal *et al.* 2007; Filippi *et al.* 2013). In addition, the strong curvature of the neural spine and the excavation of the anterior surface of the neural spine summit by the dorsal extension of the SPRF make the structure of the caudal arch and spine of *Tambatitanis* unique among sauropods.

Such large morphological deviation of the caudal elements from those of other titanosauriforms is remarkable. This is especially true when compared with *Phuwiangosaurus*, which is highly similar to *Tambatitanis* in dental

morphology (Saegusa and Tomida 2011). High morphological diversity of the caudal elements appears to be the general tendency in East Asian basal titanosauriforms, because the caudal vertebral articulation morphology is also highly diverse in this group (D'Emic *et al.* 2013). Such wide range of the morphology of the caudal elements observed in a clade possibly endemic to a continent is intriguing, and in a sense an enigma. Currently we have little idea about the functional interpretations for this peculiar morphological variation, in contrast to the dental diversity in Euhelopodidae, which can be interpreted as a consequence of presumed dietary diversity (D'Emic *et al.* 2013). The functional morphology and the adaptive significance of the equally elongate structure located on the opposite side of the sauropod body, the neck, has been the subject of intense debate for more than a decade (*e.g.,* Christian and Dzemski 2011; Christian *et al.* 2013; Klein *et al.* 2012; Stevens and Parrish 1999; Taylor *et al.* 2009), while that of tail has been discussed only sporadically (*e.g.,* Powell 2003; Gallina and Otero 2009; Otero *et al.* 2012). We hope that the peculiar morphology of the caudal vertebrae of *Tambatitani*s ignite a renewed interest in the functional morphology and adaptive significance of the sauropod tail, especially that of titanosauriforms.

Conclusion

1 A new genus and species of a titanosauriform sauropod, *Tambatitanis amicitiae* **gen. et sp. nov.**, is erected based on a partial skeleton found in the Lower Cretaceous Sasayama Group of Hyogo Prefecture, SW Japan.
2 *Tambatitanis amicitiae* **gen. et sp. nov.**, is diagnosed by eight unique characters of the braincase, caudal vertebrae and chevrons.
3 A phylogenetic analysis suggests *Tambatitanis amicitiae* is a basal titanosauriform, possibly belonging to the East Asian endemic clade Euhelopodidae.
4 The caudal vertebrae and chevrons described in detail in this paper exhibit highly autapomorphic features, as well as potentially phylogenetically informative characters.
5 The uniqueness of the caudal elements of *Tambatitanis* suggests that East Asian titanosauriforms were highly diverse both in terms of the number of the taxa and the morphology of caudal elements during the Cretaceous.
6 The braincase of *Tambatitanis* exhibits derived features which have almost exclusively been described in titanosaurs (Paulina Carabajal 2012). This may imply that these features were distributed more widely among the non-titanosaur titanosauriforms or that *Tambatitanis* is a titanosaur.

Acknowledgements

We wish to express our sincere gratitude to S. Murakami and K. Adachi for their discovery of the holotype skeleton of *Tambatitanis amicitiae*. We are grateful the volunteers who support the excavation of the skeleton. Thanks are also owing to staff of MNHAH and Tamba City, for their support and assistance during the excavation. We thank preparators of MNHAH for exquisite preparation of the holotype specimen of *Tambatitanis amicitiae*. We thank You Hailu and Lü Junchang (both Chinese Academy of Geological Sciences, Beijing, China), Li Daqing (Gansu Provincial Bureau of Geo-exploration and Mineral Development, Lanzhou, China), Xu Li (Henan Geological Museum, Zhengzhou, China), Xu Xing (Institute of Vertebrate Paleontology and Paleoanthropology, Beijing, China), Jin Xingsheng (Zhejiang Museum of Natural History, Hangzhou, China), Pang Qiqing (Shijiazhuang University of Economics, Shijiazhuang, China), Suravech Suteethorn (Mahasarakham University, Maha Sarakham, Thailand), Khishigjav Tsogtbaatar (Mongolian Academy of Sciences, Ulaanbaatar, Mongolia), Varavudh Suteethorn (Department of Mineral Resources, Bangkok, Thailand) and Yoichi Azuma (Fukui Prefectural Dinosaur Museum, Katsuyama, Japan) for collections access. Kazunori Miyata (Fukui Prefectural Dinosaur Museum, Katsuyama, Japan) CT scanned the caudal vertebrae of MNHAH D-1029280 for which we are grateful. We would like to express our gratitude to Philip D. Mannion (Imperial Colledge, London, UK) and Michael D. D'Emic (Stony Brook University, New York, USA) for the critical reading and valuable comments on earlier version of our manuscript. We appreciate very much Stephen L. Brusatte's suggestions for improvement of our text. We also thank James Kirkland (Utah Geological Survey, Salt Lake City, USA), Hideo Nakaya (Kagoshima University, Kagoshima, Japan) and Ren Hirayama (Waseda University, Tokyo, Japan) for literature Information. This work was supported in part by a Grant-in-Aid for Scientific Research (B) (no. 20340145) from the Japan Society for the Promotion of Science (JSPS) awarded to H.S.

References

Alifanov, V.R. & Averianov, A.O. (2003) *Ferganasaurus verzilini*, gen. et sp. nov., a new neosauropod (Dinosauria, Saurischia, Sauropoda) from the Middle Jurassic of Fergana Valley, Kirghizia. *Journal of Vertebrate Paleontology*, 23, 358–372. http://dx.doi.org/10.1671/0272-4634(2003)023[0358:fvgesn]2.0.co;2

Allain, R. & Aquesbi, N. (2008) Anatomy and phylogenetic relationships of *Tazoudasaurus naimi* (Dinosauria, Sauropoda) from the late Early Jurassic of Morocco. *Geodiversitas*, 30, 345–424.

Azuma, Y. & Shibata, M. (2010) *Fukuititan nipponensis*, a new titanosauriform sauropod from the Early Cretaceous Tetori Group of Fukui Prefecture, Japan. *Acta Geologica Sinica*, 84, 454–462. (English Edition)

Balanoff, A.M., Bever, G.S. & Ikejiri, T. (2010) The Braincase of *Apatosaurus* (Dinosauria: Sauropoda) Based on Computed Tomography of a New Specimen with Comments on Variation and Evolution in Sauropod Neuroanatomy. *American Museum Novitates*, 3677, 1–32. http://dx.doi.org/10.1206/591.1

Berman, D.S. & McIntosh, J.S. (1978) Skull and relationships of the Upper Jurassic sauropods Apatosaurus (Reptilia, Saurischia). *Bulletin of Carnegie Museum of Natural History*, 8, 1–35.

Bonaparte, J.F. (1996) Cretaceous tetrapods of Argentina. *Münchner Geowissenschaftliche Abhandlungen R. (A)*, 30, 73–130.

Bonaparte, J.F., Heinrich, W.-D. & Wild, R. (2000) Review of *Janenschia* Wild, with the description of a new sauropod from the Tendaguru beds of Tanzania and a discussion on the systematic value of procoelous caudal vertebrae in the Sauropoda. *Palaeontographica A*, 256 (1–3), 25–76.

Borsuk-Białynicka, M. (1977) A new camarasaurid sauropod *Opisthocoelicaudia skarzynskii* gen. n., sp. n. from the Upper Cretaceous of Mongolia. *Palaeontologia Polonica*, 37, 5–64.

Calvo, J.O., González-Riga, B.J. & Porfiri, J.D. (2008) A new titanosaur sauropod from the Late Cretaceous of Neuquén, Patagonia, Argentina. *Arquivos do Museu Nacional, Rio de Janeiro*, 65, 485–504.

Calvo, J.O. & Kellner, A.W.A. (2006) Description of a sauropod dinosaur braincase (Titanosauridae) from the Late Cretaceous Rio Colorado Subgroup, Patagonia. *Anais da Academia Brasileira de Ciências*, 78, 175–182. http://dx.doi.org/10.1590/s0001-37652006000100015

Calvo, J.O. & Salgado, L. (1995) *Rebbachisaurus tessonei* sp. nov. a new Sauropoda from the Albian-Cenomanian of Argentina; new evidence on the origin of the Diplodocidae. *Gaia*, 11, 13–33.

Campos, D.A. & Kellner, A.W.A. (1999) On some sauropod (Titanosauridae) pelves from the continental Cretaceous of Brazil. *In*: Tomida, Y., Rich, T.H. & Vickers-Rich, P. (Eds.), *Proceedings of the Second Gondwanan Dinosaur Symposium. Vol. 15*. National Sciences Museum Monographs, Tokyo, pp. 143–166.

Campos, D.A., Kellner, A.W.A., Bertini, R.J. & Santucci, R.M. (2005) On a titanosaur (Dinosauria, Sauropoda, Titanosauridae) vertebral column from the Bauru Group, Late Cretaceous of Brazil. *Arquivos do Museu Nacional, Rio de Janeiro*, 63, 565–593.

Canudo, J.I., Royo-Torres, R. & Cuenca-Bescós, G.A. (2008) New sauropod: *Tastavinsaurus sanzi* gen. et sp. nov. from the Early Cretaceous (Aptian) of Spain. *Journal of Vertebrate Paleontology*, 28, 712–731. http://dx.doi.org/10.1671/0272-4634(2008)28[712:anstsg]2.0.co;2

Carballido, J.L., Pol, D., Cerda, I. & Salgado, L. (2011) The Osteology of *Chubutisaurus insignis* Del Corro, 1975 (Dinosauria: Neosauropoda) from the 'Middle' Cretaceous of Central Patagonia, Argentina. *Journal of Vertebrate Paleontology*, 31, 93–110. http://dx.doi.org/10.1080/02724634.2011.539651

Carballido, J.L., Salgado, L., Pol, D., Canudo, J.I. & Garrido, A. (2012) A new basal rebbachisaurid (Sauropoda, Diplodocoidea) from the Early Cretaceous of the Neuquén Basin; evolution and biogeography of the group. *Historical Biology,* 24, 631–654. http://dx.doi.org/10.1080/08912963.2012.672416

Carballido, J.L. & Sander, P.M. (2013) Postcranial axial skeleton of *Europasaurus holgeri* (Dinosauria, Sauropoda) from the Upper Jurassic of Germany: implications for sauropod ontogeny and phylogenetic relationships of basal Macronaria. *Journal of Systematic Palaeontology*, 12 (13), 335–387 http://dx.doi.org/10.1080/14772019.2013.764935

Carvalho, I.S., Avilla, L.S. & Salgado, L. (2003) *Amazonsaurus maranhensis* gen. et sp. nov. (Sauropoda,Diplodocoidea) from the Lower Cretaceous (Aptian-Albian) of Brazil. *Cretaceous Research*, 24, 697–713. http://dx.doi.org/10.1016/j.cretres.2003.07.005

Casal, G., Martínez, R., Luna, M., Sciutto, J. & Lamnna, M. (2007) *Aeolosaurus colhuehuapensis* sp. nov. (Sauropoda, Titanosauria) de la Formación Bajo Barreal, Cretácico superior de Argentina. *Revista Brasileira de Paleontologia*, 10, 53–62.

Cerda, I.A., Salgado, L. & Powell, J.E. (2012) Extreme postcranial pneumaticity in sauropod dinosaurs from South America. *Paläontologische Zeitschrift*, 86, 441–449. http://dx.doi.org/10.1007/s12542-012-0140-6

Chatterjee, S. & Rudra, D.K. (1996) KT events in India: impact, rifting, volcanism and dinosaur extinction. *Memoirs of the Queensland Museum,* 39, 489–532.

Chatterjee, S. & Zheng, Z. (2002) Cranial anatomy of *Shunosaurus*, a basal sauropod dinosaur from the Middle Jurassic of

China. *Zoological Journal of the Linnean Society*, 136, 145–169.
http://dx.doi.org/10.1046/j.1096-3642.2002.00037.x
Chatterjee, S. & Zheng, Z. (2005) Neuroanatomy and Dentition of *Camarasaurus lentus*. *In*: Tidwell, V. & Carpenter, K. (Eds.), *Thunder-lizards: the sauropodomorph dinosaurs.* Indiana University Press, Bloomington, pp. 199–211.
Christian, A. & Dzemski, G. (2011) Neck posture in sauropods. *In*: Klein, N., Remes, K., Gee, C.T. & Sander, P.M. (Eds.), *Biology of the sauropod dinosaurs: understanding the life of giants.* Indiana University Press, Bloomington, pp. 251–260.
Christian, A., Peng. G., Sekiya, T., Ye, Y., Wulf, M.G. & Steuer, T. (2013) Biomechanical Reconstructions and Selective Advantages of Neck Poses and Feeding Strategies of Sauropods with the Example of *Mamenchisaurus youngi*. *PLoS ONE*, 8 (10), e71172.
http://dx.doi.org/10.1371/journal.pone.0071172
Chure, D., Britt, B.B., Whitlock, J.A. & Wilson, J.A. (2010) First complete sauropod dinosaur skull from the Cretaceous of the Americas and the evolution of sauropod dentition. *Naturwissenschaften*, 97, 379–39.
http://dx.doi.org/10.1007/s00114-010-0650-6
Curry Rogers, K.A. (2005) Titanosauria: A Phylogenetic Overview. *In*: Curry Rogers, K.A. & Wilson, J. (Eds.), *The Sauropods: Evolution and Paleobiology.* University of California Press, Berkeley, pp. 50–103.
Curry Rogers, K.A. (2009) The postcranial osteology of *Rapetosaurus krausei* (Sauropoda: Titanosauria) from the Late Cretaceous of Madagascar. *Journal of Vertebrate Paleontology*, 29, 1046–1086.
http://dx.doi.org/10.1671/039.029.0432
Curry Rogers, K. & Forster, C.A. (2004) The skull of Rapetosaurus krausei (Sauropoda: Titanosauria) from the Late Cretaceous of Madagascar. *Journal of Vertebrate Paleontology*, 24,121–144.
http://dx.doi.org/10.1671/a1109-10
D'Emic, M.D. (2012) The early evolution of titanosauriform sauropod dinosaurs. *Zoological Journal of the Linnean Society*, 166, 624–671.
http://dx.doi.org/10.1111/j.1096-3642.2012.00853.x
D'Emic, M.D. (2013) Revision of the sauropod dinosaurs of the Lower Cretaceous Trinity Group, southern USA, with the description of a new genus. *Journal of Systematic Palaeontology,* 11, 707–726.
http://dx.doi.org/10.1080/14772019.2012.667446
D'Emic, M.D., Mannion, P.D., Upchurch, P., Benson, R.B.J., Pang, Q. & Cheng, Z. (2013) Osteology of *Huabeisaurus allocotus* (Sauropoda: Titanosauriformes) from the Upper Cretaceous of China. *PLoS ONE*, 8 (8), e69375.
http://dx.doi.org/10.1371/journal.pone.0069375
D'Emic, M.D. & Wilson, J.A. (2011) New remains attributable to the holotype of the sauropod dinosaur *Neuquensaurus australis*, with implications for saltasaurine systematics. *Acta Palaeontologica Polonica,* 56, 61–73.
http://dx.doi.org/10.4202/app.2009.0149
Díez Díaz, V., Pereda Suberbiola, X. & Sanz, J.L. (2011) Braincase anatomy of the sauropod dinosaur *Lirainosaurus astibiae* (Titanosauria) from the Late Cretaceous of the Iberian Peninsula. *Acta Palaeontologica Polonica,* 56, 521–533.
http://dx.doi.org/10.4202/app.2010.0043
Díez Díaz, V., Tortosa, T., & Le Loeuff, J. (2013) Sauropod diversity in the Late Cretaceous of southwestern Europe: The lessons of odontology. *Annales de Paléontologie*, 99,119–129.
http://dx.doi.org/10.1016/j.annpal.2012.12.002
Filippi, L.S., García, R.A. & Garrido, A.C. (2011) A new titanosaur sauropod dinosaur from the Upper Cretaceous of North Patagonia, Argentina. *Acta Palaeontologica Polonica,* 56, 505–520.
http://dx.doi.org/10.4202/app.2010.0019
Filippi, L.S. & Garrido, A.C. (2008) *Pitekunsaurus macayai* gen. et sp. nov., nuevo titanosaurio (Saurischia, Sauropoda) del Cretácico Superior de la Cuenca Neuquina, Argentina. *Ameghiniana*, 45, 575–590.
Filippi, L.S., Martinelli, A.G. & Garrido, A.C. (2013) Registro de un dinosaurio Aeolosaurini (Sauropoda, Titanosauria) en el Cretácico Superior (Formación Plottier) del norte de la Provincia de Neuquén, Argentina, y comentarios sobre los Aeolosaurini sudamericanos. *Revista Brasileira de Paleontologia*, 16,147–156.
http://dx.doi.org/10.4072/rbp.2013.1.11
Gallina, P.A. & Apesteguía, S. (2011) Cranial anatomy and phylogenetic position of the titanosaurian sauropod *Bonitasaura salgadoi. Acta Palaeontologica Polonica*, 56, 45–60.
http://dx.doi.org/10.4202/app.2010.0011
Gallina, P.A. & Otero, A. (2009) Anterior caudal transverse processes in sauropod dinosaurs: morphological, phylogenetic and functional aspects. *Ameghiniana*, 46, 165–176.
Galton, P.M. & Knoll, F. (2006) A saurischian dinosaur braincase from the Middle Jurassic (Bathonian) near Oxford, England: from the theropod *Megalosaurus* or the sauropod *Cetiosaurus*? *Geological Magazine*, 143, 905–921.
http://dx.doi.org/10.1017/s0016756806002561
García, R.A., Paulina Carabajal, A. & Salgado, L. (2008) Un nuevo basicráneo de titanosaurio de la Formación Allen (Campaniano–Maastrichtiano), Provincia de Río Negro, Patagonia, Argentina. *Geobios*, 41, 625–633.
http://dx.doi.org/10.1016/j.geobios.2007.11.005
Gillette, D.D. (1991) *Seismosaurus halli,* gen. nov. et sp. nov., a new sauropod dinosaur from the Morrison Formation (Upper Jurassic/Lower Cretaceous) of New Mexico, USA. *Journal of Vertebrate Paleontology*, 11, 417–433.

http://dx.doi.org/10.1080/02724634.1991.10011413
Gilmore, C.W. (1933) On the dinosaurian fauna of the Iren Dabasu formation. *Bulletin of the American Museum of Natural History,* 67, 23–78.
Gilmore, C.W. (1936) Osteology of *Apatosaurus*, with special references to specimens in the Carnegie Museum. *Memoirs of the Carnegie Musseum*, 11, 175–300.
Gilmore, C.W. (1946) Reptilian fauna of the North Horn formation of central Utah. *United States Geological Survey, Professional Paper,* 210, 1–52.
Gomani, E.M. (2005) Sauropod Dinosaurs from the Early Cretaceous of Malawi, Africa. *Palaeontologia Electronica,* 8, 1–37.
González Riga, B.J. (2003) A new titanosaur (Dinosauria, Sauropoda) from the Upper Cretaceous of Mendoza, Argentina. *Ameghiniana,* 40, 155–172.
http://dx.doi.org/10.5710/amgh.24.12.2013.1889
González Riga, B.J., Previtera, E. & Pirrone, C.A. (2009) *Malarguesaurus florenciae* gen. et sp. nov., a new titanosauriform. *Cretaceous Research*, 30, 135–148.
http://dx.doi.org/10.1016/j.cretres.2008.06.006
Harris, J.D. (2006) The axial skeleton of the dinosaur *Suuwassea emilieae* (Sauropoda: Flagellicaudata) from the Upper Jurassic Morrison Formation of Montana, USA. *Palaeontology*, 49, 1091–1121.
http://dx.doi.org/10.1111/j.1475-4983.2006.00577.x
Harris, J.D. & Dodson, P. (2004) A new diplodocoids sauropod dinosaur from the upper Jurassic Morrison Formation of Montana, USA. *Acta Palaeontologica Polonica*, 49, 197–210.
Hatcher, J.B. (1901) *Diplodocus* (Marsh): its osteology, taxonomy, and probable habits, with a restoration of the skeleton. *Memoirs of the Carnegie Museum*, 1, 1–63.
http://dx.doi.org/10.5962/bhl.title.46734
Hatcher, J.B. (1903) Osteology of *Haplocanthosaurus* with description of a new species, and remarks on the probable habits of the Sauropoda and the age and origin of the Atlantosaurus beds. *Memoirs of the Carnegie Museum*, 2, 1–72.
Hayashi, K., Matuskawa, M., Ohira, H., Chen, P., Zhen, J., Ito, M., Koarai, K. & Obata, I. (2010) Revised age of the Sasayama Group, southwest Japan, based on ostracoda and conchostracan biostratigraphy and zircon fission-track dating. *Journal of the Geological Society of Japan,* 116, 283–286. [in Japanese with English abstract]
Hocknull, S.A., White, M.A., Tischler, T.R., Cook, A.G., Calleja, N.D., Sloan, T. & Elliot, D.A. (2009) New Mid-Cretaceous (Latest Albian) Dinosaurs from Winton, Queensland, Australia. *PLoS ONE*, 4 (7), e6190.
http://dx.doi.org/10.1371/journal.pone.0006190
Holland, W.J. (1905) The osteology of *Diplodocus* Marsh: with special reference to the restoration of the skeleton of *Diplodocus*. *Memoirs of the Carnegie Museum of Natural History*, 2, 225–276.
Ikejiri, T. (2008) Slender and robust skeletal morphotypes of *Camarasaurus* (Dinosauria, Sauropoda) from the Morrison Formation (Upper Jurassic) of the Rocky Mountain Region and their implications for sexual dimorphism. *In*: Farleym, G.H. & Choate, J.R. (Eds.), *Unlocking the Unknown: papers honoring Dr. Richard J. Zakrzewski Fort Hays Studies Special Issue Number*, 2, pp. 31–44.
Ikejiri, T., Tidwell, V. & Trexler, D.L. (2005) New adult specimens of *Camarasaurus lentus* highlights ontogenetic variation within the species. *In*: Tidwell, V. & Carpenter, K. (Eds.), *Thunder-lizards: the sauropodomorph dinosaurs.* Indiana University Press, Bloomington, pp. 154–179.
Jain, S.L. & Bandyopadhyay, S. (1997) New titanosaurid (Dinosauria: Sauropoda) from the Late Cretaceous of central India. *Journal of Vertebrate Paleontology,* 17, 114–136.
http://dx.doi.org/10.1080/02724634.1997.10010958
Janensch, W. (1929) Die Wirbelsäule der Gattung *Dicraeosaurus. Palaeontographica* Supplement 7*,* 2, 37–133.
Janensch, W. (1935–1936) Die Schädel der Sauropoden *Brachiosaurus, Barosaurus* und *Dicraeosaurus* aus den Tendaguru-Schichten Deutsch-Ostafrika. *Palaeontographica*, Supplement 7, 2, 147–298.
Janensch, W. (1950) Die Wirbelsäule von Brachiosaurus brancai. *Palaeontographica*, Supplement 7, 3, 27–93.
Kellner, A.W.A., Campos, D.A., Azevedo, S.A.K., Trotta, M.N.F., Henriques, D.D.R., Craik, M.M.T. & Silva, H.P. (2006) On a new titanosaur sauropod from the Bauru Group, Late Cretaceous of Brazil. *Boletim do Museu Nacional (Geologia)*, 74, 1–31.
Kellner, A.W.A., Campos, D.A. & Trotta, M.N.F. (2005) Description of a titanosaurid caudal series from the Bauru Group, Late Cretaceous of Brazil. *Arquivos do Museu Nacional, Rio de Janeiro*, 63, 529–564.
Kirkland, J.I. & Bader, K. (2010) Insect trace fossils associated with Protoceratops carcasses in the Djadokhta Formation (Upper Cretaceous), Mongolia. *In*: Ryan, M.J., Chinnery-Allgeier, B.J. & Eberth, D.A. (Eds.), *New Perspectives on Horned Dinosaurs: The Royal Tyrell Museum Ceratopsian Symposium*. Indiana University Press, Bloomington, pp. 509–519.
Klein, N., Christian, A. & Sander, P.M. (2012) Histology shows elongated neck ribs in sauropod dinosaurs are ossified tendons. *Biology Letters*, 8, 1032–1035.
http://dx.doi.org/10.1098/rsbl.2012.0778
Knoll, F. & Schwarz-Wings, D. (2009) Palaeoneuroanatomy of *Brachiosaurus. Annales de Paléontologie*, 9, 165–175.
http://dx.doi.org/10.1016/j.annpal.2009.06.001
Knoll, F., Ridgely, R.C., Ortega, F., Sanz, J.L. & Witmer, L.M. (2013) Neurocranial Osteology and Neuroanatomy of a Late

Cretaceous Titanosaurian Sauropod from Spain *(Ampelosaurus* sp.). *PLoS ONE*, 8 (1), e54991. http://dx.doi.org/10.1371/journal.pone.0054991
Knoll, F, Witmer, L.M., Ortega, F., Ridgely, R.C. & Schwarz-Wings, D. (2012) The braincase of the basal sauropod dinosaur *Spinophorosaurus* and 3D reconstructions of the cranial endocast and inner ear. *PLoS ONE*, 7 (1), e30060. http://dx.doi.org/10.1371/journal.pone.0030060
Ksepka, D.T. & Norell, M.A. (2006) *Erketu ellisoni*, a long-necked sauropod from Bor Guvé (Dornogov Aimag, Mongolia). *American Museum Novitates,* 3508, 1–16. http://dx.doi.org/10.1206/0003-0082(2006)3508[1:eealsf]2.0.co;2
Kusuhashi, N., Tsutsumi, Y., Saegusa, H., Horie, K., Ikeda, T., Yokoyama, K. & Shiraishi, K. (2013) A new Early Cretaceous eutherian mammal from the Sasayama Group, Hyogo, Japan. *Proceedings of the Royal Society B,* 280, 1–8. http://dx.doi.org/10.1098/rspb.2013.0142
Läng, E. & Mahammed, F. (2010) New anatomical data and phylogenetic relationships of Chebsaurus algeriensis (Dinosauria, Sauropoda) from the Middle Jurassic of Algeria. *Historical Biology*, 22, 142–164. http://dx.doi.org/10.1080/08912960903515570
Li, L., Li, D., You, H. & Dodson, P. (2014) A New Titanosaurian Sauropod from the Hekou Group (Lower Cretaceous) of the Lanzhou-Minhe Basin, Gansu Province, China. *PLoS ONE*, 9 (1), e85979. http://dx.doi.org/10.1371/journal.pone.0085979
Lü, J., Azuma, Y., Chen, R., Zheng, W. & Jin, X. (2008) A new titanosauriform Sauropod from the Early Late Cretaceous of Dongyang, Zhejiang Province. *Acta Geologica Sinica*, 82, 225–235. http://dx.doi.org/10.1111/j.1755-6724.2008.tb00572.x
Lü, J., Xu, L., Jia, S., Zhang, X., Zhang, J., Yang, L., You, H. & Ji, Q. (2009a) A new gigantic sauropod dinosaur from the Cretaceous of Ruyang, Henan, China. *Geological Bulletin of China*, 28, 1–10.
Lü., J., Xu, L., Jiang, X., Jia, S., Li, M., Yuan, C., Zhang, X. & Ji, Q. (2009b) A preliminary report on the new dinosaurian fauna from the Cretaceous of the Ruyang Basin, Henan Province of central China. *Journal of the Palaeontological Society of Korea*, 25, 43–56.
Lü, J., Xu, L., Pu, H., Zhang, X., Zhang, Y., Jia, S., Chang, H., Zhang, J. & Wei, X. (2013) A new sauropod dinosaur (Dinosauria, Sauropoda) from the late Early Cretaceous of the Ruyang Basin (central China). *Cretaceous Research*, 44, 202–213. http://dx.doi.org/10.1016/j.cretres.2013.04.009
Lü, J., Xu, L., Zhang, X., Hu, W., Wu, Y., Jia, S. & Ji, Q. (2007) A new gigantic sauropod dinosaur with the deepest known body cavity from the Cretaceous of Asia. *Acta Geologica Sinica*, 81, 167–176. http://dx.doi.org/10.1111/j.1755-6724.2007.tb00941.x
Lull, R.S. (1919) The sauropod dinosaur Barosaurus Marsh. *Memoires of the Connecticut Academy of Arts and Science*, 6, 1–42.
Madsen, J.H. (1976) *Allosaurus fragilis*: a revised osteology. Utah Geologocal Society, Bulletin, 109, 1–163.
Madsen, J.H. Jr., McIntosh, J.S. & Berman, D.S. (1995) Skull and atlas-axis complex of the Upper Jurassic sauropod *Camarasaurus* Cope (Reptilia: Saurischia). *Bulletin of Carnegie Museum of Natural History*, 31, 1–115.
Maltese, A. (2002) Discovery of a divided initial chevron in *Camarasaurus* (Dinosauria, Sauropoda). *Journal of VertebratePaleontology,* 22 (Supplement 3), 83A.
Mannion, P.D. (2011) A reassessment of *Mongolosaurus haplodon* Gilmore, 1933, a titanosaurian sauropod dinosaur from the Early Cretaceous of Inner Mongolia, People's Republic of China. *Journal of Systematic Palaeontology*, 9, 355–378. http://dx.doi.org/10.1080/14772019.2010.527379
Mannion, P.D. & Calvo, J.O. (2011) Anatomy of the basal titanosaur (Dinosauria, Sauropoda) *Andesaurus delgadoi* from the mid-Cretaceous (Albian–early Cenomanian) Río Limay Formation, Neuquén Province, Argentina: implications for titanosaur systematic. *Zoological Journal of the Linnean Society,* 163, 155–181. http://dx.doi.org/10.1111/j.1096-3642.2011.00699.x
Mannion, P.D. & Otero, A. (2012) A reappraisal of the Late Cretaceous Argentinean sauropod dinosaur *Argyrosaurus superbus*, with a description of a new titanosaur genus. *Journal of Vertebrate Paleontology,* 32, 614–638. http://dx.doi.org/10.1080/02724634.2012.660898
Mannion, P.D., Upchurch, P., Barnes, R.N. & Mateus, O. (2013) Osteology of the Late Jurassic Portuguese sauropod dinosaur *Lusotitan atalaiensis* (Macronaria) and the evolutionary history of basal titanosauriforms. *Zoological Journal of the Linnean Society,* 168, 98–206. http://dx.doi.org/10.1111/zoj.12029
Mannion, P.D., Upchurch, P. & Hutt, S. (2011) New rebbachisaurid (Dinosauria: Sauropoda) material from the Wessex Formation (Barremian, Early Cretaceous), Isle of Wight, United Kingdom. *Cretaceous Research*, 32, 774–780. http://dx.doi.org/10.1016/j.cretres.2011.05.005
Marpmann, J.S., Carballido, J.L., Sander, P.M. & Knötschke, N. (2014) Cranial anatomy of the Late Jurassic dwarf sauropod *Europasaurus holgeri* (Dinosauria, Camarasauromorpha): ontogenetic changes and size dimorphism. *Journal of Systematic Palaeontology.* [published online] http://dx.doi.org/10.1080/14772019.2013.875074
Marsh, O.C. (1878) Principal characters of American Jurassic dinosaurs. Part 1. *American Journal of Science*, 16, 411–416.

http://dx.doi.org/10.2475/ajs.s3-16.95.411
Marsh, O.C. (1896) The dinosaurs of North America. *U.S. Geological Survey Annual Report,* 16, 133–244.
Martin, V., Suteethorn, V. & Buffetaut, E. (1999) Description of the type and referred material of *Phuwiangosaurus sirindhornae* Martin, Buffetaut et Suteethorn, 1994, a sauropod from the Lower Cretaceous of Thailand. *Oryctos,* 2, 39–91.
Martinelli, A.G. & Forasiepi, A.M. (2004) Late Cretaceous vertebrates from Bajo de Santa Rosa (Allen Formation), Río Negro Province, Argentina, with the description of a new sauropod dinosaur (Titanosau- ridae). *Revista del Museo Argentino de Ciencias Naturales,* Nuevo Serie*,* 6, 257–305.
Martínez, R.D., Giménez, O., Rodríguez, J., Luna, M. & Lamanna, M.C. (2004) An articulated specimen of the basal titanosaurian (Dinosauria: Sauropoda) *Epachthosaurus sciuttoi* from the early Late Cretaceous Bajo Barreal Formation of Chubut Province, Argentina. *Journal of Vertebrate Paleontology*, 24, 107–120.
http://dx.doi.org/10.1671/9.1
Matsuura, H. & Yoshikawa, T. (1992) Radiometric ages of the Early Cretaceous Sasayama Group, Hyogo Prefecture, Southwest Japan. *Journal of the Geological Society of Japan,* 98, 635–643. [in Japanese with English abstract]
http://dx.doi.org/10.5575/geosoc.98.635
McIntosh, J.S. (2005) The genus *Barosaurus* Marsh (Sauropoda, Diplodocidae). *In:*Tidwell, V. & Carpenter, K. (Eds.), *Thunder-lizards: The Sauropod Dinosaurs. Bloomington*. Indiana University Press. Bloomington, pp. 38–77.
McIntosh, J.S., Miles, C.A., Cloward, K.C. & Parker, J.R. (1996a) A new nearly complete skeleton of *Camarasaurus. Bulletin of Gunma Museum of Natural History*, 1, 1–87.
McIntosh, J.S., Miller, W.E., Stadtman, K.L. & Gillette, D.D. (1996b) The osteology of *Camarasaurus lewisi* (Jensen 1988). *Brigham Young University Geology Studies*, 41, 73–115.
Mo, J., Huang, C., Zhao, Z., Wang, W. & Xu, X. (2008) A new titanosaur (Dinosauria: Sauropoda) from the Late Cretaceous of Guangxi, China. *Vertebrata PalAsiatica,* 46, 147–156.
Mo, J., Wang, W., Huang, Z., Huang, X. & Xu, X. (2006) A basal titanosauriform from the Early Cretaceous of Guangxi, China. *Acta Geologica Sinica (English Edition),* 80, 486–489.
http://dx.doi.org/10.1111/j.1755-6724.2006.tb00267.x
Mo, J., Xu, X. & Buffetaut, E. (2010) A New Eusauropod Dinosaur from the Lower Cretaceous of Guangxi Province, Southern China. *Acta Geologica Sinica (English Edition)*, 84, 1328–1335.
http://dx.doi.org/10.1111/j.1755-6724.2010.00331.x
Nesbitt, S.J. (2011) The early evolution of archosaurs: relationships and the origin of major clades. *Bulletin of the American Museum of Natural History*, 352, 1–292.
http://dx.doi.org/10.1206/352.1
O'Connor, P.M. (2007) The postcranial axial skeleton of *Majungasaurus crenatissimus* (Theropoda: Abelisauridae) from the Late Cretaceous of Madagascar. *In:* Sampson, S.D. & Krause, D.W. (Eds.), *Majungasaurus crenatissimus (Theropoda: Abelisauridae) from the Late Cretaceous of Madagascar. Society of Vertebrate Paleontology Memoir*, 8, pp. 127–162.
Osborn, H.F. (1904) Manus, Sacrum, and Caudals of Sauropoda. *Bulletin of the American Museum of Natural History,* 20, 181–190.
Osborn, H.F. & Mook, C.C. (1921) *Camarasaurus, Amphicoelias*, and other sauropods of Cope. *Memoirs of the American Museum of Natural History,* 3, 247–387.
Ostrom, J.H. & McIntosh, J.S. (1966) *Marsh's Dinosaurs.* Yale University Press, New Haven, 388 pp.
Otero, A., Gallina, P.A., Canale, J.I. & Haluza, A. (2012) Sauropod haemal arches: morphotypes, new classification and phylogenetic aspects. *Historical Biology*, 24, 243–256.
http://dx.doi.org/10.1080/08912963.2011.618269
Ouyang, H. & Ye, Y. (2002) *The First Mamenchisaurian Skeleton with Complete Skull: Mamenchisaurus youngi.* Sichuan Science and Technology Press, Chengdu, 111 pp.
Owen, R. (1842) Report on British Fossil Reptiles. Part II. *Reports of the British Association for the Advancement of Science*, 11, 60–204.
Paik, I.S. (2000) Bone chip-filled burrows associated with bored dinosaur bone infloodplain paleosols of the Cretaceous Hasandong Formation, Korea. *Palaeogeography, Palaeoclimatology, Palaeoecology*, 157, 213–225.
http://dx.doi.org/10.1016/s0031-0182(99)00166-2
Pang, Q. & Cheng, Z. (2000) A new family of sauropod dinosaur from the Upper Cretaceous of Tianzhen, Shanxi province, China. *Acta Geologica Sinica (English Edition),* 74, 117–125.
http://dx.doi.org/10.1111/j.1755-6724.2000.tb00438.x
Paulina Carabajal, A. (2012) Neuroanatomy of titanosaurid dinosaurs from the Upper Cretaceous of Patagonia, with comments on endocranial variability within Sauropoda. *The Anatomical Record,* 295, 2141–2156.
http://dx.doi.org/10.1002/ar.22572
Paulina Carabajal, A., Coria, R.A. & Chiappe, L.M. (2008) An incomplete Upper Cretaceous titanosaur (Sauropoda) braincase: new insights on the dinosaurian inner ear and endocranium. Cretaceous Research, 29, 643–648.
http://dx.doi.org/10.1016/j.cretres.2008.01.011
Powell, J.E. (1992) Osteología de *Saltasaurus loricatus* (Sauropoda-Titanosauridae) del Cretácico Superior del Noroeste Argentino. *In*: Sanz, J.L. & Buscalioni, A.D. (Eds.), *Los dinosaurios y su enterno biotico. Actas del Segundo Curso de*

Paleontologia en Cuenca. Instituto "Juan de Valdes", Ayuntamiento de Cuenca, pp.165–230.
Powell, J.E. (2003) Revision of South American Titanosaurid dinosaurs: palaeobiological, palaeobiogeographical and phylogenetic aspects. *Records of the Queen Victoria Museum*, 111, 1–173.
Remes, K. (2006) Revision of the Tendaguru sauropod dinosaur *Tornieria africana* (Fraas) and its relevance for sauropod paleobiogeography. *Journal of Vertebrate Paleontology*, 26, 651–669.
http://dx.doi.org/10.1671/0272-4634(2006)26[651:rottsd]2.0.co;2
Rose, P.J. (2007) A new titanosauriform sauruopod (Dinosauria: Saurischia) from the Early Cretaceous of Central Texas and its phylogenetic relationships. *Paleontologica Electronica*, 10, 1–65.
Royo-Torres, R. (2009) El saurópodo de Peñarroya de Tastavins. *Instituto de Estudios Turolenses-Fundación Conjunto Paleontológico de Teruel-Dinópolis, Monografías Turolenses,* 6, 1–548.
Royo-Torres, R. & Upchurch, P. (2012) The cranial anatomy of the sauropod *Turiasaurus riodevensis* and implications for its phylogenetic relationships. *Journal of Systematic Palaeontology*, 10, 553–583.
http://dx.doi.org/10.1080/14772019.2011.598577
Saegusa, H., Tanaka, S., Ikeda, T., Matsubara, T., Frutani, H. & Handa, K. (2008) On the occurrence of sauropod and some associated vertebrate fossils from the Lower Cretaceous Sasayama Group of Hyogo Prefecture, SW Japan. *Journal of Fossil Research*, 41, 2–12. [in Japanese with English abstract]
Saegusa, H., Tanaka, S. & Ikeda, T.(2010) Preliminary observations on the dinosaur teeth from the Lower Cretaceous Sasayama Group in Tamba City, Hyogo Prefecture and additional notes on the pneumaticity of the postcranial skeleton of Tamba sauropod. *Journal of Fossil Research*, 42, 52–65. [in Japanese with English abstract]
Saegusa, H. & Tomida, Y. (2011) Titanosauriform teeth from the Cretaceous of Japan. *Anais da Academia Brasileira de Ciências*, 83, 247–265.
http://dx.doi.org/10.1590/s0001-37652011000100014
Salgado, L., Apesteguía, S. & Heredia, S. (2005) A new specimen of *Neuquensaurus australis*, a Late Cretaceous saltasaurine titanosaur from north Patagonia J*ournal of Vertebrate Paleontology*, 25, 623–634.
http://dx.doi.org/10.1671/0272-4634(2005)025[0623:ansona]2.0.co;2
Salgado, L. & Calvo, J.O. (1992) Cranial osteology of *Amargasaurus cazui* Salgado and Bonaparte (Sauropoda, Dicraeosauridae) from the Neocomian of Patagonia. *Ameghiniana*, 29, 337–346.
Salgado, L. & Coria, R.A. (1993) El genero *Aeolosaurus* (Sauropoda, Titanosauridae) en la Formacion Allen (Campaniano-Maastrichtiano) de la Provincia de Rio Negro, Argentina. *Ameghiniana*, 30, 119–128.
Salgado, L., Coria, R.A. & Calvo, J.O. (1997) Evolution of titanosaurid sauropods. I: phylogenetic analysis based on the postcranial evidence. *Ameghiniana*, 34, 3–32.
Santucci, R.M. & Arruda-Campos, A.C. (2011) A new sauropod (Macronaria, Titanosauria) from the Adamantia Formation, Bauru Group, Upper Cretaceous of Brazil and the phylogenetic relationships of Aeolosaurini. *Zootaxa*, 3085, 1–33.
Santucci, R.M. & Bertini, R.J. (2006) A new titanosaur from western Sao Paolo State, Upper Cretaceous Bauru Group, south-east Brazil. *Palaeontology,* 49, 59–66.
http://dx.doi.org/10.1111/j.1475-4983.2005.00527.x
Sanz, J.L., Buscalioni, A.D., Casanovas, M.-L. & Santafé, J.-V. (1987) Dinosaurios del Cretácico inferior de Galve (Teruel, España). *Estudios Geologicos, Volumen Extraordinario Galve-Trem,* 45–64.
http://dx.doi.org/10.3989/egeol.8743extra625
Sanz, J.L., Powell, J.E., LeLoeuff, J., Martínez, R. & Superbiola, X.P. (1999) Sauropod remains from the Upper Cretaceous of Laño (northcentral Spain). Titanosaur phylogenetic relationships. *Estudios del Museo de Ciencias Naturales de Alava*, 14 (Número Especial 1), 235–255.
Seeley, H.G. (1887) On the classification of the fossil animals commonly called Dinosauria. *Proceedings of the RoyalSociety of London*, 43, 165–171.
Sereno, P.C., Wilson, J.A., Witmer, L.M., Whitlock, J.A., Maga, A., Ide, O. & Rowe, T.A. (2007) Structural Extremes in a Cretaceous Dinosaur. *PLoS ONE*, 2 (11), e1230.
http://dx.doi.org/10.1371/journal.pone.0001230
Stevens, K.A. & Parrish, M.J. (1999) Neck posture and feeding habits of two Jurassic sauropod dinosaurs. *Science*, 284, 798–800.
http://dx.doi.org/10.1126/science.284.5415.798
Suteethorn, S., Le Loeuff, J., Buffetaut, E. & Suteethorn, V. (2010) Description of topotypes of *Phuwiangosaurus sirindhornae*, a sauropod from the Sao Khua Formation (Early Cretaceous) of Thailand, and their phylogenetic implications. *Neues Jahrbuch für Geologie und Paläontologie Abhandlungen*, 256, 109–121.
http://dx.doi.org/10.1127/0077-7749/2010/0036
Suteethorn, S., Le Loeuff, J., Buffetaut, E., Suteethorn, V., Talubmook, C. & Chonglakman, C. (2009) A new skeleton of *Phuwiangosaurus sirindhornae* (Dinosauria,Sauropoda) from NE Thailand. *In*: Buffetaut, E., Cuny, G., Le Loeuff, J. & Suteethorn, V. (Eds.), *Late Palaeozoic and Mesozoic Ecosystems in SE Asia.* Geological Society, London, Special Publications, 315, pp. 189–215.
http://dx.doi.org/10.1144/sp315.14
Swofford, D.L. (2002) *PAUP*: phylogenetic analysis using parsimony (*and other methods), version 4.0b10*. Sunderland, Sinauer Associates, MA:

Tang, F., Kang, X, Jin, X., Wei, F. & Wu, W. (2001) A new sauropod dinosaur of Cretaceous from Jiangshan, Zhejiang Province. *Vertebrata PalAsiatica*, 39, 272–281.
Taylor, M.P. (2009) A re-evaluation of *Brachiosaurus altithorax* Riggs 1903 (Dinosauria, Sauropoda) and its generic separation from *Giraffatitan brancai* (Janensch 1914). *Journal of vertebrate paleontology,* 29, 787–806. http://dx.doi.org/10.1671/039.029.0309
Taylor, M.P., Wedel, M.J. & Cifelli, R.L. (2011) A new sauropod dinosaur from the Lower Cretaceous Cedar Mountain Formation, Utah, USA. *Acta Palaeontologica Polonica,* 56, 75–98. http://dx.doi.org/10.4202/app.2010.0073
Taylor, M.P., Wedel, M.J. & Naish, D. (2009) Head and neck posture in sauropod dinosaurs inferred from extant animals. *Acta Palaeontologica Polonica,* 54, 213–220.
Tidwell, V. & Carpenter, K. (2003) Braincase of an Early Cretaceous titanosauriform sauropod from Texas. *Journal of Vertebrate Paleontology*, 23, 176–180. http://dx.doi.org/10.1671/0272-4634(2003)23[176:boaect]2.0.co;2
Tidwell, V., Carpenter, K. & Brooks, W. (1999) New sauropod from the Lower Cretaceous of Utah, USA. *Oryctos*, 2, 21–37.
Tidwell, V., Carpenter, K. & Meyer, S. (2001) New titanosauriform (Sauropoda) from the Poison Strip Member of the Cedar Mountain Formation (Lower Cretaceous), Utah. *In*: Tanke, D. & Carpenter, K. (Eds.), *Mesozoic Vertebrate Life.* Indiana University Press, Bloomington, pp. 139–165.
Torcida Fernández-Baldor, F., Canudo, J.I., Huerta, P., Montero, D., Pereda Suberbiola, X. & Salgado, L. (2011) *Demandasaurus darwini,* a new rebbachisaurid sauropod from the Early Cretaceous of the Iberian Peninsula. *Acta Palaeontologica Polonica,* 56, 535–552. http://dx.doi.org/10.4202/app.2010.0003
Upchurch, P. (1995) The evolutionary history of sauropod dinosaurs. *Philosophical Transactions of the Royal Society of London, SeriesB*, 349, 365–390. http://dx.doi.org/10.1098/rstb.1995.0125
Upchurch, P. (1998) The phylogenetic relationships of sauropod dinosaurs. *Zoological Journal of the Linnean Society*, 124, 43–103. http://dx.doi.org/10.1111/j.1096-3642.1998.tb00569.x
Upchurch, P., Barrett, P.M. & Dodson, P. (2004a) *The Sauropoda. In*: Weishampel, D.B., Dodson, P. & Osmolska, H. (Eds.), *The Dinosauria*. University of California Press, Berkeley, pp. 259–322.
Upchurch, P. & Mannion, P.D. (2009) The first diplodocid from Asia and its implications for the evolutionary history of sauropod dinosaurs. *Palaeontology*, 52, 1195–1207. http://dx.doi.org/10.1111/j.1475-4983.2009.00909.x
Upchurch, P. & Martin, J. (2002) The Rutland Cetiosaurus: the anatomy and relationships of a Middle Jurassic British sauropod dinosaur. *Palaeontology*, 45, 1049–1074. http://dx.doi.org/10.1111/1475-4983.00275
Upchurch, P. & Martin, J. (2003) The anatomy and taxonomy of Cetiosaurus (Saurischia, Sauropoda) from the Middle Jurassic of England. *Journal of Vertebrate Paleontology,* 23, 208–231. http://dx.doi.org/10.1671/0272-4634(2003)23[208:taatoc]2.0.co;2
Upchurch, P., Tomida, Y. & Barrett, P.M. (2004b) A new specimen of *Apatosaurus ajax* (Sauropoda: Diplodocidae) from the Morrison Formation (Upper Jurassic) of Wyoming, USA. *National Science Museum Monographs*, 26, 1–107.
von Huene, F. (1929) Los saurisquios y ornitisquios del Cretácico Argentino. *Anales del Museo de La Plata*, Series 2*,* 3, 1–196.
Wang, X., You, H., Meng, Q., Gao, C., Chang, X. & Liu, J. (2007). *Dongbeititan dongi*, the first sauropod dinosaur from the Lower Cretaceous Jehol Group of western Liaoning Province, China. *Acta Geologica Sinica*, 81, 911–916. [English Edition] http://dx.doi.org/10.1111/j.1755-6724.2007.tb01013.x
Wedel, M.J. (2009) Evidence for bird-like air sacs in saurischian dinosaurs. *Journal of Experimental Zoology,* 311 A, 611–628. http://dx.doi.org/10.1002/jez.513
White, T.E. (1958) The braincase of Camarasaurus lentus (Marsh). *Journal of Paleontology*, 32, 477–494.
Whitlock, J.A., D'Emic, M.D. & Wilson, J.A. (2011) Cretaceous diplodocids in Asia? Re-evaluating the phylogenetic affinities of a fragmentary specimen. *Palaeontology*, 54, 351–364. http://dx.doi.org/10.1111/j.1475-4983.2010.01029.x
Wilson, J.A. (1999) A nomenclature for vertebral laminae in sauropods and other saurischian dinosaurs. *Journal of Vertebrate Paleontology,* 19, 639–653. http://dx.doi.org/10.1080/02724634.1999.10011178
Wilson, J.A. (2002) Sauropod dinosaur phylogeny: critique and cladistic analysis. *Zoological Journal of the Linnean Society,* 136, 217–276. http://dx.doi.org/10.1046/j.1096-3642.2002.00029.x
Wilson, J.A. (2005) Redescription of the Mongolian sauropod *Nemegtosaurus mongoliensis* Nowinski (Dinosauria: Saurischia) and comments on Late Cretaceous sauropod diversity. *Journal of Systematic Palaeontology*, 3, 283–318. http://dx.doi.org/10.1017/s1477201905001628
Wilson, J.A. (2012) New vertebral laminae and patterns of serial variation in vertebral laminae of sauropod dinosaurs.

Contributions from the Museum of Paleontology, University of Michigan, 32, 91–110.
Wilson, J.A., D'Emic, M.D., Curry Rogers, K.A., Mohabey, D. & Sen, S. (2009) Reassessment of the sauropod dinosaur *Jainosaurus* (='*Antactosaurus*') *septentrionalis* from the Upper Cretaceous of India. *Contributions from the Museum of Paleontology, University of Michigan,* 32, 17–40.
Wilson, J.A., D'Emic, M.D., Ikejiri, T., Moacdieh, E.M. & Whitlock, J.A. (2011) A Nomenclature for Vertebral Fossae in Sauropods and Other Saurischian Dinosaurs. *PLoS ONE*, 6 (2), e17114.
http://dx.doi.org/10.1371/journal.pone.0017114
Wilson, J.A. & Sereno, P.C. (1998) Early evolution and higherlevel phylogeny of sauropod dinosaurs. *Society of Vertebrate Paleontology*, Memoir 5, 1–68.
http://dx.doi.org/10.2307/3889325
Wilson, J.A. & Upchurch, P. (2009) Redescription and reassessment of the phylogenetic affinities of *Euhelopus zdanskyi* (Dinosauria:Sauropoda) from the Early Cretaceous of China. *Journal of Systematic Palaeontology*, 7, 199–239.
http://dx.doi.org/10.1017/s1477201908002691
Wiman, C. (1929) Die Kriede-Dinosaurier aus Shantung. *Palaeontologia Sinica*, Series C, 6, 1–67.
Witmer, L.M. & Ridgely, R.C. (2009) New insights into the brain, braincase, and ear region of *Tyrannosaurs* (Dinosauria, Theropoda), with implications for sensory organization and behavior. *The Anatomical Record,* 292, 1266–1296.
http://dx.doi.org/10.1002/ar.20983
Witmer, L.M., Ridgely, R.C., Dufeau, D.L. & Semones, M.C. (2008) Using CT to Peer into the Past: 3D Visualization of the Brain and Ear Regions of Birds, Crocodiles, and Nonavian Dinosaurs. *In*: Endo, H. & Frey, R. (Eds]), *Anatomical Imaging Towards a New Morphology*. Springer-Verlag, Tokyo, pp. 67–87.
Wu, W., Dong, Z., Sun, Y., Li, C. & Li, T. (2006) A New Sauropod Dinosaur from the Cretaceous of Jiutai, Jilin, China. *Global Geology*, 25, 6–9. [in Chinese]
Xu, X., Zhang, X., Tan, Q., Zhao, X. & Tan, L. (2006) A new titanosaurian sauropod from Late Cretaceous of Nei Mongol, China. *Acta Geologica Sinica* 80, 20–26. [English Edition]
http://dx.doi.org/10.1111/j.1755-6724.2006.tb00790.x
Yoshikawa, T. (1993) Stratigraphy and structure of the Early Cretaceous Sasayama Group in the Sasayama area, Hyogo Prefecture, Southwest Japan. *Journal of the Geological Society of Japan,* 99, 29–38. [in Japanese with English abstract]
http://dx.doi.org/10.5575/geosoc.99.29
You, H., Ji, Q., Lamanna, M.C., Li, J. & Li, Y. (2004) A titanosaurian sauropod dinosaur with opisthocoelous caudal vertebrae from the early Late Cretaceous of Liaoning Province, China. *Acta Geologica Sinica (English Edition),* 78, 907–911.
http://dx.doi.org/10.1111/j.1755-6724.2004.tb00212.x
You, H. & Li, D. (2009) The first well-preserved Early Cretaceous brachiosaurid dinosaur in Asia. *Proceedings of the Royal Society B*: *Biological Sciences*, 276, 4077–4028.
http://dx.doi.org/10.1098/rspb.2009.1278
You, H., Li, D., Zhou, L. & Ji, Q. (2006) *Huanghetitan liujiaxiaensis.* a new sauropod dinosaur from the Lower Cretaceous Hekou Group of Lanzhou Basin, Gansu Province, China. *Geological Review*, 52, 668–674.
You, H., Li, D., Zhou, L. & Ji, Q. (2008) *Daxiatitan binglingi*: a giant sauropod dinosaur from the Early Cretaceous of China. *Gansu Geology*, 17, 1–10.
You, H., Tang, F. & Luo, Z. (2003) A new basal titanosaur (Dinosauria: Sauropoda) from the Early Cretaceous of China. *Acta Geologica Sinica,* 77, 424–429. [English Edition]
Young, C. & Zhao, X. (1972) *Mamenchisaurus hochuanensis*. *Institute of Vertebrate Paleontology and Paleoanthropology Monographs,* Series A, 8, 1–30. [in Chinese]
Zaher, H., Pol, D., Carvalho, A.B., Nascimento, P.M., Riccomini, C., Larson, P., Juarez-Valieri, R., Pires-Domingues, R., da Silva, N.J. & Campos, D.A. (2011) A complete skull of an Early Cretaceous sauropod and the evolution of advanced titanosaurians. *PLoS ONE,* 6 (2), e16663.
http://dx.doi.org/10.1371/journal.pone.0016663
Zhang, X., Lü, J., Xu, L., Li, J., Yang, L., Hu, W., Jia, S., Ji, Q. & Zhang, C. (2009) A New Sauropod Dinosaur from the Late Cretaceous Gaogou Formation of Nanyang, Henan Province. *Acta Geologica Sinica (English Edition)*, 83, 212–221.
http://dx.doi.org/10.1111/j.1755-6724.2009.00032.x

APPENDIX. Taphonomy of Caudal Elements.

In Cd1–Cd11, Cd1 is most severely damaged by postmortem distortion, being represented only by a fragment of the summit of a neural spine and a fragment composed of the right transverse process and the posterior half of the right lateral margin of the centrum. These fragments of Cd1 were found to be surrounded by the second caudal, the fragments of sacral spines and the ilium in the quarry. On the other hand, Cd2 to Cd8 were found semi-articulated, lying on their right side (Fig.2). As one moves posteriorly through Cd2 to Cd8, the postmortem distortion decreases, and major damage of the caudal vertebrae is restricted to the left side of Cd2 to Cd6. The left transverse process is missing in Cd2–Cd6. In Cd2, the summit of the neural spine was found detached from the rest of the spine and, in Cd3 and Cd4, the left border of the neural spine summit is missing. The following portion of the centrum is missing in each caudal: in Cd2, a third of the centrum, including the left ventrolateral corner of the posterior articular surface and two thirds of the anterior articular surface; in Cd3–Cd5, a quarter of the centrum including four fifths of the left margin of the anterior articular surface; and in Cd6, the anteroventral surface of the centrum. From Cd7 onward, no notable pre-burial damage is recognized, except for the loss of the summit of the neural spine and slight erosion of the anteroventral corner of the right lateral surface of the centrum in Cd11. Cd9 and Cd10 were found in anatomical order just behind Cd8, but they were flipped backward and lying on their left side in the bed. Cd11 was found about 5m apart from Cd10, but close similarity between them suggests they are consecutive.

The extent of the damage of the caudal vertebrae is roughly related to the original transverse width of the element, and judging from this pattern of distortion, the skeleton was not completely buried by the initial depositional event. The entirety of Cd1 and the left sides of Cd2–Cd6 appear to have been exposed on the ground surface and suffered from various ground surface processes for some time prior to the completion of the burial by succeeding depositional events.

There are worm-shaped trace fossils composed of a mixture of bone chips and matrix on the surfaces of the centra of Cd2–Cd10 (tf in Figs. 10–18). Similar bone-debris filled burrows are reported from the Korean Lower Cretaceous and Mongolian Upper Cretaceous (Paik 2000; Kirkland and Bader 2010). There are two types of bone-debris filled burrows. One ranged from 1.5 to 2 cm and sticks out from the surface of the bone at a high angle and extends into the surrounding sediments. The other has a diameter in the range 0.4–0. 6 cm and runs along the surface of the bone.

In Cd2 and Cd11, the height of the centrum is almost equal to its width, whereas in Cd3–Cd10, it is, as preserved, dorsoventrally higher than transversely wide (Table 4). However, the laterally compressed shape of Cd3–Cd10 can be considered as the product of the postmortem distortion rather than original morphology because large cracks running sagittaly on the anterior and posterior articular surfaces of these caudal vertebrae indicates that these centra have been shortened along these cracks by the lateral compressional force, which must have been exerted by sedimentary load. Cd2 is less deformed laterally than Cd3–Cd10 because it lay in the bed such that its articular surface inclines less steeply than those of other caudal vertebrae. Therefore, the subcircular shape of the centrum of Cd2 must represent the original shape of the centrum.

In addition to this lateral shortening of the centrum, Cd2–Cd11 have suffered some shear deformation: Cd2–Cd8 are deformed such that the anterior articular surface of the centrum is displaced rightward relative to its posterior articular surface and the sagittal plane of the bone is redirected clockwise about 10 degrees in dorsal view (Figs. 10–16). On the other hand, on Cd9 and Cd10, the centra are deformed in the opposite direction, with their anterior articular surface displaced leftward relative to their posterior articular surface and the sagittal plane of the bone redirected counterclockwise about 10 degrees in dorsal view (Figs. 17–18). This difference between these two groups of caudal vertebrae in the direction of the shear deformation is obviously related to the orientation of the caudal vertebrae in the bed. From Cd2 to Cd8, the left sides of their centra face slightly posteriorly and dorsally, and the anterior articular surfaces face anteriorly and slightly leftward in the bed. Consequently, the compressional force exerted by the vertical load of the sediments is not directed parallel to the articular facets of the centrum, but posteriorly and rightwards. This oblique force caused the slanted deformation of the centrum of Cd2 to Cd8 as described above. On the other hand, because the orientation of Cd9 and 10 is opposite to that of Cd2–Cd8 in the bed, the direction of the compressional force acting on the former becomes opposite to that of the latter and consequently the direction of the deformation of the former becomes opposite to that of the latter.

Cdx1–Cdx11 have not been damaged by the ground surface process (Figs. 20, 21), except for parallel thin grooves on the right sides of Cdx5 and Cdx11. The parallel grooves on these centra are not artifacts because these grooves were found beneath the matrix during the preparation. On both caudal vertebrae, grooves run obliquely on the posterior part of the right side of the centrum, and may have been made by theropod bites (Saegusa *et al.* 2008). The postzygapophyses of Cdx5 and Cdx11 and the prezygapophyses of the former were lost during the excavation.

In addition to the distortions described above, Cd7, Cd9 and Cdx1 were deformed by minute faults. In the former, two minute faults run from the dorsal margin of the anterior articular surface to the posteroventral border of the neural spine. In the latter, a minute fault obliquely traverses the middle of the centrum and neural arch. The parts separated by these minute faults are displaced from each other for a few cm and the narrow zones along the faults are mashed up and replaced by calcite veins.